ADVANCED MASTERS IN STRUCTURAL ANALYSIS
OF MONUMENTS AND HISTORICAL CONSTRUCTIONS

Master's Thesis

Aikaterini Maria Koukouviki

Mechanical characterization of traditional connections in half-timbered walls: experimental results and retrofitting solutions

This Masters Course has been funded with support from the European Commission. This publication reflects the views only of the author, and the Commission cannot be held responsible for any use which may be made of the information contained therein.

Portugal | 2013

DECLARATION

Name: Aikaterini Maria Koukouviki

Email: ckoukouviki@hotmail.com

Title of the Msc Dissertation: Mechanical characterization of traditional connections in half-timbered walls: experimental results and retrofitting solutions

Supervisor(s): Graça Vasconcelos, Jorge Branco

Year: July 2013

I hereby declare that all information in this document has been obtained and presented in accordance with academic rules and ethical conduct. I also declare that, as required by these rules and conduct, I have fully cited and referenced all material and results that are not original to this work.

I hereby declare that the MSc Consortium responsible for the Advanced Masters in Structural Analysis of Monuments and Historical Constructions is allowed to store and make available electronically the present MSc Dissertation.

University: University of Minho

Date: 24 July 2013

Signature:

_____

To that power that dwells within each one of us…

A strength that has no limits or boundaries!

ACKNOWLEDGEMENTS

First of all, I would like to express my gratitude to the European Commission for the scholarship that I was granted. Without this financial help, it would have been impossible for me to attend this Master's Programme.

My appreciation and special thanks go to my supervisor Professors; Graça Vasconcelos and Jorge Branco, who were always willing to help me and did not stress me at all, throughout the entire time that I was preparing my Thesis, while they provided useful information whenever asked.

At this point, I need to say, that I have more than just appreciated the constant and valuable assistance and guidance that came from Elisa Poletti at all times. She has been too patient with me and I am not using "too" by accident.

While spending sleepless days and nights with Elisa Poletti, at the laboratory performing tests, the help and advice that we received, by the staff: Marco Jorge, António Matos and Alfredo Carlos Lemos was precious. Their kindness will not be forgotten by any of us.

Of course to every person associated with the SAHC Programme, from the teachers that opened new horizons to our knowledge, to Mrs. Ana Fonseca who had to manage all our trouble from time to time, I should say a cordial thank you.

I could not fail to mention both my Professors from the Aristotle University of Thessaloniki, where I completed my previous studies, that apart from knowledge during my studying years, they provided me with the necessary recommendation letters: Professors Dimitrios Aravantinos and Kosmas Stilianidis.

Additionally, I am grateful to Professor Aikaterini Tsikaloudaki who was kind enough to help me with additional information from a relevant previous dissertation that she had supervised.

I would like to thank my colleagues for all the support (moral and scientific), as we all realize how difficult it is to live away from your country. Even though the experience is unique and for many, a once-in-a-lifetime opportunity, it can still become very stressful.

For the same reason I would like to send my warm hugs to all of my family members and my friends in Greece, that were there to lift my spirit!

Last but not least, I am more than obliged to my personal, digital hero, Vítor Costa; the computer technician at the University of Minho, that helped prevent total failure of my laptop several times.

Needless to say, that although difficult and highly demanding; SAHC Programme does not cease to fulfill its purpose, as with the completion of my Thesis, I fill more confident academically.

ABSTRACT

Connections are an important part of timber frame structures, as is the case of half-timbered walls and play a major role in their overall behaviour. Therefore, focusing on the connections' behaviour is essential when addressing the study of seismic response of traditional timber structures.

Half-timbered walls are well known as one of the most efficient seismic resistant structures in the world. The origin of half-timbered structures probably goes back to the Roman Empire and examples can be found in Europe, Asia and the American continent. In Portugal, these buildings, called Pombalino buildings, consist of outer masonry walls and an internal timber cage filled with rubble or brick masonry. Half-timbered walls act as shear walls in these structures and it is essential to study their response to horizontal loads both in their original state and after retrofitting, since a great effort has been made in the last years from a rehabilitation point of view.

In half-timbered walls, and timber frame walls in general, seismic damage is concentrated in the connections. Therefore, the main points of intervention are usually the traditional timber joints. In this study, an experimental campaign on overlapped connections has been carried out studying the response to compressive and horizontal loads and evaluating adequate retrofitting solutions.

In order to better characterize the response of traditional overlapped connections, cyclic in plane tests have been performed in order to obtain information on their seismic behaviour, taking into account their hysteretic behaviour and their dissipative capacity. Moreover, pull-out tests have been performed on the same type of connection in order to better characterize the rocking behaviour observed in traditional half-timbered walls, resulting in important uplift displacements of the bottom overlapped connections.

In this work, results on both these types of tests on traditional timber connections are presented, concerning their unreinforced and their retrofitted states, and recommendations are provided on the retrofitting solutions.

RESUMO

As ligações constituem uma parte importante de estruturas de madeira tal como no caso de paredes tradicionais de madeira e têm um papel fulcral no comportamento mecânico. Assim, o foco colocado no comportamento das ligações é essencial quando se quer estudar o comportamento sísmico de estruturas tradicionais de madeira.

As paredes de frontal são bem conhecidas como sendo um dos elementos construtivos mais eficientes em termos de resistência sísmica. A origem das paredes tradicionais de madeira remontam ao tempo do império Romano e vários exemplos podem ser encontrados na Europa, Asia e no continente americano. Em Portugal, o sistema construtivo com as paredes de frontal são designados de edifícios Pombalinos e apresentam as paredes exteriores em alvenaria de pedra e a estrutura interna constituída por gaiolas que resultam de uma associação de paredes de frontal preenchidas com alvenaria de pedra irregular ou alvenaria de tijolo. As paredes de frontal funcionam como paredes de contraventamento, sendo essencial o estudo do seu comportamento a ações horizontais, com e sem reforço dado que um grande esforço necessário na reabilitação destas paredes.

Em paredes de frontal e paredes de madeira tradicionais, o dano sísmico é concentrado maioritariamente nas ligações. Deste modo, os pontos de intervenção são usualmente as ligações de madeira. Neste trabalho, foi levada a cabo uma campanha experimental em ligações designadas de "ligações meia-madeira" para caracterização do comportamento mecânico a esforços de tração e ações laterais cíclicas e para a avaliação de diferentes técnicas de reforço. Para o efeito, ensaios cíclicos no plano foram feitos para avaliar o comportamento sísmico com base nos diagramas histeréticos força-deslocamento e capacidade de dissipação de energia. Adicionalmente foram feitos ensaios de tração cíclicos no mesmo tipo de ligações com o objetivo de caracterização o seu comportamento em tração, dado que as ligações meia-madeira da base da parede de frontal estão sujeitos a este tipo de ação devido ao comportamento tipo "rocking" das paredes de frontal sujeitas a ações laterais. Neste trabalho, os resultados de ambos os tipos de ensaios são apresentados em provetes sem e com reforço e recomendações são fornecidas acerca das soluções de reforço.

ΠΕΡΙΛΗΨΗ

Χαρακτηρισμός των παραδοσιακών συνδέσμων στις ξυλόπηκτες τοιχοποιίες:

Πειραματικά αποτελέσματα και λύσεις ενίσχυσης

Οι σύνδεσμοι αποτελούν σημαντικό τμήμα στις τοιχοποιίες με ξύλινο σκελετό, όπως οι ξυλόπηκτες, και έχουν μείζοντα ρόλο στην συνολική τους συμπεριφορά. Ως εκ τούτου, η έμφαση στη συμπεριφορά των συνδέσεων είναι απαραίτητη για την μελέτη της σεισμικής απόκρισης των παραδοσιακών ξύλινων κατασκευών.

Οι ξυλόπηκτες τοιχοποιίες, ως γνωστόν είναι από τις πιο αποτελεσματικές, σεισμικά ανθεκτικές δομές στον κόσμο. Η προέλευση τους, πιθανώς πηγαίνει πίσω στην Ρωμαϊκή Αυτοκρατορία και παραδείγματα μπορούν να βρεθούν στην Ευρώπη, την Ασία και την Αμερικανική ήπειρο. Στην Πορτογαλία, τα κτίρια που φέρουν αυτήν την τεχνοτροπία, ονομάζονται “Pombalino” κι αποτελούνται απο την εξωτερική τοιχοποιία λιθοδομής κι έναν εσωτερικό ξύλινο σκελετό – «κλουβί», του οποίου τα κενά συμπληρώνονται με λίθους ακανόνιστου σχήματος και κονίαμα ή οπτοπλινθοδομή. Στην περίπτωση αυτή, οι ξυλόπηκτες τοιχοποιίες συμπεριφέρονται ως τοιχεία, επομένως είναι απαραίτητη η μελέτη της απόκρισής τους σε οριζόντια φορτία, τόσο στην αρχική τους κατάσταση αλλά και αφότου ενισχυθούν, δεδομένου ότι τα τελευταία χρόνια έχει γίνει μια μεγάλη προσπάθεια από πλευράς αποκατάστασης-αναμόρφωσης των εν λόγω κατασκευών.

Στις ξυλόπηκτες και στις τοιχοποιίες με ξύλινο σκελετό, η σεισμική βλάβη σε γενικές γραμμές, συγκεντρώνεται στις συνδέσεις. Επομένως, τα σημεία όπου επικεντρώνονται οι επεμβάσεις είναι συνήθως ο παραδοσιακοί, ξύλινοι σύνδεσμοι. Σε αυτή τη διπλωματική εργασία, έχει διεξαχθεί μια πειραματική εκστρατεία με σκοπό τη μελέτη της απόκρισης των επικαλυπτόμενων ξύλινων συνδέσεων κατά την ταυτόχρονη υποβολή τους σε θλιπτικά και οριζόντια φορτία και την αξιολόγηση κατάλληλων λύσεων ενίσχυσής τους.

Με σκοπό τον καλύτερο χαρακτηρισμό της απόκρισης στις προαναφερθείσες συνδέσεις, πραγματοποιήθηκαν πειράματα επαναλαμβανόμενης οριζόντιας μετατόπισης εντός επιπέδου με διαφορετικά επίπεδα αξονικής φόρτισης, ώστε να ληφθούν πληροφορίες σχετικά με την σεισμική τους συμπεριφορά, μέσω των βρόχων υστέρησης και της ικανότητας διάχυσης ενέργειας. Παράλληλα, πραγματοποιήθηκαν πειράματα επαναλαμβανόμενης κατακόρυφης μετατόπισης εντός επιπέδου στον ίδιο τύπο συνδέσεων, ώστε να χαρακτηριστεί η παρατηρηθείσα συμπεριφορά «λικνισμού» κατά τη διάρκεια πειραμάτων σε ξυλόπηκτες τοιχοποιίες, που είχε ως αποτέλεσμα σημαντικές μετατοπίσεις ανύψωσης στις επικαλυπτόμενες συνδέσεις της βάσης.

Στη δεδομένη εργασία διπλωματικής διατριβής, παρουσιάζονται τα αποτελέσματα για τους δυο προηγούμενους τύπους πειραμάτων στις παραδοσιακές, ξύλινες συνδέσεις, πριν και μετά την ενίσχυσή τους και παρέχονται συστάσεις για λύσεις ενίσχυσής τους.

TABLE OF CONTENTS

LIST OF FIGURES

LIST OF TABLES

Chapter 1

Introduction

1.1 General

Nowadays, buildings are mainly constructed with reinforced concrete, especially in areas affected by seismic events of a non-negligible magnitude, on a regular basis. Although the resistance capacity of this type of structures to seismic loads is undoubtedly high, there have been many cases where apart from the expected damages that are allowed during their designing, deformations surpassed those values by far, reaching even total failure and collapse. Furthermore, the seismic design regulations have to be reviewed quite often, since earthquakes do not always fall within the expected and predefined range. After all, concepts as seismicity and seismic hazard are relatively new [1].

On the other hand, traditional buildings made with empirical knowledge, much lighter materials and a clear disadvantage concerning strength and rigidity towards reinforced concrete, such as half-timbered structures, appear to have exceptionally good behavior with high ductility and relatively small damages, under seismic loads [2].

Half-timbered structures consist of a frame made of vertical, horizontal and diagonal wooden elements, which are joined together at the connections. A masonry infill of stones, adobes or bricks and mortar, is wedged in the areas formed between the wooden elements providing further stiffness [2].

Additionally, the declaration of certain traditional settlements, where this type of structure is found, as an important part of cultural heritage, leads to the need for their repairing and preservation, while changes in use require further strengthening and rehabilitation works. The same applies also to the unique case, of “Pombalino” buildings in Lisbon, Portugal, where this type of structures was used for the first time as a solution for higher seismic resistance of buildings, after the devastating effects from the earthquake of 1755 [3].

Experimental research has verified the importance of connections in half-timbered structures, as energy is dissipated mainly at these parts of the wall, while the infill masonry which is easily repairable can sustain relatively small damages [2], [4].

1.2 Objectives and methodology

Upon the completion of the experimental research on real size wall specimens, the need for further knowledge upon the mechanical behavior of traditional connections of half-timbered walls arose.

As time for the conclusion of the Thesis was limited, only one of the connections was chosen to be studied: a lower corner connection where the post and beam are joined together through overlapping. The diagonal wooden element was not taken into consideration.

The behavior of this type of connection, during the in-plane quasi-static cyclic tests that were performed on the wall specimens, was governed by combined shear and bending. For this reason the main objectives of this work are centered in the understanding of the individual behavior of this type of

connections, aiming at obtained information that further enable its correlation to the behavior of the wall. For this, an experimental campaign was designed based on distinct types of load configurations, which are considered to be representative of the mechanical behavior of the connection under in-plane lateral loads. Therefore, in detail the major goals of the present work are:

- Analysis of the results of pull-out tests to evaluate its performance while subjected to cyclic uplifting displacements.
- Analysis of the results of in-plane cyclic tests regarding the studied connection to obtain information about the hysteresis properties under mixed flexure and shear loads.
- Assessment of the results of distinct retrofitting solutions on the hysteretic performance of the connections.

1.3 Outline of the Thesis

After this introductory chapter, follows Chapter 2, which intends to familiarize the reader with the subject. Initially, a brief historical overview of the half-timbered structures is provided, along with the architectural description and construction details of a representative, traditional building in Greece. Furthermore, the connection typologies from the “Pombalino” walls are stated, while there is also a brief state of the art on the existing studies relevant to the studied traditional half-timbered walls and timber connections.

In Chapter 3, information about the geometry of the specimens along with some physical properties of the wood is provided. Moreover, the two different types of tests that were performed (pull-out and in-plane cyclic) on the unreinforced timber connections, as well as their setups, instrumentations and procedures are explained in detail. After each test, follows the analysis and commenting of the results and the clarification of certain calculations that took place. The results concerning the in-plane cyclic tests were grouped in relation to their pre-compression load level.

A detailed description of the retrofitting techniques that were decided to be applied after the observation of the damage patterns in the unreinforced specimens is given in Chapter 4. Moreover, there is a brief discussion of additional techniques, which were not used to strengthen the tested connections.

After the tests of the retrofitted connections were performed, the results that were obtained, were evaluated and they are presented in Chapter 5. Each test is analyzed separately, while for the in-plane cyclic tests the results were grouped according to the retrofitting technique which was applied.

Finally, the conclusions that derived from this experimental campaign, as well as recommendations for future studies regarding traditional connections in half-timbered walls, are listed in Chapter 6.

In order to help the reader follow the analysis, whenever there was a large number of graphs to be displayed, they were gathered in appendixes:

Appendix A: The figures with all the force versus displacement graphs of the pull-out and the in-plane cyclic tests were gathered in this section.

Appendix B: The figures with all the vertical versus out-of-plane displacement graphs of the pull-out tests were gathered in this section.

References

1] Penelis G.G., Kappos A.I., Earthquake resistant constructions from concrete (in Greek), ZITIS Publising, Thessaloniki 1999

[2] Kappos A.I., Kouris L.A., Modelling of Traditional Timber-Framed Masonry Structures (in Greek), 3rd National Conference on Earthquake Engineering and Engineering Seismology, 5-6 of November 2008, Paper No. 2013

[3] Paula R., Coias V., Rehabilitation of Lisbon's old seismic resistant timber framed buildings using innovative techniques, International Workshop on “Earthquake Engineering on Timber Structures”, Coimbra, Portugal, November, 2006

[4] Poletti E,, Vasconcelos G,, Oliveira D.V., Influence of infill on the cyclic behaviour of traditional half-timbered walls. In: Proceedings of International Conference on Rehabilitation and Restoration of Structures, Chennai, India, 2013.

Chapter 2

State-of-the-art for half-timbered walls and their connections

2.1 Historical overview of the half-timbered wall structure

As wood is a material that is found extensively in nature, while it is also workable through easy ways and has good mechanical properties, it has been used in the construction of different types of structures for thousands of years.

Wooden elements have been used throughout time to create a whole structure, as huts or parts of it, like roofs, walls and floors. Specifically referring to walls, wooden elements have been used horizontally embedded within the walls, as they evolved vertically (*ksilodesies* in Greek, Figure 2.1a). Additionally, to make bearing walls, light structures were created with vertical, wooden, supporting elements that were filled with wattled reeds or nailed laths and covered with plaster (*ksiloplekti tichopiia* or *badgatotichos* in Greek, Figure 2.1b) or by wooden frames which were filled with bricks, rubble or adobe and usually covered with plaster (*ksilopikti tichopiia* or *tsatmas* in Greek, Figure 2.1c) [5]. The latter is the description of a half-timbered wall structure.

a)

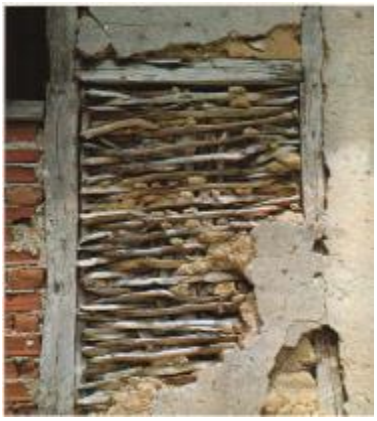

b)

c)

Figure 2.1 – a) Horizontally, embedded, wooden elements within the wall, b) Wall made of vertical, wooden, supporting elements that were filled with wattled reeds or nailed laths and covered with plaster (*ksiloplekti tichopiia*), c) Half-timbered wall (*ksilopikti tichopiia*) [6].

Chronologically, the first two story half–timbered wall structure can be found in the less known archaeological site of Herculaneum, which is close to Pompeii, Italy and was also buried under lava

after the eruption of Mount Vesuvius' volcano in 79AD. According to Vitruvius' masonry construction typologies the structure could be described as *Craticii* or *Opus Craticium [7]*.

Eventually, due to the simplicity of its construction and the use of cheap materials, this structure spread throughout the Mediterranean basin, as well as the rest of Europe, parts of Asia and South America. Since the 8th century until recently it has been greatly used in Turkey, where it is called *himis* (Figure 2.3a) and in Greece, *tsatmas* is a very common, traditional structure ever since the Byzantine era (Figure 2.3b) [7],[8]. Other local names to describe the studied structure would be (Figure 2.2): *colombage* in France, *fackwerkbau* in Germany, *telar de medianeria* in Spain, half-timber in Britain, *dhajji-dewari* in Kashmir, India (Figure 3-c) and *bindingverk* in Scandinavia (Figure 2.3d) [8], [9].

In Central America a variation between half-timbered walls and the ones created by vertical, wooden, supporting elements that were filled with wattled reeds or nailed laths and covered with plaster (named *bagdadi* in Turkey and Greece and *quincha* in Peru) can be found in Nicaragua, called *taquezal* or "pocket" system and in El Salvador, called *bahareque.* In this case the "pockets" that were formed as the wooden laths or bamboos were nailed across the studs, were then filled with layers of small stones or adobe. Finally the wall would be covered with plaster [7].

It is noteworthy, that the first time, half-timbered walls were used because of the observation of their seismic resistance ability, was after the earthquake of Lisbon, Portugal in 1755, and the one in Calabria, Italy in 1783. An anti-seismic inner wall system of half-timbered walls was created in both cases, in order to resist horizontal loads and dissipate energy, while it was also tied to the outer stone masonry walls in order to prevent their out-of-plane overturning. The developed systems were named *gaiola (=cage)* or *Pombalino construction* and *Casa Baraccata* respectively [7],[3].

Figure 2.2 – Local names to describe the studied structure [7],[8],[9].


a)

b)
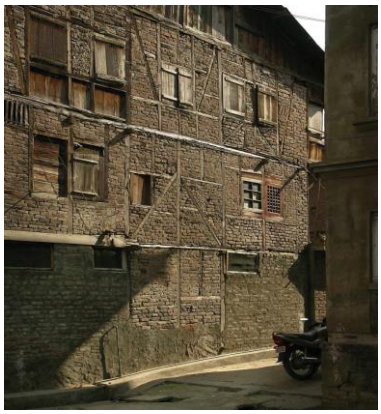
c)


d)

Figure 2.3 – a) *Himis* in Turkey, b) *Ksilopikti tichopiia* in Athens, Greece, c) *Dhajji-dewari* in Kashmir, India, d) B*indingverk* in Sweden [9],[10],[7],[8].

2.2 Architectural description of a typical half-timbered building in Greece

The historical building which is described below in detail is located in Ractivan Street 23, Thessaloniki, Greece. The upper part of the city, called Ano Poli, has been declared as a traditional settlement and most of its noticeable buildings, where created while the city was under the reign of the Ottoman Empire, since 1432 and for almost five centuries after, but the buildings are mainly from the 19th century [11].

2.2.1 Foundation

The so called shallow foundation is made of rough stones and clay mortar. The stones are laid in the perimeter of the building, in a pit that has a depth of no more than 60cm and a width of 70÷80cm depending on the width of the masonry walls of the ground floor, which were usually made of stone (Figure 2.4) [11].

2.2.2 Ground floor

Usually the bearing walls of this floor would be made of stone masonry, but the lighter half-timbered structure can also be seen here in some occasions [6]. The structural materials are limestones from the area of Thessaloniki and clay mortar mixed with hay. The stones are slightly hewed in order to form a proper laying surface for the ones lying over and underneath them. The joints are continuous only concerning the horizontal direction. These joints are no bigger than 2cm and in some parts they have been filled with small rubble stones or tile pieces. The width of the wall is between 60÷70cm and at a height of 70cm, as well as at the highest point of the wall, there are horizontally embedded, wooden elements (Figure 2.4) [11].

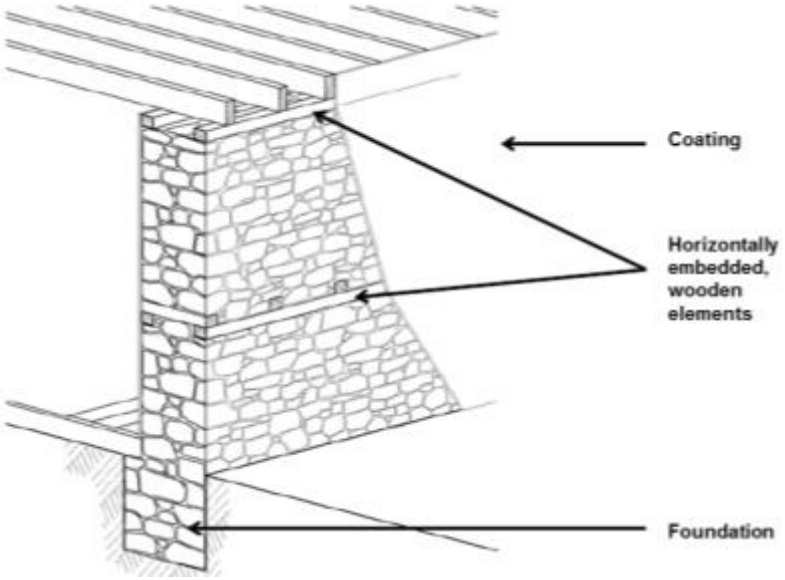

Figure 2.4 – Structural detail of the stone masonry wall and the foundation [11].

2.2.3 Upper storeys

2.2.3.1 Half-timbered structure

All the bearing walls of the upper storeys are half-timbered structures. They consist of a frame made of horizontal, vertical and diagonal wooden elements jointed together in plane. The first horizontal wooden base-beam is nailed upon the wooden floor boards which are right above the wooden beams of the floor. The nails used are placed in an inclined way and they are made of steel with a square section. The vertical columns are nailed upon the horizontal base-beam without having a mortise and tenon connection, while the stabilization of the connections is ensured by the existence and wedging of the appropriately shaped, diagonal elements. At the highest point of the wall the beams are supported on the columns through an inserted, wooden element that has a mortise and tenon connection with its ends formed into chamfers. The infill masonry includes adobes or bricks, mud, small stones and pieces of tiles in a clay mortar mixed with hay. The width of this type of wall along with the coating is around 20cm (Figure 2.5) [11].

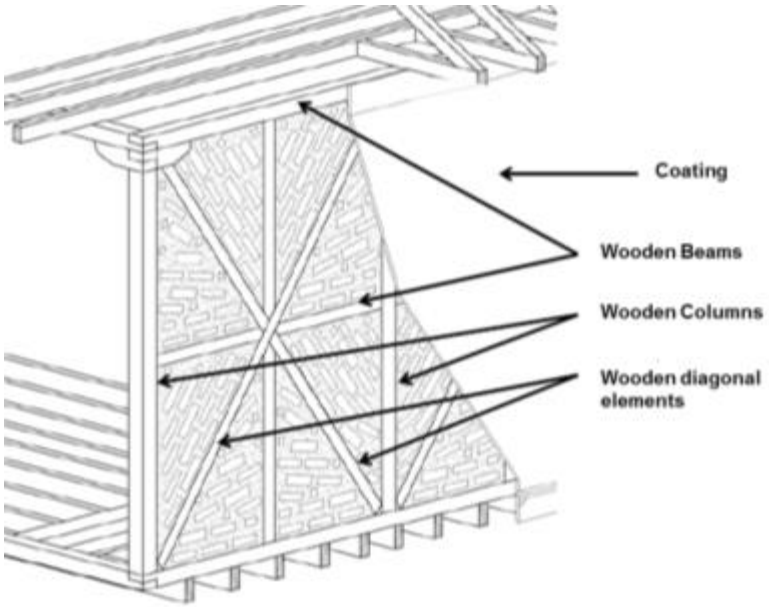

Figure 2.5 – Structural detail of the half-timbered wall [11].

2.2.3.2 Inner walls

Light, wooden walls were used to separate the interior spaces with different uses. These structures which are called *bagdadi* in Turkey and also in Greece are constructed by wooden beams and columns that form a frame, where wooden laths of an approximate thickness 1,5÷2cm and width 3÷5cm were nailed on both columns with a vertical gap of 2cm. These gaps would ensure better adhesion and stabilization of the coating that was applied afterwards. Another technique was the placement of wattled reeds instead of nailed laths (Figure 2.6) [11],[6].

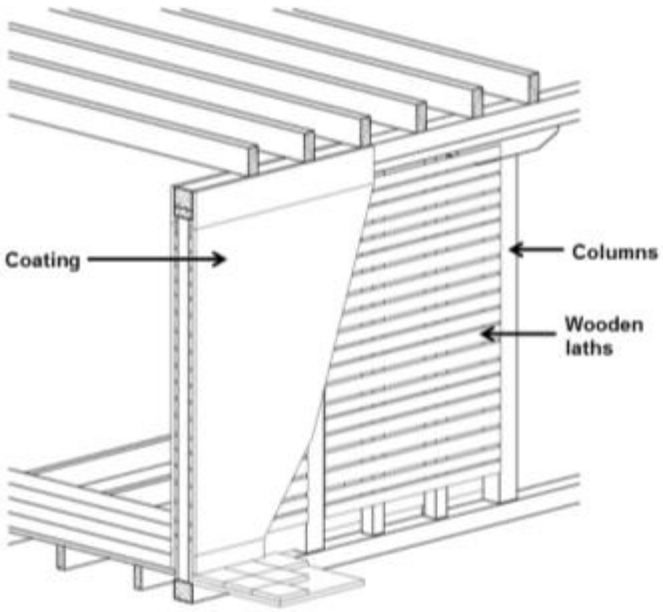

Figure 2.6 – Structural detail of the inner *bagdadi* wall [11].

2.2.3.3 Jetty

When the room of an upper floor has greater dimensions than its inferior and its projection protrudes towards the pavement, it creates an architectural differentiation which is called, *jetty* or overhanging upper storey [7]. In this case the floor beams extend further than the building line, as cantilevers. At the edge of the beams, there is a beam that connects them in a lateral way, and which redistributes the loads to the struts that support the jetty. The struts end at the outer wall of the lower floor diagonally and they can have different architectonic variations (Figure 2.7) [11]. Additionally, jetties serve a structural purpose, as they apply a compressive force to the walls below them, which adds to their strength against lateral forces [7].

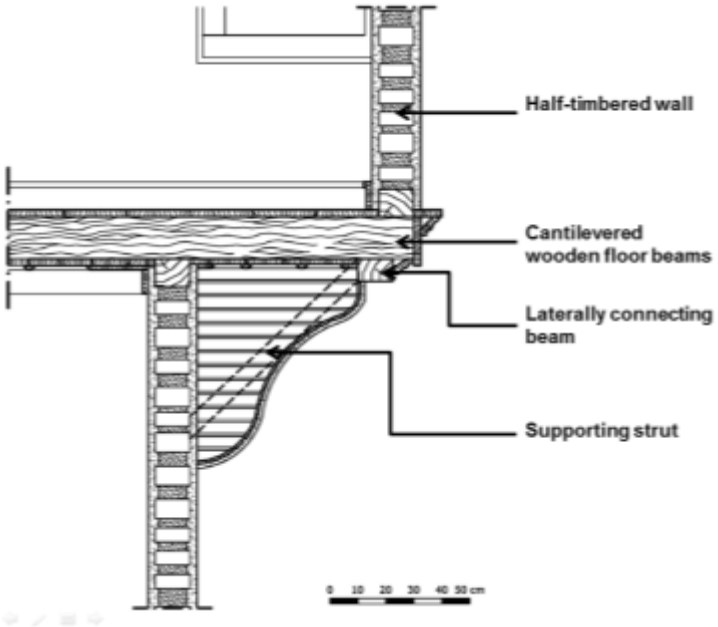

Figure 2.7 – Structural detail of the jetty [11].

2.2.4 Floor

It was common practise, for the ground floor to be the previously existing earth, which would be leveled with shovels. On a frequent basis some water, mud and manure was applied on the floor to prevent dust from rising and to keep its surface smooth [12].

The wooden floors of the upper storeys, consist of the beams that have a section of 7x15 (cm), placed every 40÷50cm, in a way parallel to the small side of the wall. It should be mentioned that traditional houses usually had a rectangular shape, with a good orientation regarding energy-saving [12]. The floor boards have a width of 18÷22cm and a thickness of 2,5cm. In the intersection between the floor and the wall there is a skirting board with a height of 7cm. The ceiling is also covered with wooden boards and a decorative wooden strip around the perimeter of the rooms (Figure 2.8) [11].

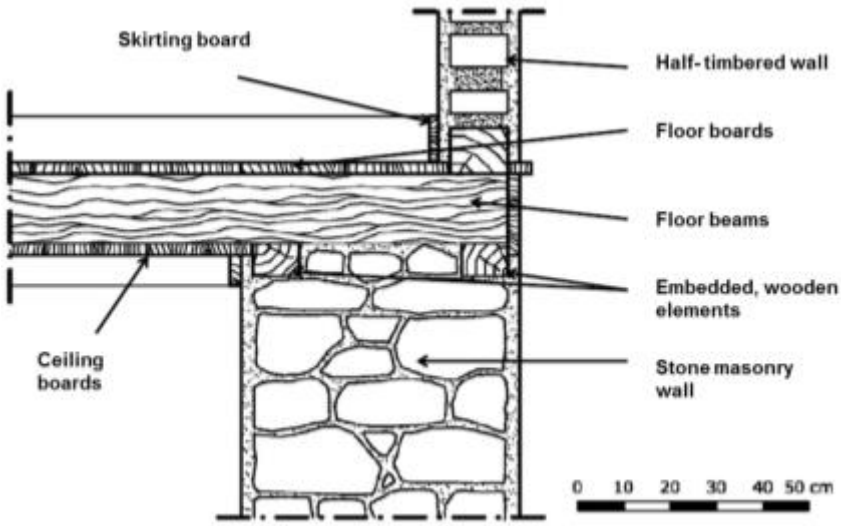

Figure 2.8 – Structural detail of the wooden floor [11].

2.2.5 Roof

The building has a wooden roof with a height of 1,95m and an inclination that ranges between 50÷55%. The ridge beam, the tie beams of the ceiling from the underlying floor, the beams that form the half -timbered wall frames, in the perimeter of the roof plan and the collar beams that exist along the height between the previous, are the horizontal elements of the wooden trusses. Additionally, there are main and secondary posts positioned vertically while rafters and wooden boards are placed inclined, concluding the wooden frame structure of the roof. The roof is covered with tiles (Figure 2.9) [11].

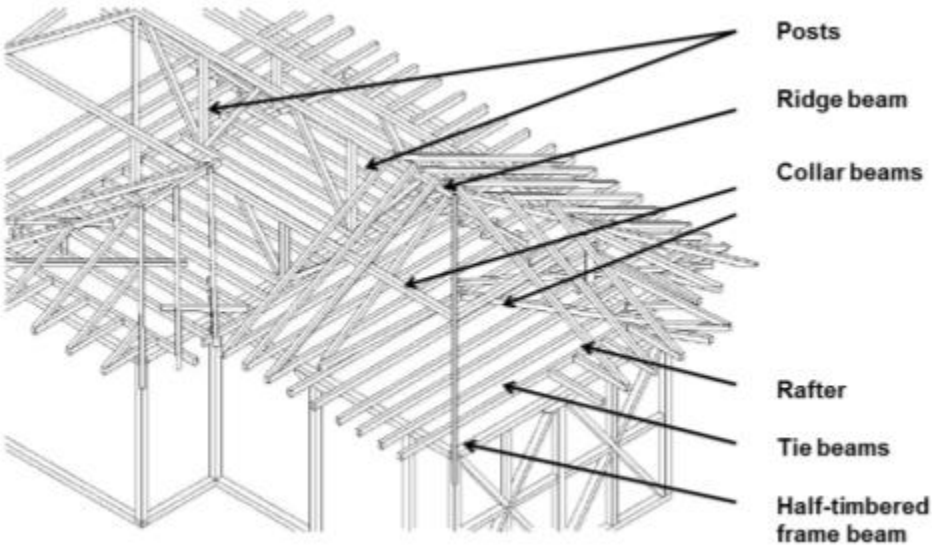

Figure 2.9 – Axonometric configuration of the wooden frame structure of the roof [11].

2.2.6 Function and distribution of spaces

Traditional buildings that date back to the 19th century bear common features, such as a rectangular plan shape, two or three storeys and rooms arranged in a row. Access was usually possible through the transitional room in the middle of the floor plan, which served as a hallway or a living room and leaded to the rooms on each one of its sides [11].

The openings were fewer on the ground floor, since it was generally meant to accommodate secondary uses, as stables or storage rooms [6]. Additionally, openings are not found distributed equally on each side of the building, which could lead to the assumption that local constructors had empirically observed that it was more efficient, as far as it concerned energy losses to minimize the presence of openings on the north side of the building, while on the contrary it was feasible for the south side [12].

The upper floors housed the social and private life of the family, while additional, roughly constructed buildings in the surrounding area of the main building, served as oven or secondary kitchen, laundry room, toilets or storerooms [11],[12].

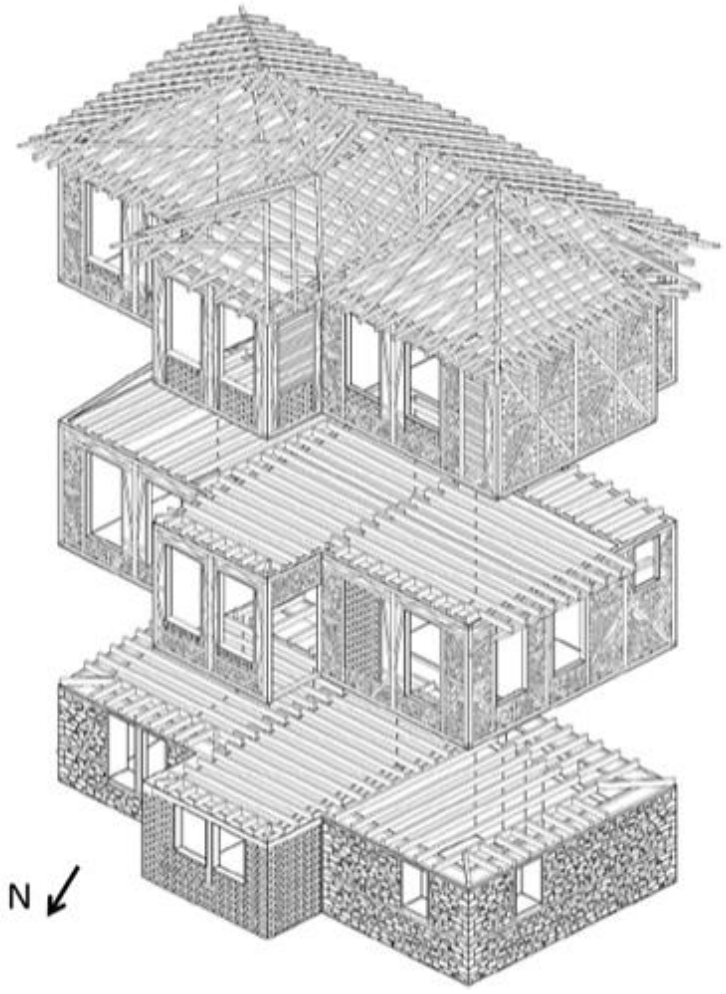

Figure 2.10 – Axonometric configuration of the load bearing structure of the building [11].

2.3 Description of the connection typologies in half-timbered frames

The architectural description of a half-timbered wall in Greece has been provided in a previous paragraph (See 2.2.3.1).

Nevertheless, the experimental part of this project will be referring to the “Pombalino” buildings of Lisbon that bear the “gaiola” or “cage” system, therefore it is essential that the main differences of these two systems are stated.

While, the half-timbered frame walls were used in Greece, to form the exterior walls of the upper storeys as a rather economical construction that they intuitively and empirically related to strength and flexibility, in Lisbon they were used in the interior of the buildings as a previously observed seismic resistant system, after the earthquake of 1755. The latter system was being knowingly used in order to make the construction resistant to horizontal loads and to dissipate substantial amounts of energy and prevent the overturning of the external stone masonry walls. In fact, the two-directional vertical bracing system of timber framed walls was connected to the façade pilasters, which were confined by horizontally embedded wooden elements (Figure 2.11) [3].

Since, the “gaiola” system was in the interior of the buildings, it had a lower number of openings, which means that it had more diagonal wooden members that contributed to a higher stiffness against horizontal loads in plane [10]. Additionally, the positioning angle of the diagonal elements, in the case of “gaiola” was usually 45º, which was easily achieved in the absence of openings while in the Greek system this angle varies. The infill material in Lisbon consisted mainly of rubble masonry made of small stones and ceramic elements set in lime mortar and there was no use of adobes or bricks as in the case of Greece. Another difference between these two cases is the number of floors, which was usually 4÷5 in Lisbon, while in Greece 2÷3 which influences the applied vertical loads in each case [3], [6].

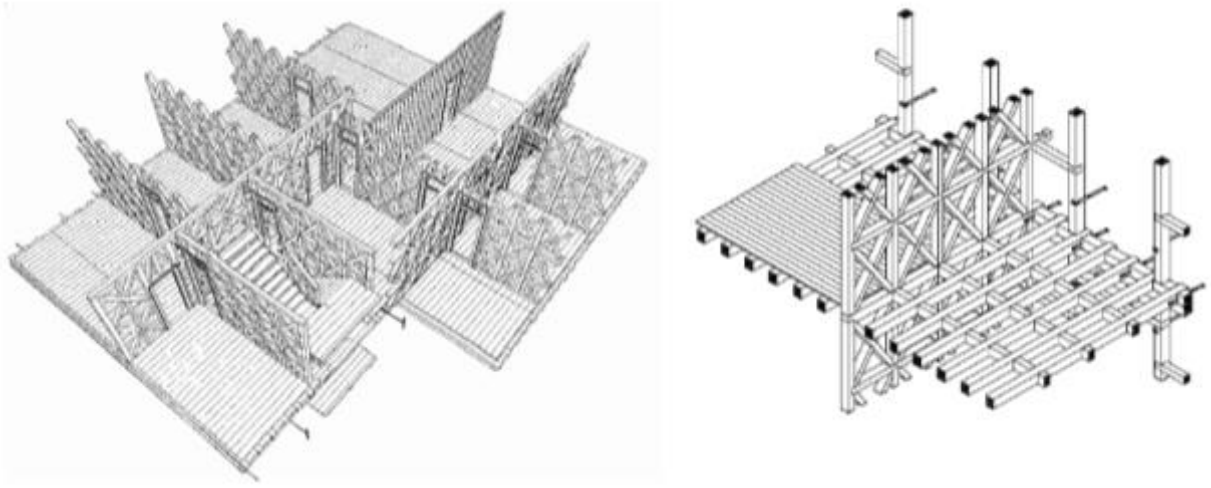

Figure 2.11 – Axonometric configuration and structural details of the “Pombalino” structure [3].

The presence of a mortise and tenon connection between the posts, beams and diagonal parts of the timber-framed walls, was not very common in Greece [11], although in some cases a round tenon of approximately 6cm was connecting the vertical posts to the horizontal elements [10]. However, in common practice the vertical posts were connected to the horizontal elements by a single iron nail, while the diagonal elements were usually wedged in the corners that were formed by the vertical posts and the horizontal elements and an iron nail was used sometimes to secure that they stayed in place [10], [11]. On the other hand, in case of the "Pombalino" structure, the timber elements that constituted it, where usually notched together with crossed edge half lap or edge half lap through joints (Figure 2.12) or connected by nails or iron ties, while there have also been cases where dovetail connections were present (Figure 2.13) [13], [14], [16] .

More precisely, three different types of connection typologies can be identified in the "gaiola" system for the case where a wall with three posts and three beams in considered along with its diagonal bracing elements (Figure 2.12):

i. The corner connection, where the post is connected to the beam with an edge half lap through joint and a nail, although there have been cases where only the vertical elements were cut in half thickness, while the beams maintain their original form [15].
ii. The central connection and
iii. The connection between the diagonal elements, where the timber elements are connected by a crossed edge half lap joint (and a nail in the case of ii).

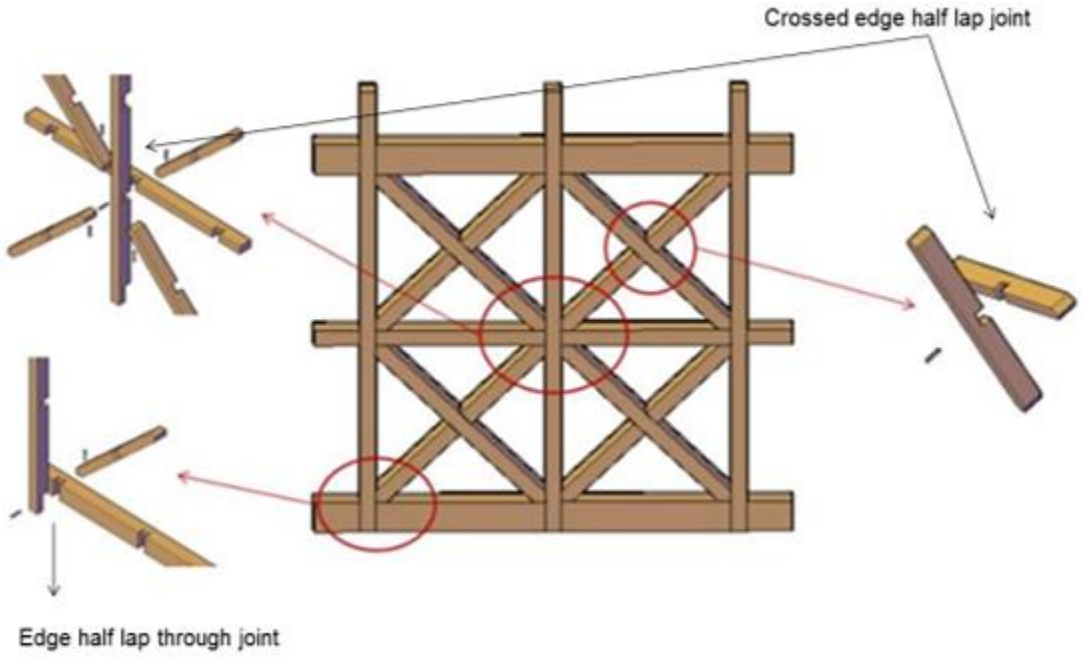

Figure 2.12 – Configuration and structural details of the connections in the "Pombalino" structure [4], [14].

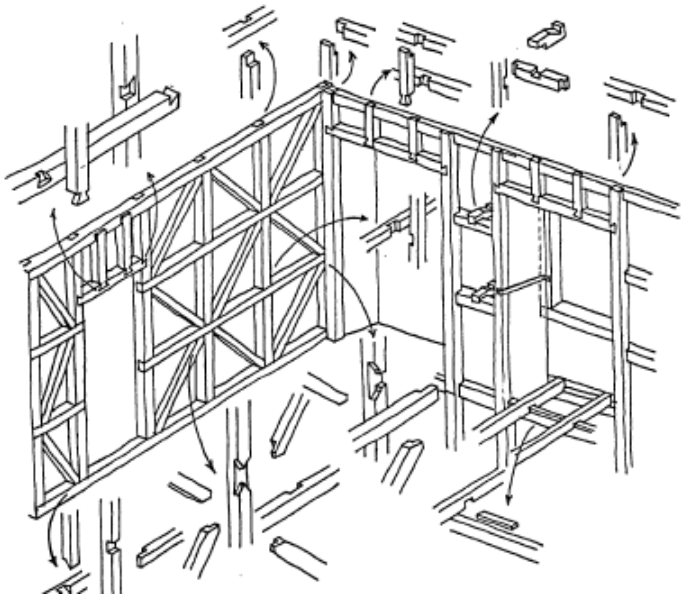

Figure 2.13 – Configuration and structural details of dovetail connections in a “Pombalino” structure [16].

2.4 Existing studies on half-timbered walls

The attempt to have a better insight and analyze the seismic behavior of half-timbered walls is a difficult task, as it involves material and geometrical dissimilarities, while there are no distinct regulations and standards to take into consideration. This leads to inevitable assumptions and simplifications and the resort to limited, relevant information in the codes [17].

Seismic evaluation of such structures is attainable through various ways:

- From observations in the pathology of buildings that have been affected by a recent earthquake. This can be regarded as an “experiment” in the true scales of space and time [18]. Indeed, such inspections of buildings in the past have provided the following conclusions:

    i) First appears detachment of the infill masonry from the timber frame, while at the same time occurs separation and falling of the coating,

    ii) Subsequently, cracking of the infill masonry and possible falling out-of-plane and

    iii) At the end damages take place at the timber frame, which could lead to its collapse.

    It is important to clarify that the last type of damage can be found in cases where buildings have been out of use and neglected for years and that generally, the damages that are found tend to be less when the materials had better quality and the engineering efficacy was adequate [2],[9],[19].

- Through numerical modeling with the use of different, available software such as Diana, Sap, ABAQUS, ANSYS etc. The studied structure is simulated in the form of finite elements with

certain degrees of freedom and mathematical functions and they have to be chosen carefully in order to give the correct results, while the analyst should be able to evaluate the final results and realize the existence of probable mistakes [18].

Nevertheless, it is challenging to appropriately simulate half-timbered walls, as some of the problems that rise are:

i) The sliding of the diagonal timber elements which are in tension, when seismic horizontal forces are implemented. This action leaves these elements almost in disuse.

ii) The connections should not be assumed as rigid and their flexibility has to be taken into account.

iii) The existence or not of openings and the adequate reproduction of the surrounding timber frame.

iv) Finally, the consideration or not of the masonry infill and the material properties that will be used [2],[17].

- Finally, helpful information to the scientific community is provided through the performance of experiments on real size walls which are either manufactured [4],[15] or removed from buildings (Figure 2.14) [7]. In the first case it is possible to perform tests on walls with or without infill and openings as well. Additionally, it is possible to examine the cases of repairing, strengthening and rehabilitation [20],[21]. Such a research is ongoing at the moment at the University of Minho in Portugal (Figure 2.15) [4].

  Scale models of this type of walls, unreinforced and with reinforcement, have also been tested in the past in diagonal compression [28] and in plane cyclic tests [29].

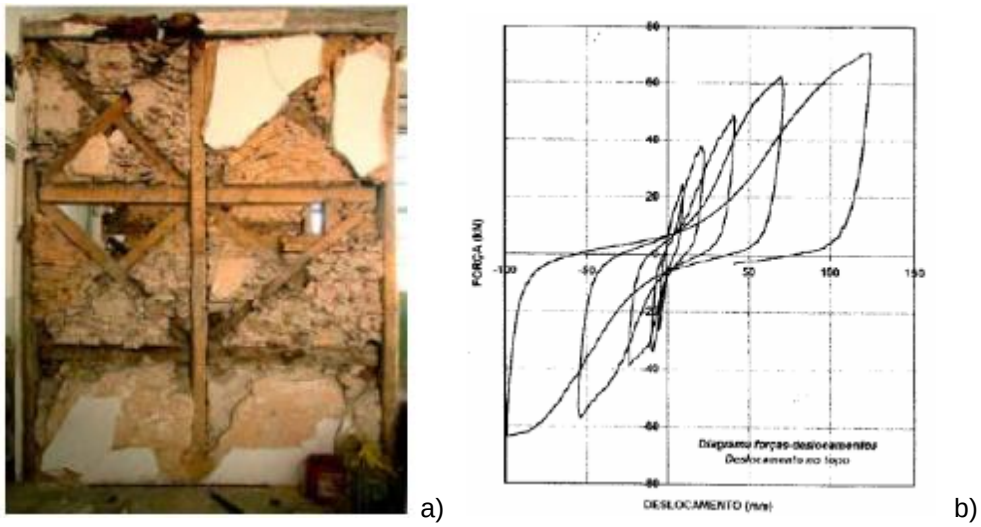

a) b)

Figure 2.14 – a) Removed wall from “Pombalino” building and tested for strength and stiffness in the Portuguese National Lab by Coias e Silva, b) F-d graph of one from the three walls that were tested, which shows that structural integrity was not lost [7].

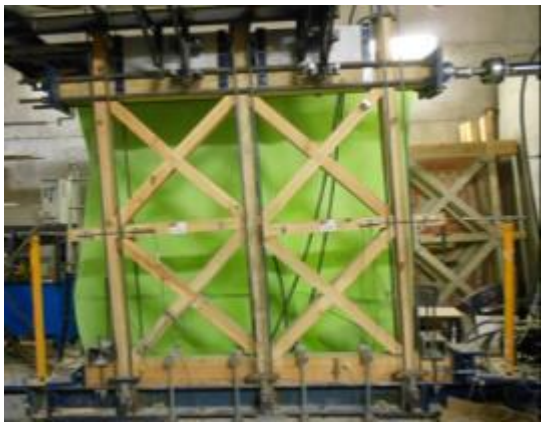

a)

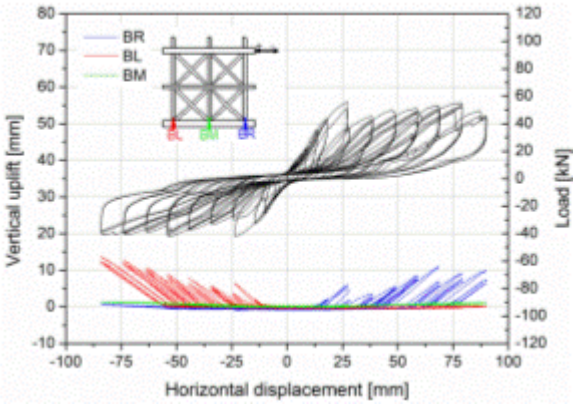

b)

Figure 2.15 – a) Timber-framed wall without infill tested at the University of Minho, Portugal, b) Corresponding F-d graph for the lower considered vertical load (25KN) [4].

2.5 Existing studies on relevant timber connections

While the timber frame of the studied walls could be described as a wooden truss [17], the connection typologies between half-timbered walls and roof trusses, for example, are quite different.

The background literature in overlapping connections is very limited, as opposed to the one referring to tests and strengthening techniques applied on typical carpentry connections found in traditional roof trusses such as single step frontal (Birdsmouth) joint, single posterior step (Birdsmouth) joint and double step joint for the connection between tie beams and rafters (Figure 2.16a-c) [22],[23],[24], or mortise and tenon connections for the struts (Figure 2.16 d) [25],[26],[27].

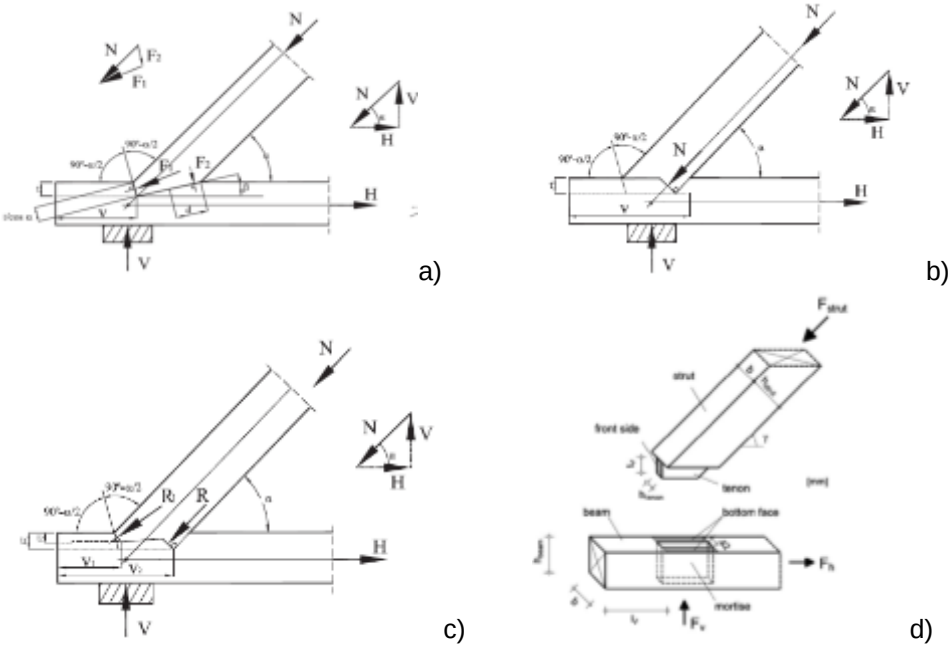

a) b) c) d)

Figure 2.16 – a) Single step frontal joint, b) Single posterior step joint, c) Double step joint and d) Tapered mortise and tenon joint [22], [25].

This indicates that experimental campaigns are necessary in order to provide engineers with sufficient knowledge regarding the mechanical behavior of overlapped connections that are representative of half-timbered walls. According to EC8, for wooden trusses with nails in their joints, only the area of the connection will be considered to dissipate energy, while their diagonal members can be taken into consideration as linearly elastic [17].

Therefore, once all the connection typologies are tested and their results are evaluated and verified through numerical analysis, it could be possible to correlate the results with the ones from timber-framed walls that have been tested without their infill.

References

[2] Kappos A.I., Kouris L.A., Modelling of Traditional Timber-Framed Masonry Structures (in Greek), 3rd National Conference on Earthquake Engineering and Engineering Seismology, 5-6 of November 2008, Paper No. 2013

[3] Paula R., Coias V., Rehabilitation of Lisbon's old seismic resistant timber framed buildings using innovative techniques, International Workshop on “Earthquake Engineering on Timber Structures”, Coimbra, Portugal, November, 2006

[4] Poletti E,, Vasconcelos G,, Oliveira D.V., Influence of infill on the cyclic behaviour of traditional half-timbered walls. In: Proceedings of International Conference on Rehabilitation and Restoration of Structures, Chennai, India, 2013.

[5] Stilianidis K., Ignatakis C., Masonry Structures(according to Eurocodes 6 and 8) (in Greek), Thessaloniki 2010

[6] Morphology - Rhythmology, Theory of Architectural Forms & Rhythms, Traditional Architecture (in Greek), Student Notes from Democritus University of Thrace, Ksanthi
Available at: http://morfologia.arch.duth.gr/3o_etos/3o_exam_VI/paradosiaka.pdf (7.7.2013)

[7] Langenbach R., From “Opus Craticium” to the “Chicago Frame”: Earthquake-Resistant Traditional Construction, International Journal of Architectural Heritage (2007),1:1, 29 — 59

[8] Copani P., Timber-Frame Buildings in Scandinavia: High Deformation Prevent the System from Collapse, ICOMOS IWC - XVI International Symposium: From Material to Structure - Mechanical Behaviour and Failures of the Timber Structures, Florence, Venice and Vicenza, 11th -16th November 2007

[9] Gülkan P., Langenbach R., The earthquake resistance of traditional timber and masonry dwellings in turkey, 13th World Conference on Earthquake Engineering, Vancouver, B.C., Canada, August 1-6, 2004, Paper No. 2297

[10] Tsakanika-Theohari E., Mouzakis H., A post-byzantine mansion in Athens. The restoration project of the timber structural elements, World Conference on Timber Engineering 2010

[11] Anastasiadis C., Papadopoulos D., Restoration and energy efficiency of a historical building in Ano Poli, Master Thesis, Civil Engineering Dept., Aristotle University of Thessaloniki, 2010

[12] Koukouviki A.M., Inspection of insulation efficiency of a rural area residence in Megalo Seirini, Grevena, Greece, according to the Regulation of Energy Performance of Buildings and suggestions on its improvement (in Greek), Master Thesis, Civil Engineering Dept., Aristotle University of Thessaloniki, 2011

[13] Cardoso R., Lopes M., Bento R., Seismic evaluation of old masonry buildings. Part I: Method description and application to a case-study, Engineering Structures 27: (2005), 2024–2035

[14] The Hobbit House Illustrated Glossary of Woodworking terms - Joinery terms: http://www.hobbithouseinc.com/personal/woodpics/_joineryterms.htm (7.7.2013)

[15] Meireles H.A., Seismic vulnerability of Pombalino buildings. PhD Thesis. UTL, Instituto Superior Tecnico, Lisbon 2012

[16] Mascarenhas J., Construction systems – V (in Portuguese). Livros Horizonte, Lisbon 2004

[17] Ignatakis C., Eftichidis S., Investigation of masonry infilled timber structures-Modelling proposal and analysis procedure (in Greek), 3rd National Conference on Earthquake Engineering and Engineering Seismology, 5-6 of November 2008, Paper No. 2072

[18] Roca P., Kabele P., Lourenco P., MSc SAHC Lecture, SA2.1 Purpose and Possibilities of Structural Analysis, UNIPD, Padova, Italy, 2012-2013.

[19] Gülhan D., Güney I.O., The behaviour of traditional building systems against earthquake and its comparision to reinforced concrete frame systems; experiences of Marmara earthquake damage assesment studies in Kocaeli and Sakarya.
Available at ICOMOS International Wood Committee :
http://www.icomos.org/iiwc/seismic/Gulhan.pdf (7.7.2013)

[20] Goncalves A.M., Ferreira J.G., Guerreiro L., Branco F., Seismic retrofitting of Pombalino "frontal" walls, World Conference of Earthquake Engineering, Lisbon 2012, Paper No. 5129

[21] Poletti E., Vasconcelos G., Seismic behaviour and retrofitting of timber frame walls. International conference on structural health assessment of timber structures (SHATIS'13) 4 - 6 September 2013, Trento, Italy (accepted).

[22] Branco J., Influence of the joints stiffness in the monotonic and cyclic behavior of traditional timber trusses. Assessment of the efficacy of different strengthening techniques, Ph.D. Thesis, Civil Engineering Dept., University of Minho, Portugal 2008

[23] Palma P., Garcia H., Ferreira J., Appleton J., Cruz H., Behaviour and repair of carpentry connections – Rotational behaviour of the rafter and tie beam connection in timber roof structures, Journal of Cultural Heritage 13S (2012) S64–S73

[24] Parisi M.A., Cordie C., Mechanical behavior of double-step timber joints, Construction and Building Materials: Volume 24, Issue 8, August 2010, Pages 1364–1371

[25] Koch H., Eisenhut L., Seim W., Multi-mode failure of form-fitting timber connections - Experimental and numerical studies on the tapered tenon joint, Engineering Structures 48 (2013) 727–738

[26] Feio A., Lourenco P., Machado J., Testing and modeling of a traditional timber mortise and tenon joint, Materials and Structures: DOI 10.1617/s11527-013-0056-y, 2013

[27] Shanks J.D., Walker P., Experimental performance of mortise and tenon connections in green oak, The Structural Engineer – 6 September 2005, p.40-45

[28] Cruz H., Moura J.P., Machado J.S., The use of FRP in the strengthening of timber-reinforced masonry load-bearing walls, Historical Constructions, Guimaraes, 2001, p.847-856

[29] Pilaon P., Experimental cyclic behavior of timber shear walls, SAHC Master Thesis, Civil Engineering Dept., University of Minho, Portugal 2010

Chapter 3

Pull-out and in-plane cyclic tests on unreinforced timber connections

3.1 Introduction

Taking into account that the cyclic behavior of traditional timber frame walls is controlled to a great extent by the behavior of their connections [4], it is important to focus on the experimental behavior of individual connections, in order to have a complete insight of their mechanical behavior. For this, an experimental campaign is intended, to evaluate the cyclic behavior of traditional timber joints to distinct types of loading configurations, namely pull-out forces and lateral cyclic loading. In a relevant research upon real size half-timbered wall specimens [4] it was seen that important uplift of the overlapped bottom connection occurred, being thus important to analysis the pull-out forces.

The evaluation of the deformation patterns and damage progress will assist in the further understanding of the mechanical behavior and in the selection of the best fitting retrofitting solutions for traditional timber frame walls. Notice that experimental results on the traditional connections used in the timber frame walls are lacking, on the contrary to other types of connection representative for other timber structures as timber roofs [22],[23],[24],[25],[26],[27]. Therefore, the experimental campaign is fully justified by the need of obtaining novel results on overlapped traditional timber connections which are typical for traditional timber frame walls.

In this scope, a total number of 14 specimens was decided to be tested for the mechanical characterization of the traditional connections in half- timbered walls. Pull-out tests were performed in four specimens and in-plane cyclic tests in the remaining ten. Details about the geometry of the connections, testing setup and procedures adopted will be provided. Additionally, a detailed discussion of the results that were obtained will be also given.

3.2 Description of specimens

The wood which was used for the construction of the specimens is pinus pinaster or maritime pine, which is a commonly found type of wood within the Mediterranean basin, especially in the western or southwestern area of Europe. Its average density value, ρ_m, is about 600kg/m^3. It should be noted that the wood that was used was not treated in order to simulate the aging that has taken place in the actual connections of the “Pombalino” system walls, which therefore can result to an overall better behavior in comparison to the real case, especially in cases where the degradation of timber elements is serious.

Out of the three different connection typologies which are encountered in the structure of half-timbered walls (See 2.2), one was selected to be tested; the corner connection, where the post is connected to the beam with an edge half lap through joint and a nail (Figure 3.1). The selection of this type of connections is associated to the following reasons: (1) the boundary conditions are more easy to be defined than the ones of the central connection for example; (2) the overlapped connection at the bottom takes an important role on the overall behavior of the walls, especially when flexure predominates in the response of the walls since significant uplifting was observed in this case [4].

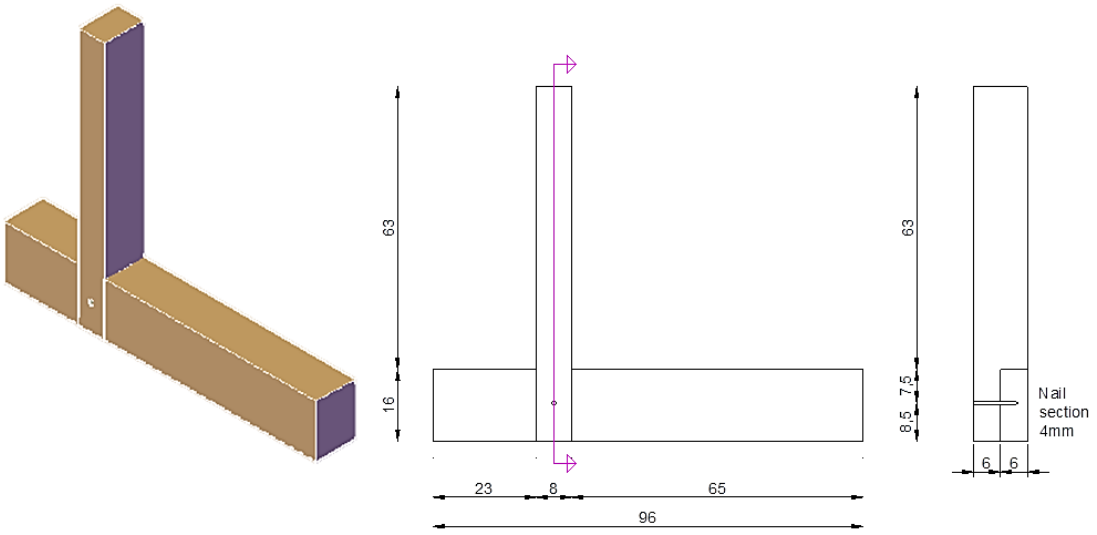

Figure 3.1 – Configuration and geometry of the overlapped bottom connection (dimensions in cm).

The only fastener of the connection is a nail of square section with a side of 4mm and 10cm length and it is positioned in the middle of the post width at approximately 8,5cm from the bottom. The dimensions adopted for the connections are related to the dimensions of posts and beams used in the experimental study carried on timber frame walls [4].

The simplifications that were made and should be taken into consideration are:

i. The complete disregard of the diagonal element, which would induce great difficulties in the setup of the test, although its presence would contribute only to the behavior of the connection in the cyclic test.
ii. The absence of infill and the further stiffness it provides concerning the cyclic test. Notice however that the present case can simulate the timber frame walls without infill.

3.3 Determination of density and moisture content of the wood

According to the International standards test pieces were taken from the wood which was used in the specimens to evaluate the density and control the moisture content. For this, prisms with a square cross-section of side 20mm and a length along the grain of 25±5mm [30],[31] were considered.

The total number of these pieces was 48, being 19 of them placed in the area of the laboratory where the tests took place and the rest 29 were positioned in a climatic chamber with a temperature of 20˚C and a relative humidity of 60%.

After two months, their mass and their dimensions along the axes of symmetry were determined to an accuracy of 0,01g and 0,1mm respectively. Subsequently the pieces were gradually dried to a constant mass at a temperature of 103±2˚C. It should be noted that “constant mass is considered to be reached if the loss in mass between two successive weighings carried out at an interval of 6 h is equal or less that 0,5% of the mass of the test piece” [31]. Once again, the specimens were weighed

and their dimensions were measured and then they were cooled in a desiccator with silica and they were weighed and had their dimensions measured for the last time [30],[31].

The calculation for the density, ρ_w, of each test piece at the moisture content *W* at the time of the test is given by the formula:

$$\rho_w = \frac{m_w}{a_w * b_w * l_w} \qquad (3.1)$$

where m_w is the mass (kg or g) and a_w, b_w and l_w are the dimensions (m or cm) of the test piece at moisture content *W* [30].

The results for the 19 test pieces which were in the area of the laboratory showed an average value of ρ_w=595,56kg/m^3, while for the 29 that were in the climatic chamber this value was ρ_w=570,19kg/m^3.

Additionally, the calculation for the density ρ_o of each test piece in the absolutely dry condition, after having reached a constant mass, is given by the formula:

$$\rho_o = \frac{m_o}{a_o * b_o * l_o} \qquad (3.2)$$

where m_o is the mass (kg or g) and a_o, b_o *and* l_o are the dimensions (m or cm) of the test piece in the absolutely dry condition [30].

The results for the 19 test pieces which were in the area of the laboratory showed an average value of ρ_o=563,95kg/m^3, while for the 29 that were in the climatic chamber this value was ρ_w=539,68kg/m^3.

As far as it concerns the calculation of moisture content *W*, of each test piece, as a percentage by mass, it is given by the formula:

$$W = \frac{m_1 - m_2}{m_2} * 100 \qquad (3.3)$$

where m_1 is the mass (g) of the test piece before drying and m_2 is the mass (g) of the test piece after cooling at the desiccator [31].

The results for the 19 test pieces which were in the area of the laboratory showed an average value of W=10,52%, while for the 29 that were in the climatic chamber this value was W=12,65%.

3.4 Determination of superficial moisture content of the wood

A hygrometer or moisture meter (Figure 3.2a) was used and several points on the surface of the specimens were punctured in a shallow depth (Figure 3.2b), in order to determine the superficial moisture content (*MC*), which is fundamental for the structural behavior of timber [32]. From the values that were gathered, an average value for the superficial *MC* was calculated separately for the beam and the post. These values are shown in Table 3.1. From the results, it is seen that no great differences on the moisture content were observed among the different timber elements

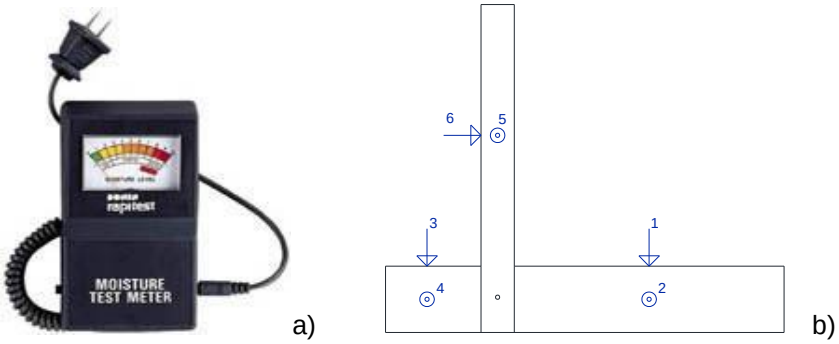

Figure 3.2 – a) hygrometer, b) the points where the superficial MC was measured [32].

Table 3.1 – Mean values of superficial moisture content for beam and post.

			Superficial MC	
Ref.number	Type of test	Test name	Mean value for beam	Mean value for post
1	Monotonic / Pull-out	URT PO1	12,21%	10,82%
2	Pull-out	URT PO2	13,23%	11,12%
3	Pull-out	URT PO3	12,67%	12,35%
4	Pull-out	URT PO4	12,82%	13,12%
5	Cyclic	URT C1_25	12,48%	12,85%
6	Cyclic	URT C2_50	13,33%	12,02%
7	Monotonic	MONO25	12,07%	11,32%
8	Monotonic	MONO50	13,02%	12,25%
9	Cyclic	URT C3_25	13,36%	12,52%
10	Cyclic	URT C4_25	13,35%	11,78%
11	Cyclic	URT C5_25	12,42%	11,65%
12	Cyclic	URT C6_50	13,68%	13,02%
13	Cyclic	URT C7_50	11,83%	11,48%
14	Cyclic	URT C8_50	12,13%	11,85%

3.5 Pull-out tests

During this test the vertical post part of the connection is being pulled upwards, while the horizontal beam part is fixed and steady. After reaching the maximum displacement which is implemented, the post is being pushed downwards until it reaches its initial position. There are no boundary conditions preventing the out of plane displacement of the post at the joint.

Pull-out tests can be performed:

- Monotonically: In this case, the test is completed after the post reaches the maximum displacement according to the predefined procedure. This type of tests aims at obtaining the non-linear behavior for this type of loading case.
- Cyclically: The test is completed after several steps of displacements are imposed, after which unloading until the initial position is required. The object of this type of tests is to provide a better approximation to the seismic behavior. This is accomplished by the comprehension of damage accumulation as well as the degradation of stiffness and the energy dissipation.

3.5.1 Test setup

The specimens were placed upon a stiff and level stabilized surface steel profile, which was fastened at the reaction floor of the laboratory (Figure 3.3a). Additionally, in order to prevent any unwanted movement at the beam of the connection, two fixing plates were positioned on the top of the beam at each side of the post and four rods were used to fix them with the steel profile (Figure 3.3b).

A hydraulic jack was fixed with bolts underneath the horizontal bottom surface of the top beam of the surrounding steel frame precisely above the set location of the top of the post. The maximum load capacity of the actuator is 150KN and the maximum plunger course is about 200mm. A load cell with a maximum measuring load capacity of 200KN was fixed at the bottom of the actuator. A hinge was fixed under the load cell.

A steel U profile is used to connect the top of the post to the actuator. Having the 4 holes of the profile as a guide, another 4 holes were drilled on the top of the post and 4 rods were placed to fasten it. Consequently, once the actuator was put in use the hinge was centered and fixed with a steel pin at the top of the U profile and the test was performed and monitored through the data acquisition system that exists at the laboratory.

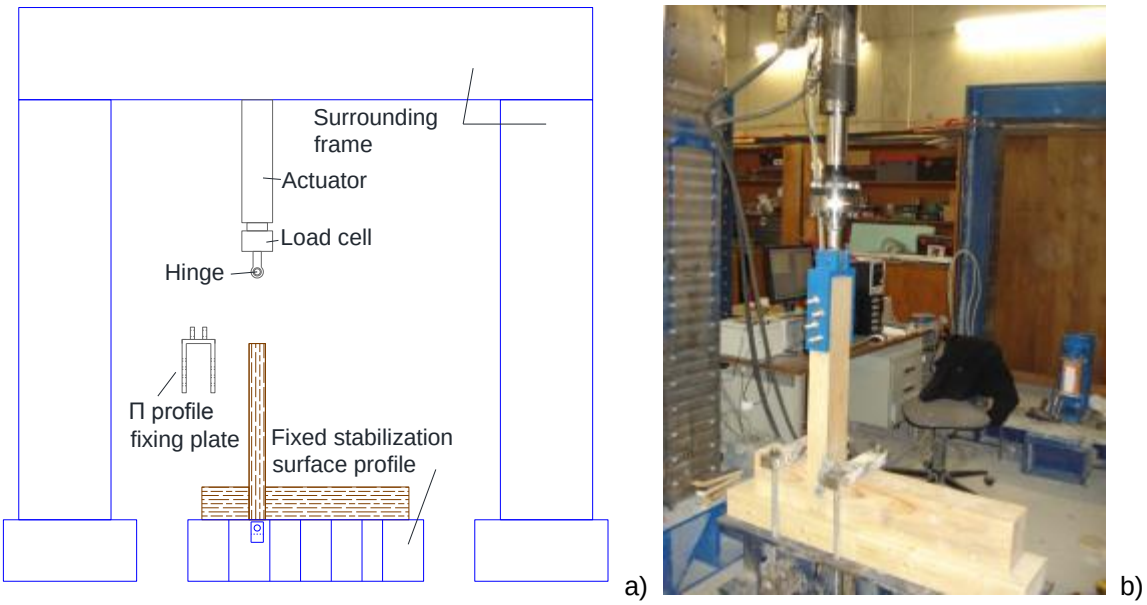

Figure 3.3 – Experimental details of the test setup for pull-out tests; a) configuration and b) a photograph of the setup for the pull-out test.

3.5.2 Instrumentation

Apart from the actuator, which is inducing the displacement at the top of the post and enables the monitoring of the force and displacement during the test through a computer, several displacement measuring devices were placed in certain positions in order to: (1) ascertain that the process was concluded as planned; (2) obtain the main deformations of the connections.

A total number of 3 to 4 linear variable differential transformers (LVDT) were used to measure and monitor the displacements in certain points of the specimens. The operating principle of these sensors is based on the fact that they consist of a rod surrounded by a transformer coil and the motion of the rod relative to the coil changes the electrical output of the transformer [34].

Each of the LVDTs that were positioned in the connections was used to measure (Figure 3.4):

- The uplifting of the beam, which should have values close to zero, since the beam was fixed (LVDT 1).
- The upward and downward displacements of the post (LVDT 2) . The displacement provided by this LVDT should be almost the same as the one recorded in the actuator and both displacements should be compared. This sensor was also used to control the test as it was carried out in displacement control, as it will be discussed in detail in the next section.
- One or two for the out of plane displacement of the post (LVDT 3 and LVDT 4); in the case where two LVDTs where used, it was possible to determine whether torsion was also present at the post during the test.

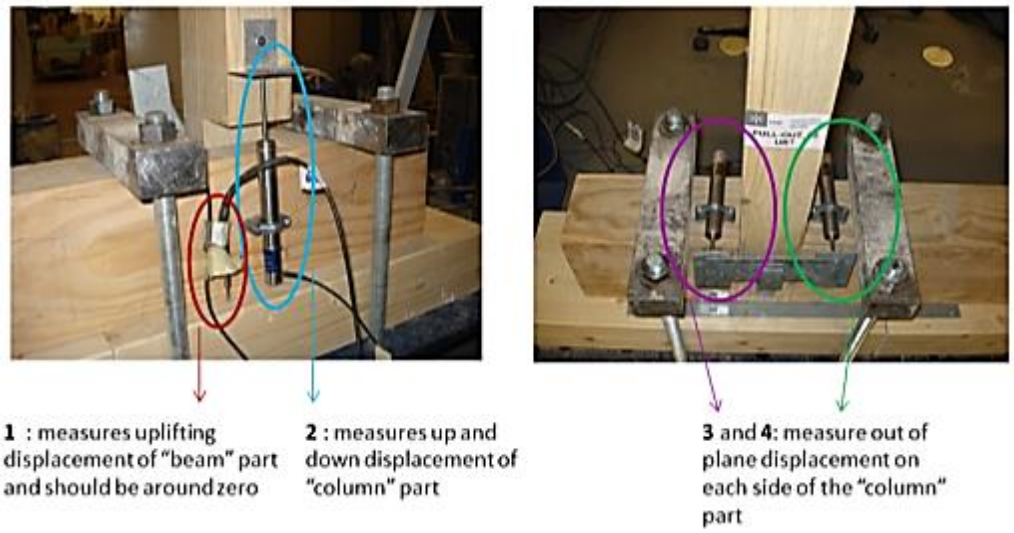

Figure 3.4 – Positions of LVDTs for the pull-out tests.

3.5.3 Test procedure

According to the predefined procedure, the pull-out tests were performed under displacement control taking into account 6 steps with certain percentages of the maximum imposed displacement, du=50mm. In four of these steps there was a repetition of 3 cycles (Table 3.2). In one case (specimen PO3) there was an addition of one more step that had one cycle, with a displacement of 60mm (120% *du) in order to achieve more softening after the peak resistance of the connection was attained.

Table 3.2 – Pull-out test procedure and graph configuration.

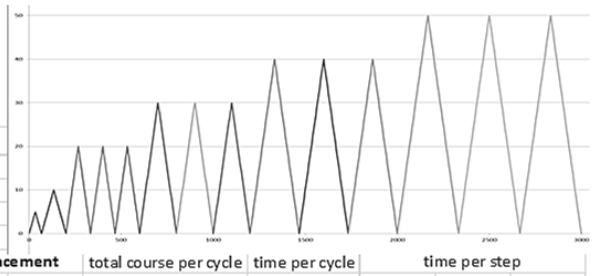

d_u	50	mm
speed 1	0,15	mm/s
speed 2	0,3	mm/s

step	nº of cycles	displacement		total course per cycle	time per cycle	time per step		
		%	mm	[mm]	[s]	[s]	[min]	[h]
1	1	10	5,00	10	66,67	66,67	1,11	0,02
2	1	20	10,00	20	133,33	133,33	2,22	0,04
3	3	40	20,00	40	133,33	400,00	6,67	0,11
4	3	60	30,00	60	200,00	600,00	10,00	0,17
5	3	80	40,00	80	266,67	800,00	13,33	0,22
6	3	100	50,00	100	333,33	1000,00	16,67	0,28

3.5.4 Analysis of results

Evaluation of the damage patterns

As a result of the pull-out force, which was applied to the specimens, the post was pulled upwards, leading to the bending of the nail (Figure 3.5a,c). The vertical area of the post right underneath the position of the nail, in its inner overlapping side, presented a splitting in the direction parallel to the grain (Figure 3.5d).

Since there was nothing to prevent the out-of-plane displacements at the connection, the nail was slowly bent into an “S” shape and it was extracted from the beam. The accumulation of the out-of-plane displacement every time the post was pushed back down occurred due to the cyclic loading, since the deformation of the nail was permanent (Figure3.5b-c). On the other hand, when it is pulled up again, the connection tended to recover some out-of plane displacements, being almost in-plane.

In the end, the nail, which was 4cm inside the beam at the beginning of the test, was totally removed, except from one case (specimen PO1), where the nail suffered abrupt failure due to fatigue.

It should be noted that the first of the four specimens that were tested with the pull-out procedure, was tested initially monotonically. Afterwards, the nail was removed and a new nail was placed at 11,5cm from the bottom, 3cm above the first position.

Apart from the permanent deformation of the nails that bended into an “S” shape and the previously mentioned splitting crack at the inner side of the post, underneath the nail, no other damages were observed during or at the end of the tests, when for every case the post was taken apart in order to register their final state (Figure 3.5e).


a)


b)

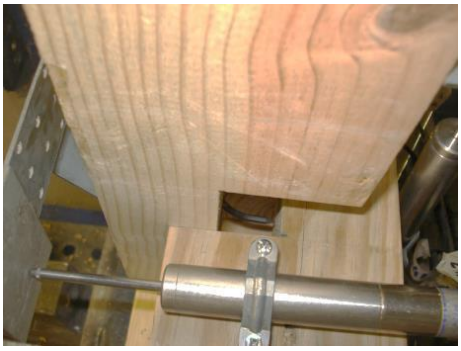
c)


d)


e)

Figure 3.5 – a) Post pulled-out and in-plane, b) Post pushed-down and out-of-plane, c) Side view of the opened joint and the bended nail, d) Deformation of nail into “S” and splitting of grain under the initial position of the nail, e) Lack of damages at the beam.

Analysis of the Force – Displacement diagrams

The typical cyclic behavior of the overlapped connections under cyclic pull-out forces is shown in Figure 3.6. The behavior is characterized by great initial stiffness and a non-linear behavior until the peak force is attained. The unloading branches also have great stiffness, being almost vertical. Two main features of the pull-out cyclic loading are identified: (1) the unloading displacement imposed to

the connection results in the appearance of important compressive stresses for high displacements, which should be associated with the difficulty of the connection to recover the displacement due to the plastic deformation of the nail. In fact, if the nail had not existed, the final stresses corresponding to the complete unloading should be zero; (2) on the other hand, there is a considerable pinching effect in the reloading branch, which should result from the clearances formed in the zone of the nail and also to the yielding of the nail. According to what was mentioned before, some concentrated damage around the nail result in the local damage of the wood.

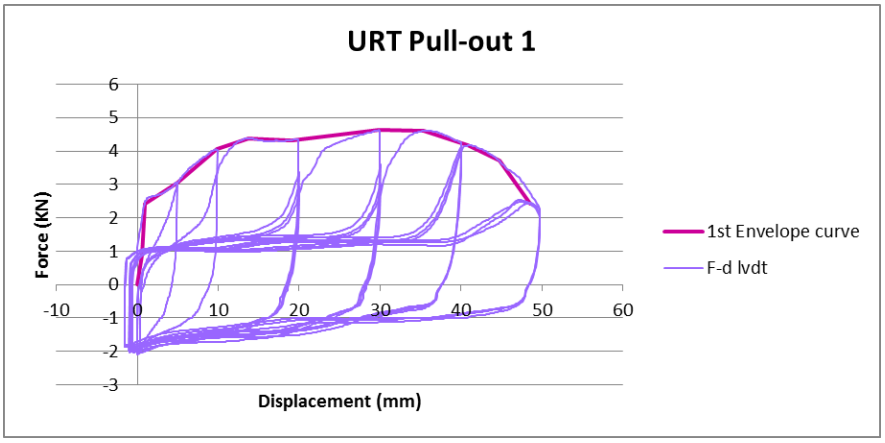

a)

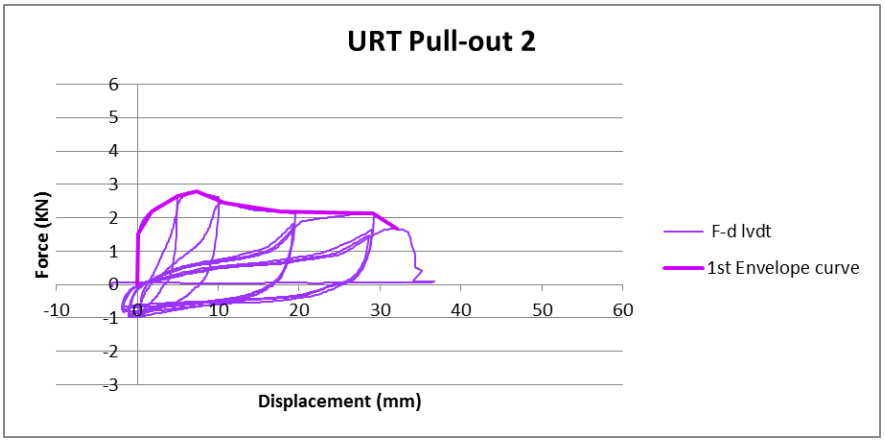

b)

Figure 3.6 – Cyclic pull-out force-displacement diagrams; a) specimen PO1, b) specimen PO2.

By comparing the force-displacement diagrams between the specimens PO1 and PO2, it is seen that there are great differences in terms of resisting force and also in terms of hysteresis loops: (1) the resistance found for specimen PO2 is considerably lower than the resistance obtained in specimen PO1; (2) the hysteresis loops in case of the force-diagrams for specimen PO1 have much higher area enclosed. This behavior should be attributed to the constructive quality of the connection. In fact, a perfect geometry of the elements that “lock” together at the joint lead to an overall better behavior under pull-out loading. By comparing the force-displacement diagrams with the perfection of the geometry of the connection some relation is found between the performance and the lateral interlocking in the following order: PO1 > PO3 > PO4 and PO2. The remaining cyclic force-displacement diagrams are in Appendix A. The differences can also be seen clearly when the

monotonic envelop of the cyclic behavior is displayed (Figure 3.7). The monotonic envelopes were obtained after connecting the points of the maximum forces for each step displacement in the first cycle, creating the backbone of each graph [35]. Due to high non–linearity, a few intermediate high values were also used in order to better approximate the graphs.

In the combined graph it is also noticeable that the monotonic test line, which captures the non-linear behavior of the pull-out loading case, is enclosing the first envelope curve lines of the tests. This is an indication of the behavioral deterioration which follows tests that are performed cyclically. However, some care should be taken when comparing the specimen PO1, being tested monotonically and cyclically. In fact, the monotonic test which was performed when the nail was at 8.5cm from the base and the cyclic test (specimen PO1) with the nail located at 11.5 cm from the base present a difference that could possibly be attributed to the new higher location of the nail, as previous deformation at the lower position of the nail could lead to that.

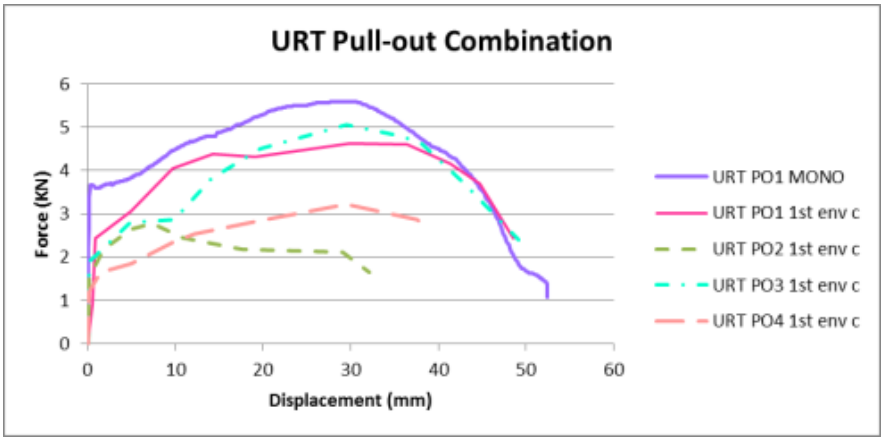

Figure 3.7 – Combination of F-d envelope curve graphs for all the pull-out tests. (URT: Unreinforced timber).

Evaluation of the out-of-plane displacement

In the diagrams that relate the out-of-plane displacement (oop) with the pull-out vertical displacement, it can be seen that the out of plane increases during the test for increasing vertical displacements and that it is cumulative.

The maximum out of plane displacement appears to be lower in the case of specimen PO1 (10cm) in relation to the other specimens that are in average 30mm at the end of the test (see also Appendix B), which was due to the loss of the LVDT.

It is also possible to realize the increasing of the out-of-plane displacement during the test each time the specimen described a downward movement and its decreasing once the post starts uplifting. The increasing out of plane displacement of the monotonic pull-out test was also recorded.

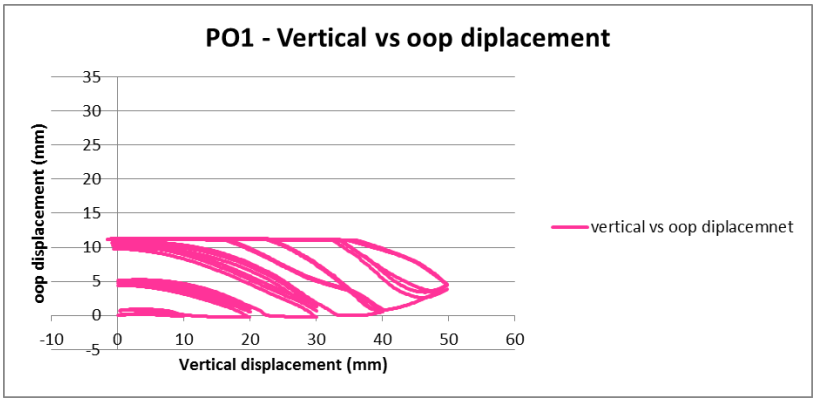

a)

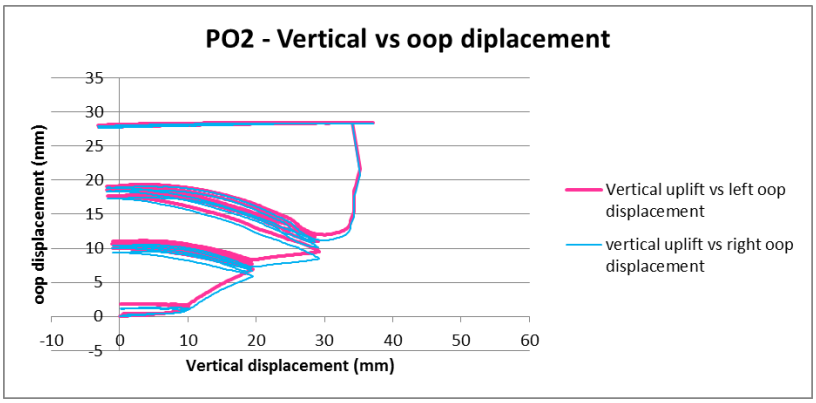

b)

Figure 3.8 - Cyclic pull-out force-displacement diagrams; a) specimen PO1, b) specimen PO2.

The lack of clearances, laterally between the post and the beam at the overlapping joint, provided friction which prevented the out-of-plane displacement and the extraction of the nail. Slight differentiations between the records of the right and left LVDT's were observed especially when there were lateral clearances between the post and beam, which indicates torsional movements of the post. In order to verify this, the out of plane final positioning of the post at the end of the tests, was measured with a digital caliper in several places and registered, showing that torsion was indeed present (Table 3.3), even though it was moderate.

Table 3.3 – Final out-of-plane displacement measured at the end of the test in the deformed shape of the connection.

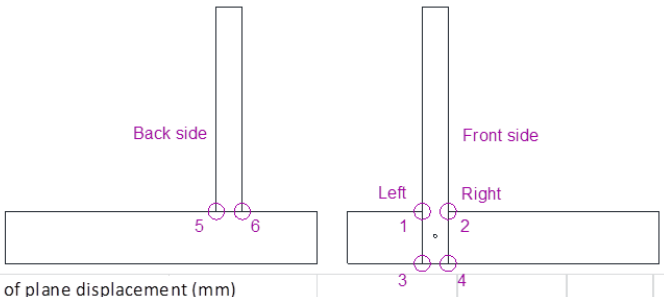

Final out of plane displacement (mm)

Position	1	2	3	4	5	6
Pull-out 1	19,03	19,24	-	23,16	18,08	17,55
Pull-out 2	31,13	-	-	-	30,77	31,21
Pull-out 3	34,24	32,21	39,76	39,32	-	32,35
Pull-out 4	43,42	44,1	42,07	42,9	45,15	43,12

Analysis of the Dissipated energy and stiffness

The area of each hysteresis loop which is formed at the force-displacement diagrams for each displacement step corresponds to the energy (E_{dis}) which is dissipated in the form of deformation due to the plastic behavior of the material [1]. These values are added step by step, for the first cycles, providing the accumulative dissipated energy for every test which was performed (Figure 3.9).

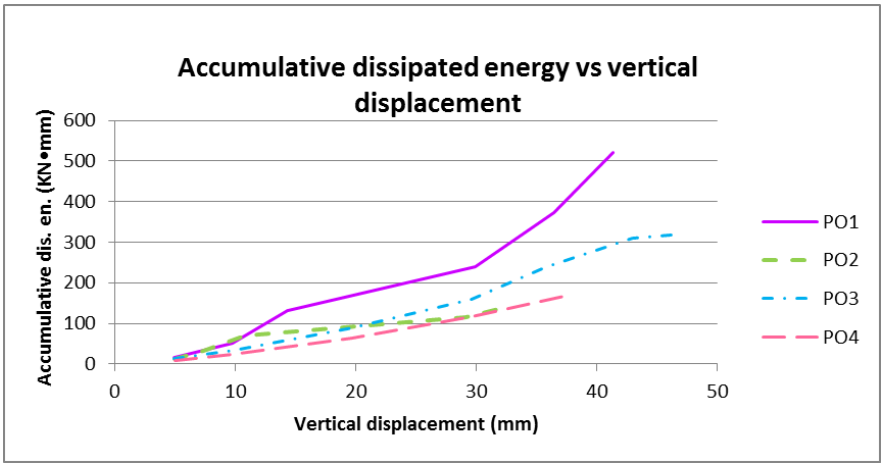

Figure 3.9 – Accumulative energy dissipated for increasing vertical displacements obtained for all the specimens.

For the steps that were concluded after three cycles, higher values of the dissipated energy are observed at the first cycle, lower at the second and even lower at the third, while the maximum force that is reached also decreases and its corresponding displacement value increases. This could be explained by the fact that the first time a certain displacement is exceeded in a new step the specimen resists more, while the second and third time this resistance lowers significantly, leaving the second and third cycles looking quite similar (Figure 3.10). More information on this trend is provided in Appendix A. Notice also that after the first cycle corresponding to a certain imposed lateral displacement the pinching effect in the reloading branch considerably increases, resulting in the decrease of the dissipated energy.

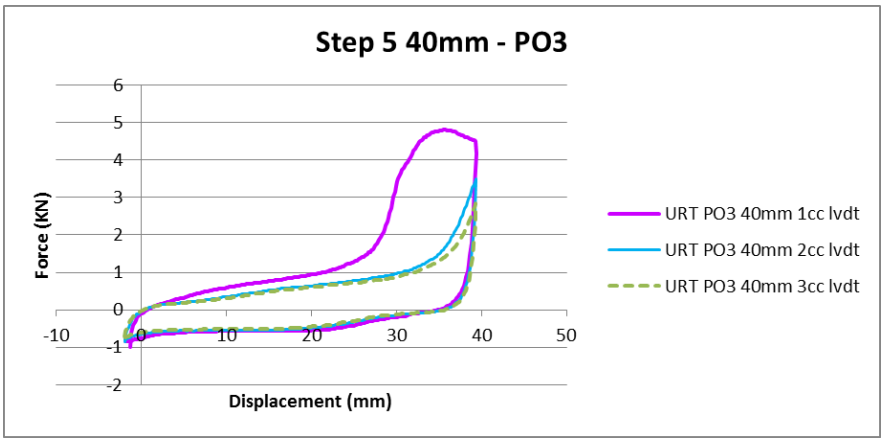

Figure 3.10 – The 3 cycles of step 5 (40mm) for specimen PO3.

Apart from the dissipated energy, the input energy E_{in}, which is a measure of the energy imposed to the specimens, can be obtained for each cycle of every step by the formula [36]:

$$E_{in} = \frac{\max F_{cc} \cdot v_{Fmax_{cc}}}{2} \qquad (3.4)$$

where *maxFcc* is the maximum force attained and v_{Fmaxcc} is the corresponding displacement. Additionally, the results can be evaluated in terms of the equivalent viscous damping ξ_{eq}, which is also a measure of the dissipated energy during the hysteretic behavior in relation to the energy given to the system. This parameter is calculated according to the following expression [36]:

$$\xi_{eq} = \frac{E_{dis}}{2\pi \cdot E_{in}} \qquad (3.5)$$

In Figure 3.11, it is noticed that the equivalent viscous damping is gradually decreasing, due to the high pinching, particularly in the last steps (Figure 3.10).

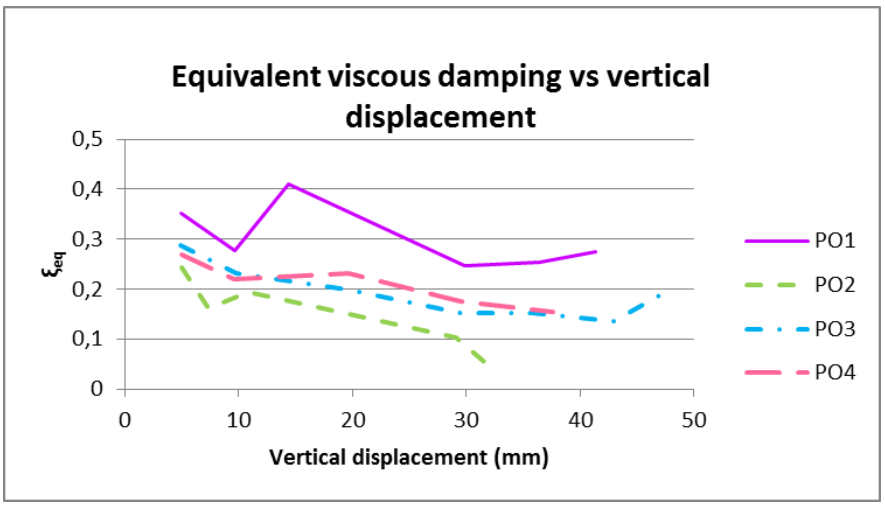

Figure 3.11 – Combination of the equivalent viscous damping graphs for all the pull-out tests.

For the characterization of the cyclic behavior of the overlapped connections to pull-out tests, the cyclic stiffness degradation is also a parameter to take into consideration. The degradation of stiffness is essentially associated to the progress of damage. The cyclic stiffness, K_{cc}, is calculated according to the equation 3.6:

$$K_{cc} = \frac{\max F_{cc}}{v_{Fmax_{cc}}} \qquad (3.6)$$

The initial stiffness for the first envelope curve of the cyclically performed pull-out test is calculated according to equation 3.7 [35]:

$$K = \frac{0{,}3 \cdot F_{max}}{v_{40\%F_{max}} - v_{10\%F_{max}}} \qquad (3.7)$$

where $v_{40\%F_{max}}$ and $v_{10\%F_{max}}$ are the displacement values obtained at 40% and 10% of the maximum force respectively for the corresponding envelope curve

The values of the initial stiffness are presented in Table 3.4 and the cyclic stiffness corresponding to the a given value of the vertical displacement is presented in Figure 3.12.

Table 3.4 – Calculated initial stiffness for the first envelope curve of each test.

	Fmax	v40%Fmax	v10%Fmax	K
Pull-out 1	4,63	0,478	0	2,906
Pull-out 2	2,79	0,814	0	1,028
Pull-out 3	5,07	0,34	0,017	4,709
Pull-out 4	3,22	0,202	0,004	4,879

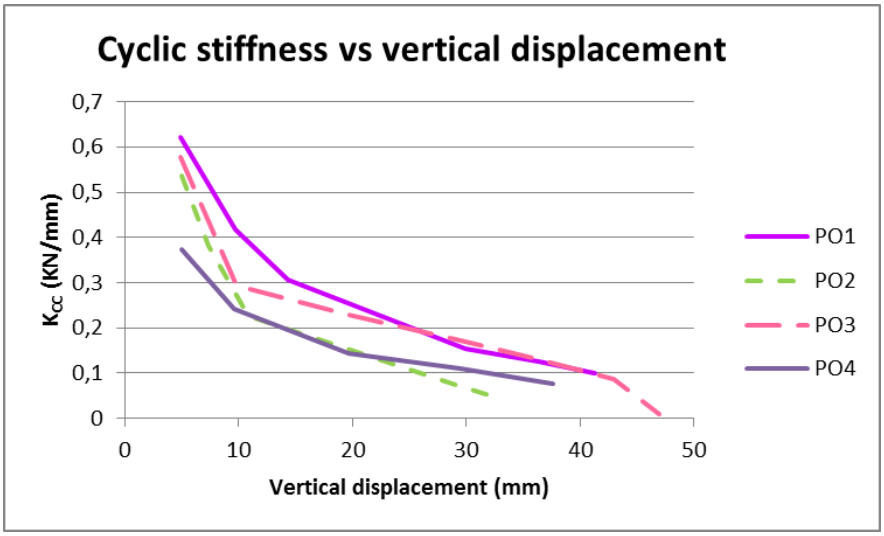

Figure 3.12 – Combination of the cyclic stiffness graphs for all the pull-out tests.

It is observed that the cyclic stiffness is higher in case of the specimen PO1, in spite of the previous monotonic test and it remains higher after the cyclic test. In all cases, the degradation follows approximately the same trend (exponential) for the decreasing stiffness for increasing vertical displacements. It is also seen that the specimens PO1 and PO3 can be grouped as the samples with higher cyclic stiffness, contrarily to the specimens PO2 and PO4 that presented the lowest values of the cyclic stiffness.

3.5.5 Estimation of the load-carrying capacity for the nail

Taking into account the behavior of the overlapped connections in relation to the low value of resistance and the possible influence of the friction at the post-beam interfaces, it was decided to investigate the role of the nail in the resistance. Therefore, it was decided to evaluate the resistance of the connection considering it as a mechanical connection fastened with a nail. As already mentioned,

a single steel nail with a square section of 4mm thickness and 10mm length is the mechanical fastener that keeps the overlapping connection fixed in place. The nail was positioned without pre-drilling.

The maritime pine wood, which was used to manufacture the specimens, is considered to have a density of ρ= 600kg/m^3. The calculations were implemented regarding the section 8.3.1.2 section of Eurocode 5 about nailed timber-to-timber connections, when the nails are laterally loaded [33].

The slip modulus *Kser* per shear plane per fastener under service load for nails without pre-drilling is given by equation 3.8 (Table 7.1- [33]):

$$K_{ser} = \frac{\rho_m{}^{1.5} \cdot d^{0.8}}{30} = \frac{600^{1.5} \cdot 4^{0.8}}{30} = 1485.09\ N/mm \qquad (3.8)$$

where ρ_m=600kg/m^3 is the mean density of maritime pine wood and *d*=4mm is the diameter of the nail.

For fasteners in single shear and timber-to-timber connections the characteristic load-carrying capacity for the nail is defined as the minimum value from the following expressions [33], which are associated to distinct failure patterns (Figure 3.13):

$$F_{v,Rk} = \min \begin{cases} f_{h,1,k} t_1 d & \text{(a)} \\ f_{h,2,k} t_2 d & \text{(b)} \\ \dfrac{f_{h,1,k} t_1 d}{1+\beta}\left[\sqrt{\beta + 2\beta^2\left[1+\dfrac{t_2}{t_1}+\left(\dfrac{t_2}{t_1}\right)^2\right]+\beta^3\left(\dfrac{t_2}{t_1}\right)^2} - \beta\left(1+\dfrac{t_2}{t_1}\right)\right] + \dfrac{F_{ax,Rk}}{4} & \text{(c)} \\ 1{,}05\dfrac{f_{h,1,k} t_1 d}{2+\beta}\left[\sqrt{2\beta(1+\beta)+\dfrac{4\beta(2+\beta)M_{y,Rk}}{f_{h,1,k} d\ t_1^2}} - \beta\right] + \dfrac{F_{ax,Rk}}{4} & \text{(d)} \\ 1{,}05\dfrac{f_{h,1,k} t_2 d}{1+2\beta}\left[\sqrt{2\beta^2(1+\beta)+\dfrac{4\beta(1+2\beta)M_{y,Rk}}{f_{h,1,k} d\ t_2^2}} - \beta\right] + \dfrac{F_{ax,Rk}}{4} & \text{(e)} \\ 1{,}15\sqrt{\dfrac{2\beta}{1+\beta}}\sqrt{2M_{y,Rk} f_{h,1,k} d} + \dfrac{F_{ax,Rk}}{4} & \text{(f)} \end{cases} \qquad (3.9)$$

with

$$\beta = \frac{f_{h,2,k}}{f_{h,1,k}}$$

where:

$F_{v,Rk}$	is the characteristic load-carrying capacity per shear plane per fastener;
t_i	is the timber or board thickness or penetration depth, with i either 1 or 2, see also 8.3 to 8.7 ;
$f_{h,i,k}$	is the characteristic embedment strength in timber member i;
d	is the fastener diameter;
$M_{y,Rk}$	is the characteristic fastener yield moment;
β	is the ratio between the embedment strength of the members;
$F_{ax,Rk}$	is the characteristic axial withdrawal capacity of the fastener, see (2).

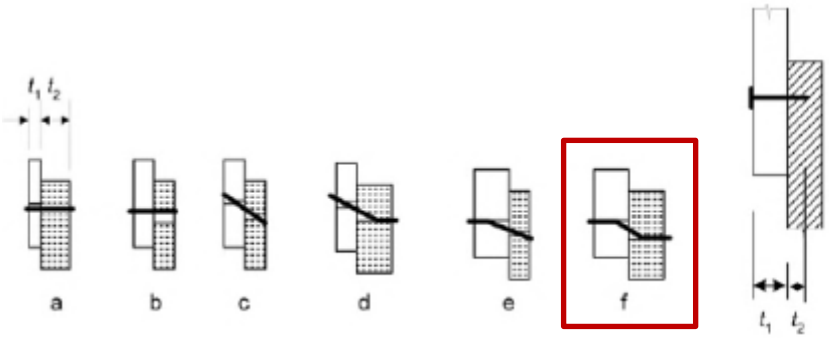

Figure 3.13 – Failure modes for timber connections in single shear and definition of t_1 and t_2 [33].

The characteristic embedment strength in timber member 1 (front-post) and 2 (posterior-beam) is the same as they are made of the same wood (equation 3.9):

$$f_{h1,k} = f_{h2,k} = 0.082 \cdot \rho_k \cdot d^{-0.3} = 0.082 \cdot 600 \cdot 4^{-0.3} = 32.46\ N/mm^2$$ and β=1.

So for failure mode (a):

$$f_{h1,k} \cdot t_1 \cdot d = 32.46 \cdot 60 \cdot 4 = 7790.37N$$

And for failure mode (b):

$$f_{h2,k} \cdot t_2 \cdot d = 32.46 \cdot 40 \cdot 4 = 5193.6N$$

In the rest of the expressions, the first term on the right hand side is the load-carrying capacity according to the Johansen yield theory, whilst the second term $F_{ax,Rk}/4$ is the contribution from the rope effect. The contribution to the load-carrying capacity due to the rope effect should be limited to following percentages of the Johansen part:

− Square nails 25 %

For failure mode (c):

$$\frac{f_{h1,k}\cdot t_1\cdot d}{1+\beta}\cdot\left[\sqrt{\beta+2\beta^2\cdot\left[1+\frac{t_2}{t_1}+\left(\frac{t_2}{t_1}\right)^2\right]+\beta^3\cdot\left(\frac{t_2}{t_1}\right)^2}-\beta\cdot\left(1+\frac{t_2}{t_1}\right)\right]$$
$$=\frac{7790.37}{2}\cdot\left[\sqrt{1+2\cdot\left[1+\frac{4}{6}+\left(\frac{4}{6}\right)^2\right]+1\cdot\left(\frac{4}{6}\right)^2}-1\cdot\left(1+\frac{4}{6}\right)\right]=2780.42N$$

So $F_{v,Rk\,(c)}=2780.42\cdot1.25=3475.52N$

For smooth nails produced from wire with a minimum tensile strength of 600 N/mm², the following characteristic values for yield moment should be used:

$$M_{y,Rk}=\begin{cases}0{,}3\,f_u\,d^{2.6} & \text{for round nails}\\ 0{,}45\,f_u\,d^{2.6} & \text{for square nails}\end{cases}$$

where:

$M_{y,Rk}$ is the characteristic value for the yield moment, in Nmm;

d is the nail diameter as defined in EN 14592, in mm;

f_u is the tensile strength of the wire, in N/mm².

The characteristic value for the yield moment is calculated as:

$M_{y,Rk}=0.45\cdot600\cdot4^{2.6}=9924.75N/mm$

For failure mode (d):

$$1.05\frac{f_{h1,k}\cdot t_1\cdot d}{2+\beta}\cdot\left[\sqrt{2\beta\cdot(1+\beta)+\frac{4\beta\cdot(2+\beta)\cdot M_{y,Rk}}{f_{h1,k}\cdot {t_1}^2\cdot d}}-\beta\right]$$
$$=1.05\frac{7790.37}{3}\cdot\left[\sqrt{2\cdot(2)+\frac{4\cdot(3)\cdot9924.75}{32.46\cdot60^2\cdot4}}-1\right]=2897.6N$$

So $F_{v,Rk\,(d)}=2897.6\cdot1.25=3622N$

For failure mode (e):

$$1.05\frac{f_{h1,k}\cdot t_2\cdot d}{1+2\beta}\cdot\left[\sqrt{2\beta^2\cdot(1+\beta)+\frac{4\beta\cdot(1+2\beta)\cdot M_{y,Rk}}{f_{h1,k}\cdot {t_2}^2\cdot d}}-\beta\right]$$
$$=1.05\frac{5193.6}{3}\cdot\left[\sqrt{2\cdot(2)+\frac{4\cdot(3)\cdot9924.75}{32.46\cdot40^2\cdot4}}-1\right]=2069.6N$$

So $F_{v,Rk\,(e)}=2069.6\cdot1.25=2587N$

For failure mode (f):

$$1.15\sqrt{\frac{2\beta}{1+\beta}}\cdot\sqrt{2M_{y,Rk}\cdot f_{h1,k}\cdot d}=\ 1.15\sqrt{\frac{2}{2}}\cdot\sqrt{2\cdot 9924.75\ \cdot 32.46\cdot 4}=1846.2N$$

So $F_{v,Rk\ (f)}=1846{,}2\cdot 1.25=2307.7N$

According to the previous calculations the characteristic load-carrying capacity for the nail is the minimum value which was acquired for failure mode f:

$$F_{v,Rk}=2307.7N\ .$$

This value could be to a certain extent, related to the experimental resistance found for specimens PO2 and PO4 taking into account that only the shear resistance of the fastener contributes for the resistance of the connection. In addition, note that the failure mode found in the experimental work is close to the one corresponding to the analytical pull-out resistance. In this case, due to the geometrical clearances (PO2 and PO4), no friction resistance at the interfaces of the post and beam should contribute for the resistance.

3.6 In-plane cyclic tests

In this testing typology, a horizontal in-plane (lateral) displacement is applied at the top part of the post, while the horizontal beam part of the connection is fixed and steady. Additionally, a constant vertical load, which remains aligned with the axis of the post during the test due to boundary conditions, is applied on top of the post, simulating the existing permanent loads above the reference post. There are no boundary conditions preventing the out of plane displacement of the post at the joint.

In-plane lateral tests provide significant knowledge concerning the seismic behavior in any studied case and can be performed:

- Monotonically: In this case the test is completed after the post reaches the maximum displacement towards one direction according to the predefined procedure. This type of tests aim at obtaining the non-linear behavior for this type of loading case.
- Cyclically: The test is completed after several steps of displacements are reached, with a certain number of cycles for each of them. The objective of this type of tests is to provide a better realization of the seismic behavior. This is accomplished by the comprehension of damage accumulation as well as the degradation of stiffness and the energy dissipation.

3.6.1 Test setup

The specimens were placed upon a stiff and level stabilized surface steel profile, which was fastened at the reaction floor of the laboratory. Additionally, in order to prevent any unwanted movement of the beam two fixing plates were positioned on top of the beam on each side of the post and four rods were

used to fix them with the previously mentioned steel profile (Figure 3.14a). In order to allow the lateral movement at the intersecting points between the post and the beam, the plates were positioned a few centimeters (~6cm) away from the post, leaving enough space for the monitoring instruments to be placed as well.

An actuator was fixed horizontally, to the steel frame, at the level of the top of the post to apply horizontal cyclic displacement to the post. The connection to the steel frame is made through a two-dimensional hinge and at the top of the post also through a hinge. The maximum load capacity of the actuator is 150KN and the maximum plunger course of the internal LVDT is 200mm. A load cell with a maximum measuring load capacity of 200KN was fixed at the end of the actuator. Nevertheless, as maximum load capacity is considered, the minimum of these two values which is 150KN.

Two steel plates and 4 rods with nuts were positioned laterally at the top of the post, (Figure 3.14b) One of these steel plates is connected to the horizontal actuator to impose the lateral displacements.

A second hydraulic jack was used to apply the vertical load upon the post. Since it was new, it was calibrated to lose the air and then tested to realize the conversion between the superimposed load (KN) and the pressure (bars). It was placed right above the post and on its higher part it bore a rectangular steel plate. The reaction system to the vertical load was achieved by connecting the top steel plate to the bottom hinges connected to the bottom steel profile through 4 steel bars. Notice that the bottom steel profile is connected to the reaction slab, thus the vertical reaction is realized by the reaction slab. The top steel plate of the vertical actuator was secured with a chain that passed above the surrounding frame, in order to restrain it for safety reasons.

The weight of the horizontally positioned actuator was withheld from underneath with an air-pressured device.

After the mounting of the specimens and the application of the vertical load, the horizontal actuator was put in use and the test was performed and monitored through a computer.

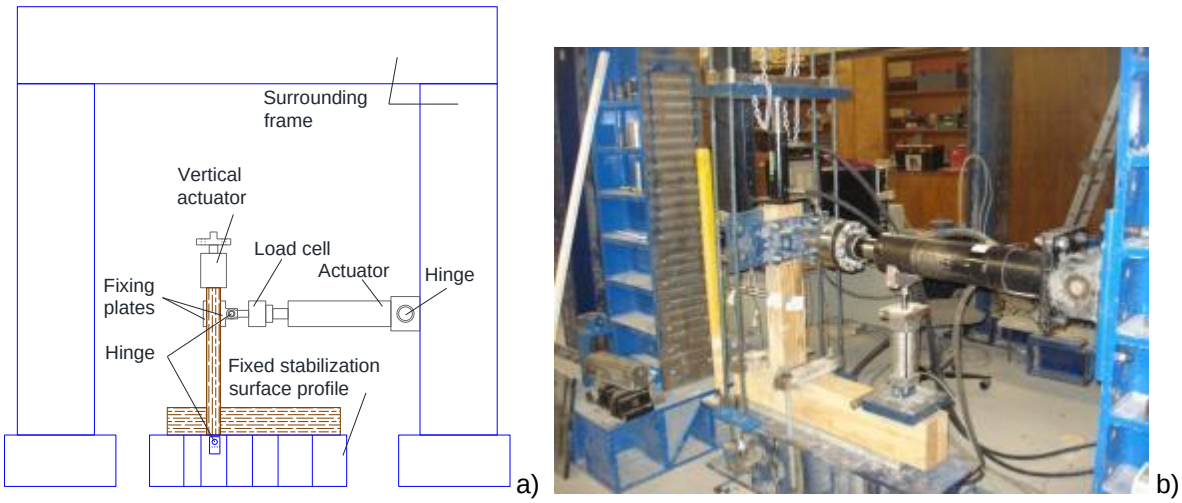

Figure 3.14 – Test setup for in-plane cyclic tests; a) configuration and b) a photograph of the setup

3.6.2 Instrumentation

Apart from the horizontal actuator, through which the horizontal displacement history is applied to the top of the post and monitors the force and displacement during the test, a computer is used to record the data. Additionally, several displacement measuring devices are placed in certain positions in order to measure the deformation of the connection and control some displacements aiming at ensuring the validity of the test setup.

A total number of 4 to 6 linear variable differential transformers (LVDT) were used to measure and monitor the displacements in certain points of the specimens (Figure 3.15).

- Two LVDTs were used to measure the horizontal displacements of the post and they were positioned at different heights. One was placed at the same height as the horizontal actuator thus it served as the control LVDT. The displacements measured by this LVDT should be similar to the ones measured by the internal LVDT of the actuator for the applied displacement and they have to be compared. Another LVDT was put at the mid-height of the post. After observations during some tests, a third one was decided to be placed at the lower part of the post, at the intersection of the post with the beam.
- One to two LVDTs were used to measure the possible uplifting displacements, due to the rotation, of the bottom part of the post at the back side.
- One LVT was used to measure for the out-of-plane displacement of the post.

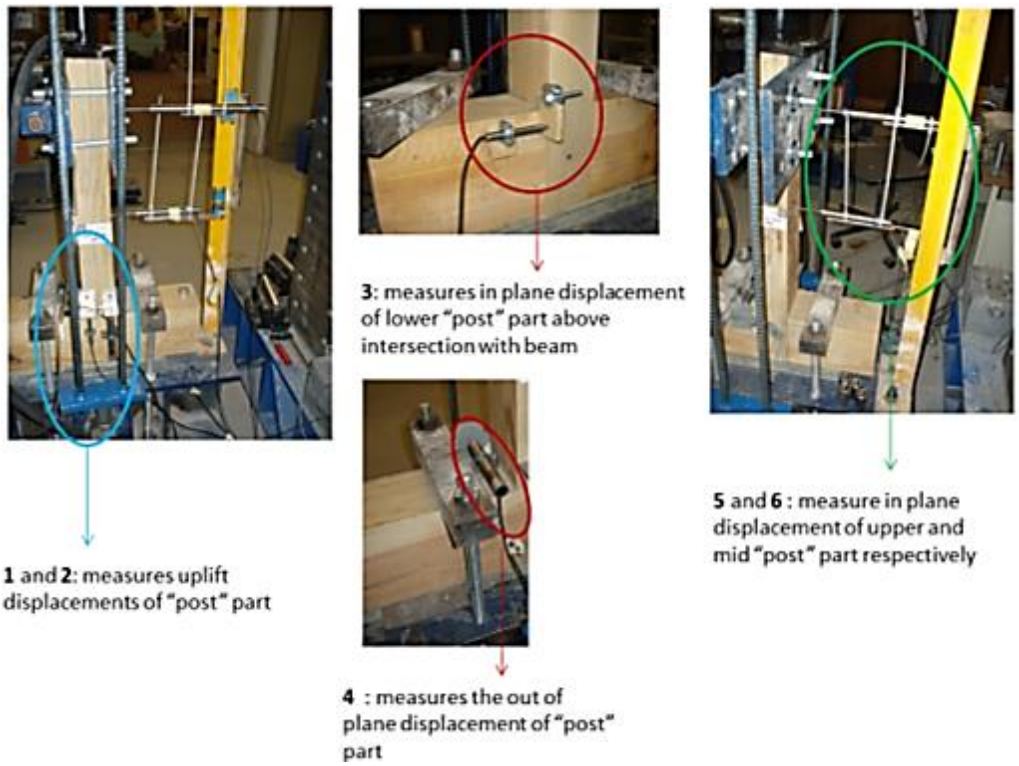

Figure 3.15 – Positions of LVDTs for the in-plane cyclic tests.

3.6.3 Test procedure

For the in-plane cyclic tests two distinct values of vertical load were considered, namely:

- **Vertical load of 25KN:** In this case, the connection is located on the first floor of a traditional Pombalino building, which has 3 more storeys above it. The value was calculated, taking into consideration the self weighs of the upper timber floors, inner half-timbered walls and live load [4].
- **Vertical load of 50KN:** The additional loads that should be considered in case of rehabilitation works, due to the use of heavier materials (steel, cement etc.) and the change in the use of the building, were taken into account by multiplying the previous value with a safety factor equal to two [4].

Initially, for the in-plane cyclic tests, a procedure was adapted to the studied connection based on cyclic tests that were performed on real scale timber-framed walls [4]. In the case of the connection, an ultimate horizontal displacement d_u of 43.5mm was adopted which was the interpolated value, based on the maximum real displacement imposed to the walls [4]. This procedure was applied on two specimens (C1_25 and C2_50) and it was concluded after 15 steps with a final maximum displacement reaching 52,2mm ($1.2d_u$).

In total 10 specimens were tested under lateral cyclic loading. Two specimens were tested under monotonic lateral load, for each vertical load in order to obtain the typical non-linear behavior for this type of testing. The results were evaluated according to the European standard for cycling testing of timber joints made with mechanical fasteners and a new procedure was decided, taking into consideration the yield value instead of the ultimate one. For both monotonic tests the yield value was estimated by assuming a load-slip curve with two well-defined linear parts and the value was found to be V_y=19.9mm [37].

The rest of the 6 specimens were tested according to the new procedure, which was concluded in 10 steps with distinct percentages of the yield value, Vy=19.9mm. In seven of these steps there was a repetition of 3 cycles (Table 3.5).

Table 3.5 – In-plane cyclic test procedure according to EN12512 [37].

d_u	19,9	mm							
speed 1	0,1	mm/s							
speed 2	0,2	mm/s							
speed 3	0,3	mm/s							
step	nº of cycles	displacement		total course per cycle	time per cycle	time per step			
		%	mm	[mm]	[s]	[s]	[min]	[h]	
1	1	25	4,98	19,9	199	199,00	3,32	0,06	3,32
2	1	50	9,95	39,8	398	398,00	6,63	0,11	9,95
3	1	75	14,93	59,7	597	597,00	9,95	0,17	19,90
4	3	100	19,90	79,6	265,3	796,00	13,27	0,22	33,17
5	3	125	24,88	99,5	331,7	995,00	16,58	0,28	49,75
6	3	150	29,85	119,4	398,0	1194,00	19,90	0,33	69,65
7	3	175	34,83	139,3	464,3	1393,00	23,22	0,39	92,87
8	3	200	39,80	159,2	530,7	1592,00	26,53	0,44	119,40
9	3	225	44,78	179,1	597,0	1791,00	29,85	0,50	149,25
10	3	275	54,73	218,9	729,7	2189,00	36,48	0,61	185,73

3.6.4 Analysis of results

Evaluation of the damage patterns

Considering the continuous part of the overlapped connection, vertical cracks develop parallel to the grain, firstly around the area of the nail. When the top of the post suffered a horizontal displacement towards the left, an area located in the right side of the joint was not working in compression, so the post would split and slide (Figure 3.16a). As expected this type of damage occurred in both sides. Those cracks would propagate upwards mainly vertically while their depth was unknown. It should be noticed that these cracks should be associated to shear stresses developed in the connection resulting from the imposed lateral displacements at the top.

As the test evolved, snapping cracks perpendicular to the grain happened in a brittle manner laterally of the post near the intersecting point with the beam. This type of damage appeared in most cases on both sides and manifested in two different ways:

i. either as an almost horizontal, linear crack perpendicular to the grain,
ii. or in the form of an arch that would appear on one side (lateral side of the post – Figure 3.16b) or in the corner of two sides (lateral and front side of the post - Figure 3.16c).


a)


b)


c)


d)


e)

f)

Figure 3.16 – a) Vertical, sliding cracks parallel to the grain, b) Perpendicular to the grain, snapping crack forming arch , c) Perpendicular to the grain, snapping crack forming arch at the corner, d) Detached “tenon” of post, e) Imprint of post at the beam.

In most cases the depth of this type of damage was unknown, whereas in others those cracks would propagate and join. There was a specimen where the “tenon” of the post got completely detached (Figure 3.16d). In the end, as the specimens were dismantled, it was observed that the bottom part of the post “tenon” was crashed, since the parallel, vertical cracks were joined in depth at this point (Figure 3.16e).

It should be noted that when the applied vertical load was higher (50KN) damages developed in a faster rate, while in most cases, after one side failed with laterally, perpendicular snapping cracks the other continued to perform well until it failed similarly, usually after a few steps.

Apart from the imprint of the post that was left on the top side of the beam which was underneath the post, no other damage was observed at the beam (Figure 3.16f).

Analysis of the Force – Displacement diagrams

As the test was in progress, it was observed that there was a side for which the test performed a little better, which could lead to the assumption that the physical properties of the material and preexisting natural defects, as knots or cracks, hold a key role to its mechanical behavior.

Relatively higher load values were observed in the case of the implemented higher vertical load (50KN), while damages in this case appeared faster, leaving one side almost inactive in a few cases.

During the application of the second procedure in the last 6 specimens (3 for each vertical load) better softening was achieved as the displacement steps were larger. By observing the cyclic force-displacement diagrams for both vertical load levels (25kN and 50kN), apart from the lateral resistance, it can be seen that no major differences are detected in the shape of the hysteresis loops. However, it should be noticed that in case of the higher vertical load level applied in the post, the unloading branches are not completely symmetrical when positive and negative directions are compared. This can be associated to the asymmetry on the damage distribution. Further information on all the force-displacement diagrams is given in Appendix A.

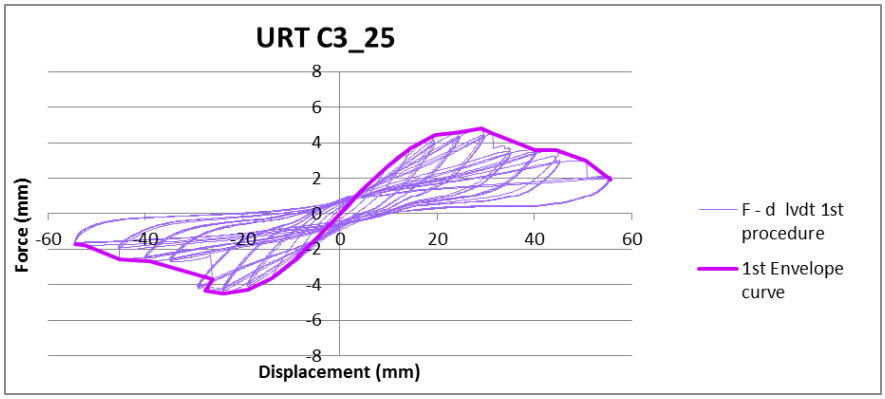

a)

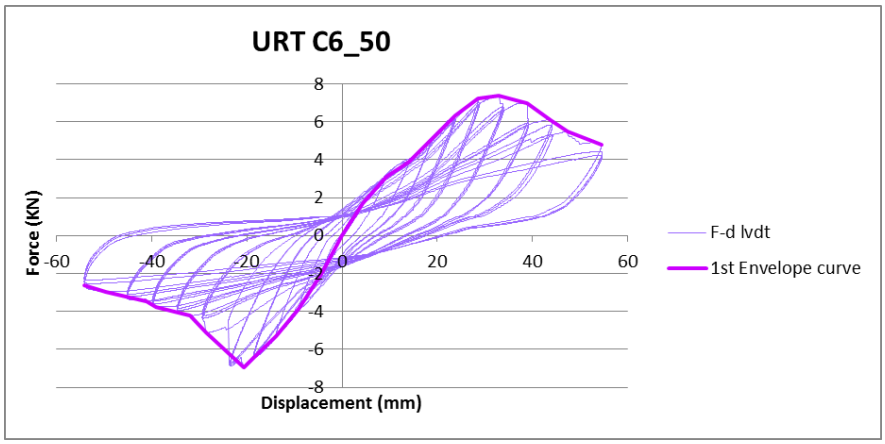

b)

Figure 3.17 – Typical in-plane cyclic force-displacement diagrams for: a) a vertical load of 25KN and b) a vertical load of 50KN.

In both cases, it is observed that good dissipation of energy is achieved. Besides, particularly in the case with a vertical load of 25kN, there is considerable stiffness degradation (Figure 3.18), which is accompanied also by a decrease on the lateral resistance, resulting in a soft post-peak regime.

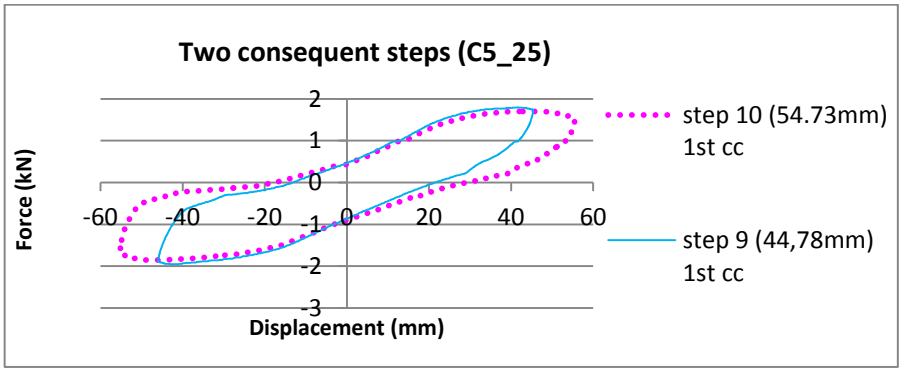

Figure 3.18 – The hysteresis loop shapes of two consecutive steps (C5_25).

The results of the monotonic tests carried out previously and the monotonic envelops calculated from the cyclic tests are shown in Figure 3.19 for both vertical load levels. It is observed that the monotonic tests exhibit a more pronounced softening branch due to the higher imposed displacements. By comparing the envelope curves for all the specimens, corresponding to each vertical load and the respective monotonic tests it is visible that the force values of the monotonic tests are comparable to the ones from the envelope curves for each case of applied vertical load.

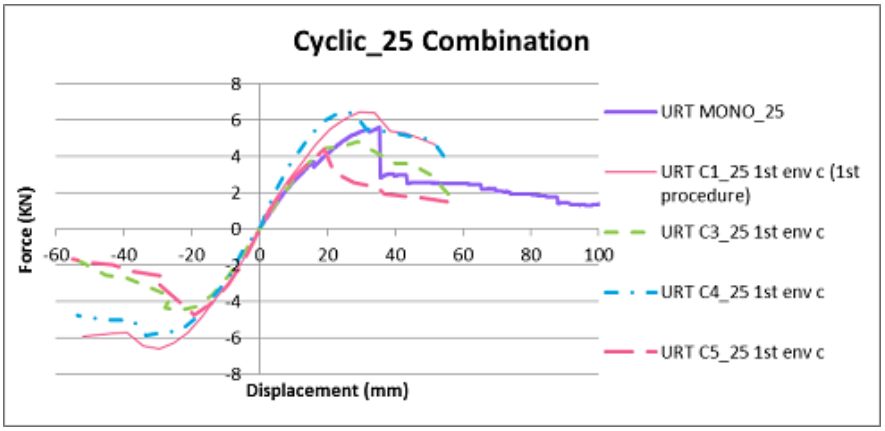

a)

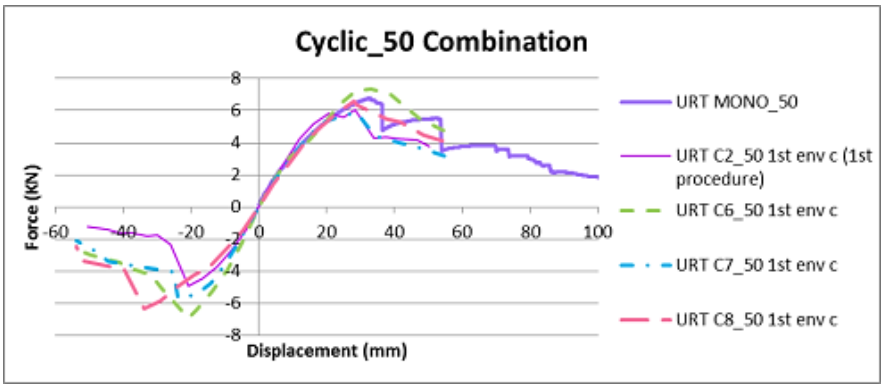

b)

Figure 3.19 – Combination of F-d monotonic and envelope curve graphs for all the cyclic tests with: a) a vertical load of 25KN and b) a vertical load of 50KN.

Analysis of the out-of-plane displacements

As the lateral imposed displacement increased, the out-of-plane displacement would increase as it is possible to notice in the representative diagrams obtained for each vertical load (Figure 3.20a-b).

The final out-of-plane displacement values varied between 1 to 2cm in the case where a lower vertical load was applied (25KN), whereas when the vertical load was higher (50KN) greater differentiations were observed (0.2 to 1,5cm) leading to the assumption that vertical load influences the out-of-plane displacement. This result is associated to further restrain provided by the higher vertical load to the lateral opening of the connection.

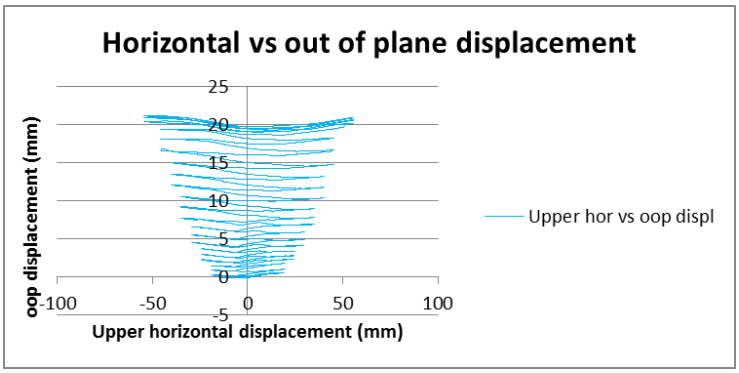

a)

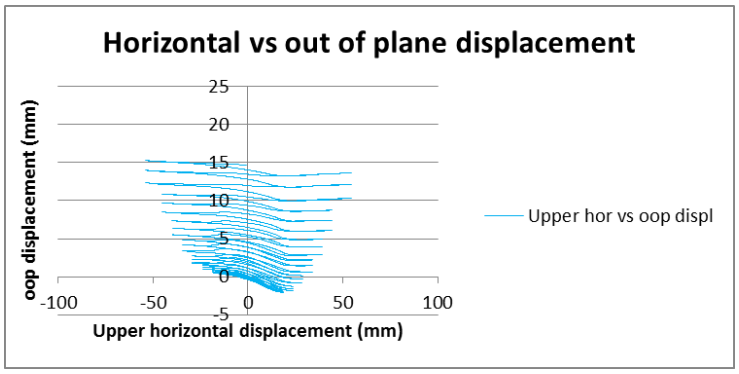

b)

Figure 3.20 – Representative horizontal-oop displacement diagrams for two cyclic tests with: a) a vertical load of 25KN (URT C3_25) and b) a vertical load of 50KN (URT C6_50). (Oop: out of plane).

Analysis of the Vertical displacement

The vertical displacement of the post was measured at the back side of the specimens, where the discontinuity between post and beam exists. Values were registered on the left and right side of the post. As expected, the post was moving simultaneously upwards on one side and downwards on the other, as it rotated towards the left or right. Note that the overlapped connection is not rigid and rotation can occur by imposing lateral displacements to the post. This is illustrated in the diagrams of Figure 3.21.

It should also be mentioned that, although no greater differences were recorded, there is a trend for higher uplift in the case of vertical load of 25kN. It should be noticed that important negative

displacements are also present, which should be the reason for the deformation observed in the horizontal interface between the beam and the post.

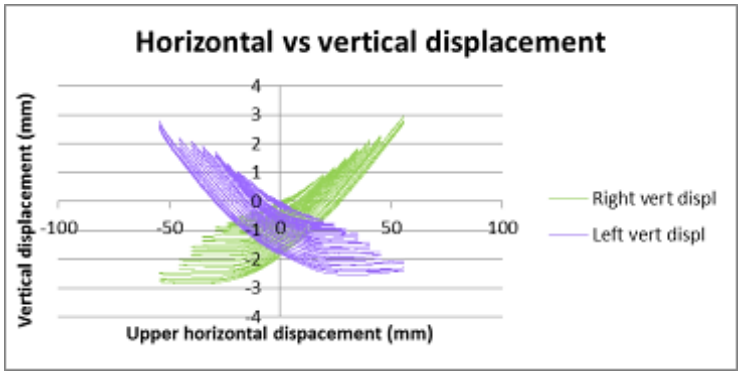

a)

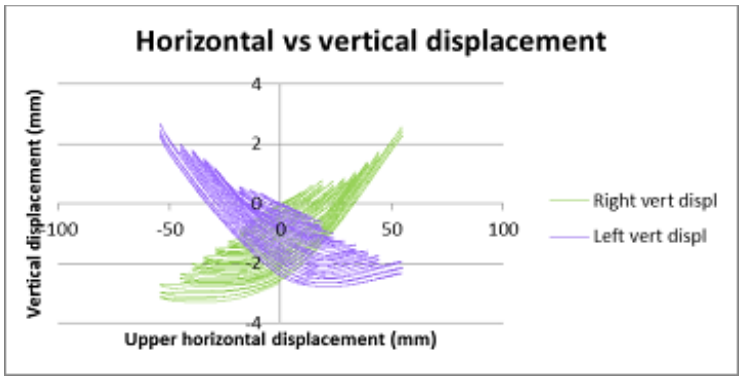

b)

Figure 3.21 – Representative horizontal-vertical displacement diagrams for two cyclic tests with: a) a vertical load of 25KN (URT C3_25) and b) a vertical load of 50KN (URT C6_50).

Analysis of the Horizontal displacement in different positions

The horizontal displacement was recorded in 3 positions as it was previously mentioned (See 3.6.2). Although a proportional displacement could be expected among the upper and the middle horizontal displacements, this was not exactly verified when the results were analyzed. Slight differentiations were recorded at the same step between those values on each side due to the permanent deformations that occurred throughout the test. In the following representative configurations two of the displacement steps (Step 4: 19.90mm and Step 10: 54.73) with their final displacement values are shown for each vertical load case (Figure 3.22a-b).

The horizontal displacement values corresponding to the intersecting part of the post and beam are slightly higher than zero as expected.

Figure 3.22 – Representative horizontal displacement configurations for two cyclic tests with: a) a vertical load of 25KN (URT C3_25) and b) a vertical load of 50KN (URT C8_50).

Analysis of the Dissipated energy and stiffness

The dissipated energy of all the hysteresis loops was calculated according to the methodology presented previously. The dissipated energy corresponding to the first cycles were taken into consideration to design the diagrams between the accumulative dissipated energy and the drift percentage.

The drift for every displacement step is the mean value of the corresponding displacements to the maximum and minimum forces of the cycle, divided by the height of application of the horizontal displacement which is 500mm. This process accommodates dimensional differences and makes the results among variant specimens comparable.

High values of the accumulative energy indicate that in a real loading case, as a seismic event, the joint can resist and withstand greater deformations (Figure 3.23a-b). In the case of higher vertical load more energy was dissipated, which should be associated to the higher damage of the connection, resulting in wider hysteresis loops of the force-displacement diagrams.

In both vertical load levels, the shape of the accumulative dissipated energy is exponential, while it should be also noticed that reduced scatter is found among the diagrams.

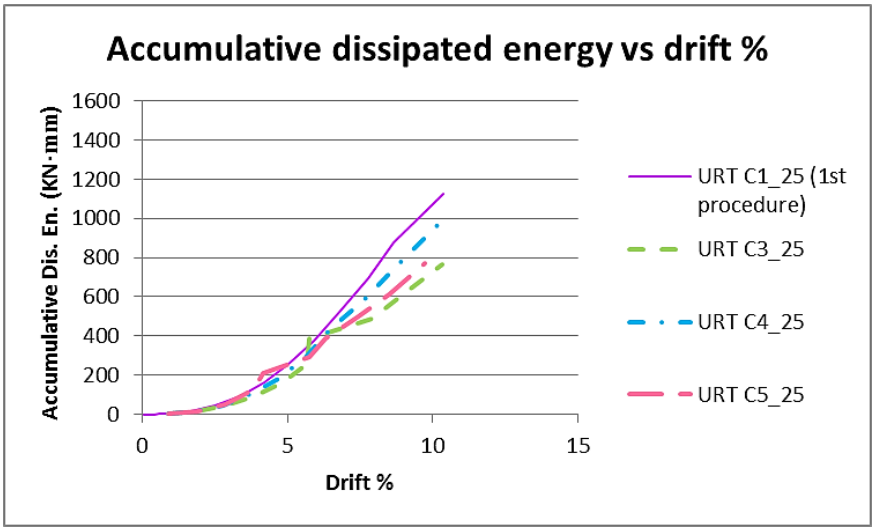

a)

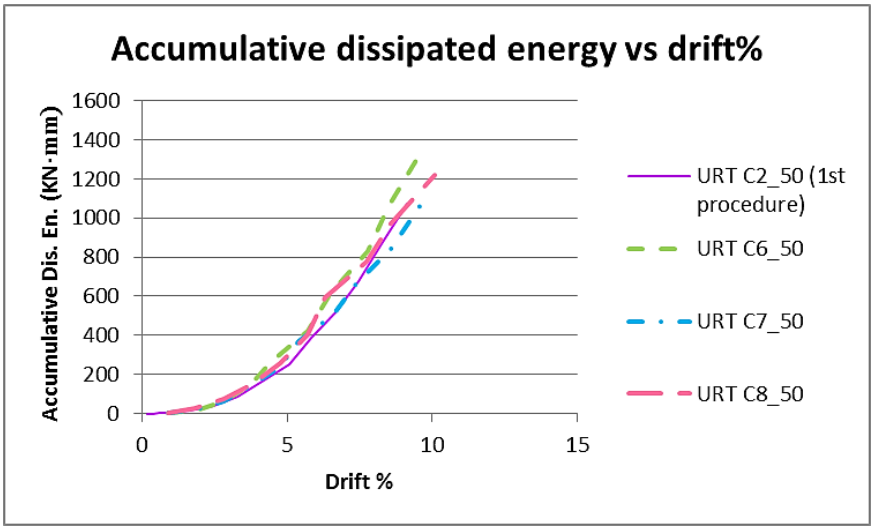

b)

Figure 3.23 – Combination of the accumulative dissipated energy – drift% graphs for all the in plane cyclic tests with: a) a vertical load of 25KN and b) a vertical load of 50KN.

Additionally, as there is a degradation of the dissipated energy among cycles, the accumulative dissipated energy also appears to have higher values at the first cycle, while the second and third are quite similar. This is observed at the representative graph in Figure 3.24.

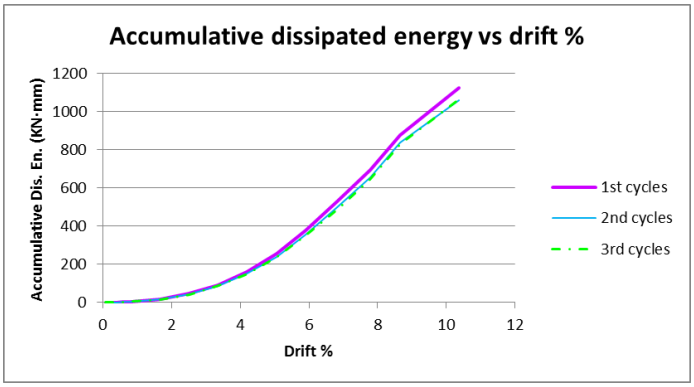

Figure 3.24 – The accumulative dissipated energy of all 3 cycles for C1_25.

The input energy E_{in}, was also calculated with the formula (3.4) and the results were evaluated in terms of the equivalent viscous damping ξ_{eq}, which is gradually increasing as does the ratio between dissipated and input energy [35]:

$$\xi_{eq} = \frac{E_{dis}}{2\pi \cdot (E_{in}^{+} + E_{in}^{-})} \qquad (3.10)$$

The equivalent viscous damping exhibits a trend for increasing as the lateral drift increases, being slightly higher in case of the vertical load of 50kN, (Figure 3.25).

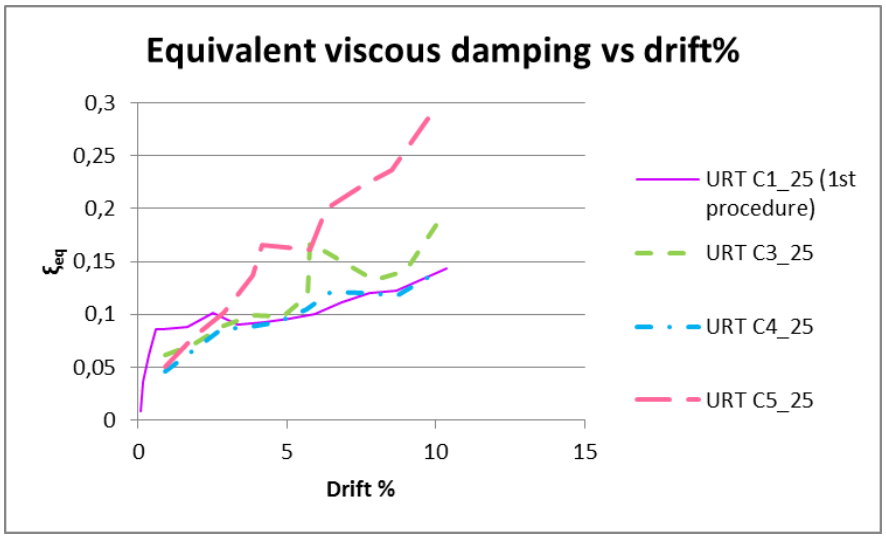

a)

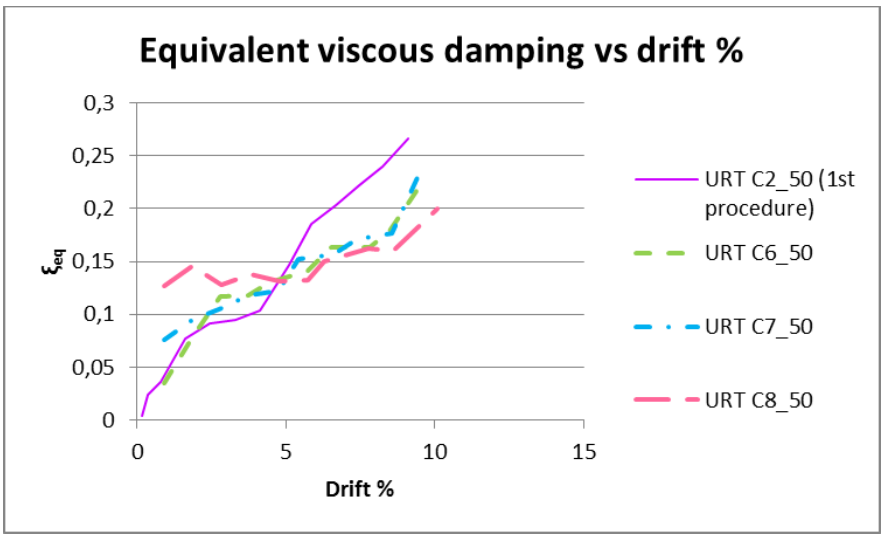

b)

Figure 3.25 – Combination of the equivalent viscous damping- drift % graphs for all the in plane cyclic tests with: a) a vertical load of 25KN and b) a vertical load of 50KN.

The degradation of stiffness, calculated according to what was done for the pull-out tests for the first cycle of every step. is shown in Figure 3.26. It is observed that in both vertical load levels there is very important stiffness degradation for increasing lateral drifts. The decreasing of stiffness is associated to the progress of damage observed in the connections.

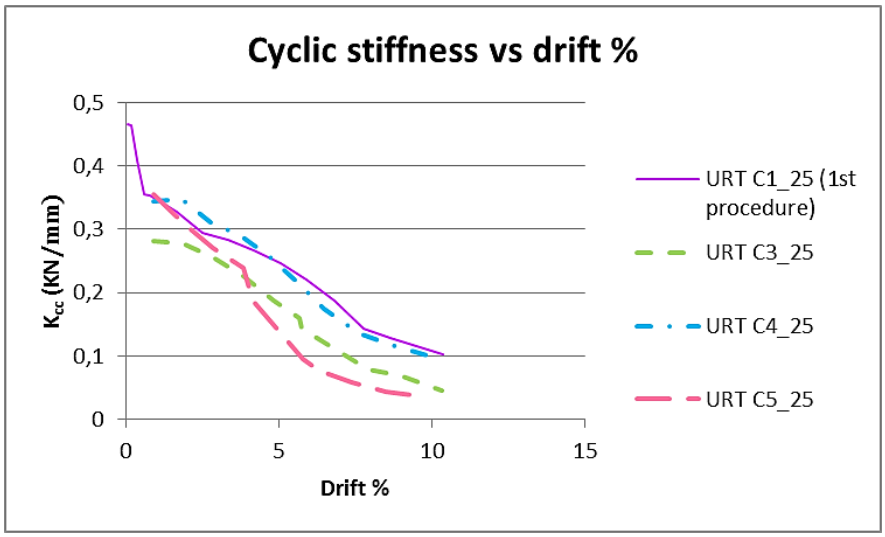

a)

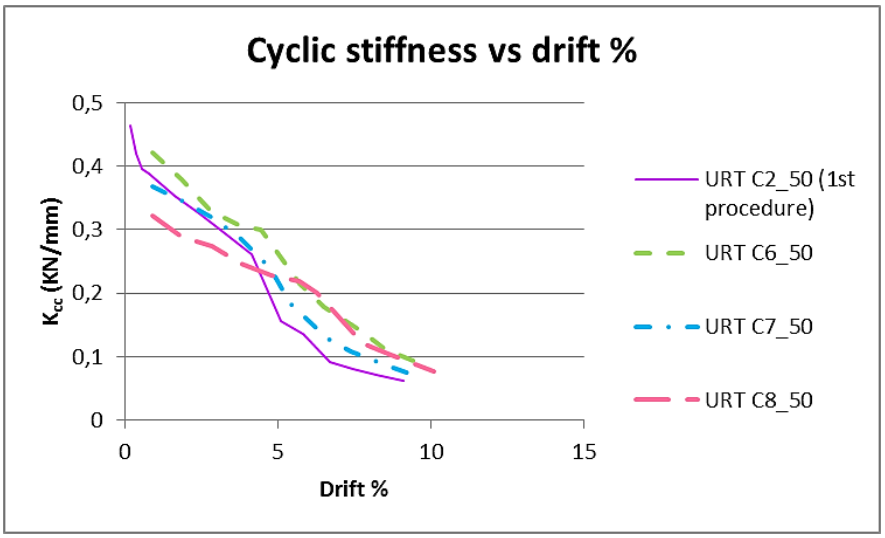

b)

Figure 3.26 – Combination of the cyclic stiffness - drift % graphs for all the in plane cyclic tests with: a) a vertical load of 25KN and b) a vertical load of 50KN.

Finally, the initial stiffness for the first envelope curve of all the in-plane cyclic tests was calculated by the formula (3.7) and it is presented in the following tables (Table 3.6-3.7). In the case with a higher vertical load, greater initial stiffness should be expected, although the final mean values between the two tables appear to not present major differences, which is probably due to the asymmetry that existed in the left and right side of the F-d graphs for the vertical load of 50KN (See Figure 3.17b).

Table 3.6 – Calculated initial stiffness for the first envelope curve of each test with a vertical load of 25KN.

Specimen	Fmax	v40%Fmax	v10%Fmax	K (kN/mm)	mean K (kN/mm)
C1_25 (+)	6,46	7,965	1,395	0,295	0,313
C1_25 (-)	6,61	7,475	1,485	0,331	
C3_25 (+)	4,81	6,635	1,12	0,262	0,274
C3_25 (-)	4,5	6,14	1,418	0,286	
C4_25 (+)	6,42	5,525	1,185	0,444	0,364
C4_25 (-)	5,84	7,385	1,225	0,284	
C5_25 (+)	4,42	5,235	1,01	0,314	0,353
C5_25 (-)	4,73	4,35	0,735	0,393	

Table 3.7 – Calculated initial stiffness for the first envelope curve of each test with a vertical load of 50KN.

Specimen	Fmax	v40%Fmax	v10%Fmax	K (kN/mm)	mean K (kN/mm)
C2_50 (+)	6,08	6,345	1,215	0,356	0,361
C2_50 (-)	4,95	5,3	1,245	0,366	
C6_50 (+)	7,38	8,51	1,46	0,314	0,395
C6_50 (-)	6,95	6,161	1,78	0,476	
C7_50 (+)	5,87	6,2	1,37	0,365	0,353
C7_50 (-)	5,68	5,685	0,695	0,341	
C8_50 (+)	6,59	8,67	1,3	0,268	0,246
C8_50 (-)	6,32	9,05	0,605	0,225	

References

[1] Penelis G.G., Kappos A.I., Earthquake resistant constructions from concrete (in Greek), ZITIS Publising, Thessaloniki 1999

[4] Poletti E,, Vasconcelos G,, Oliveira D.V., Influence of infill on the cyclic behaviour of traditional half-timbered walls. In: Proceedings of International Conference on Rehabilitation and Restoration of Structures, Chennai, India, 2013.

[22] Branco J., Influence of the joints stiffness in the monotonic and cyclic behavior of traditional timber trusses. Assessment of the efficacy of different strengthening techniques, Ph.D. Thesis, Civil Engineering Dept., University of Minho, Portugal 2008

[23] Palma P., Garcia H., Ferreira J., Appleton J., Cruz H., Behaviour and repair of carpentry connections – Rotational behaviour of the rafter and tie beam connection in timber roof structures, Journal of Cultural Heritage 13S (2012) S64–S73

[24] Parisi M.A., Cordie C., Mechanical behavior of double-step timber joints, Construction and Building Materials: Volume 24, Issue 8, August 2010, Pages 1364–1371

[25] Koch H., Eisenhut L., Seim W., Multi-mode failure of form-fitting timber connections - Experimental and numerical studies on the tapered tenon joint, Engineering Structures 48 (2013) 727–738

[26] Feio A., Lourenco P., Machado J., Testing and modeling of a traditional timber mortise and tenon joint, Materials and Structures: DOI 10.1617/s11527-013-0056-y, 2013

[27] Shanks J.D., Walker P., Experimental performance of mortise and tenon connections in green oak, The Structural Engineer – 6 September 2005, p.40-45

[30] International Organization for Standardization – International Standard ISO 3131: Wood - Determination of density for physical and mechanical tests, Switzerland 1975

[31] International Organization for Standardization – International Standard ISO 3130: Wood - Determination of moisture content for physical and mechanical tests, Switzerland 1975

[32] Brites R., MSc SAHC Lecture, SA4 Inspection and Diagnosis: Non-destructive evaluation of timber structures, UNIPD, Padova, Italy, 2012-2013.

[33] European Committee for Standardization – European Standard EN 1995-1-1:2004, Eurocode 5: Design of timber structures - Part 1-1: General - Common rules and rules for buildings, Brussels, Belgium 2004

[34] Drdácký M., Panizza M., MSc SAHC Lecture, SA4 Inspection and Diagnosis: Laboratory and in situ testing, UNIPD, Padova, Italy, 2012-2013.

[35] International Organization for Standardization – International Standard ISO/DIS 21581: Timber structures — Static and cyclic lateral load test method for shear walls, Switzerland 2008

[36] Magenes G., Calvi M., In-plane seismic response of brick masonry walls, Earthquake Engineering and Structural Dynamics, VOL. 26, 1091-1112 (1997)

[37] European Committee for Standardization – European Standard EN 12512: Timber structures - Test methods - Cyclic testing of joints made with mechanical fasteners Brussels, Belgium 2001

Chapter 4

Retrofitting solutions

4.1 Introduction

It is common for historical constructions and cultural heritage buildings the need to preserve, restore, or even to rehabilitate when there is a change in the use. Works of maintenance, repairing or strengthening are usually necessary for existing constructions, particularly, in the case of neglected or abandoned buildings. However, it is essential for the person in charge to keep in mind a few principles before proceeding with the final decisions concerning the solutions that will be applied.

The historical value of the construction along with its importance, hold a key role in the determination of solutions. Inevitably, when the significance rises, more restrictions apply. Additionally, in order to find an appropriate way to accommodate the problems in any case, a restorer should take into consideration according to ICOMOS/ISCARSAH recommendations [38]:

- First of all, a structurally and mechanically correct solution has to be applied;
- Compatible materials with physical and mechanical properties close to the ones of the original are preferable;
- As an addition to the previous, traditional techniques should be the first option and choice, but if they are inadequate, innovative techniques and materials could also be used, as long as their efficacy has been shown by scientific data and proved by experience;
- It is of great importance that the applied technique is reversible and that it holds on to the originality and authenticity of the initial, actual structure as much as possible;
- In case that a new addition is positioned, apart from the previous, it is significant that the new part is combined in a harmonious way with the older; this is meant to follow another influential point which is the aesthetical view;
- Last but not least, the financial matter and the degree of simplicity for the application also have to be kept in mind, but this should not compromise with the rest of the principles. As a matter of fact, a balance among all the previous is not always clear, but the best option between their combinations will be adopted.

4.2 Available strengthening techniques for the connections

After the completion of a series of tests on 14 specimens of a traditional connection, from the half-timbered “Pombalino” walls, it was possible to acquire a better knowledge towards their performance and damage-deformation patterns under certain loading conditions.

According to this, the retrofitting of the overlapped connections should aim to:

- Restriction of the out-of-plane displacement;
- Better fastening, confinement and lateral “interlocking”;
- Increasing of the overall strength and stiffness of the connection, especially the rotational stiffness concerning the in-plane cyclic tests.

Traditionally, steel elements would be used in order to reinforce timber connections but, nowadays, there is a tendency to experiment with innovative materials, as fiber reinforced polymers. Below there is a list with the available strengthening options, which were implemented in previous relevant studies [20],[21],[28],[29],[39].

4.2.1 Nails and screws

As it was previously pointed out, a single iron nail with a length of almost 10cm was used sometimes to connect the notched joints of the timber elements in the half-timbered walls [13]. Although the presence of the infill material provided a certain amount of further stability and stiffness in the structure, it is safe to consider that the existence of a few more steel nails or screws would improve the behavior of the connection, in the case of an earthquake or other imposed displacements (e.g. foundation settlements). The number of extra nails or screws that can be used in any case, as well as the spacing between them, has to be carefully defined [33]. Additionally, the inclination as well as the side (front or upper/lower) of positioning can also be decided, after considering the possibility of access in each occasion (Figure 4.1a).

However, it should be kept in mind that nails work better in shear, perpendicular to their axis, while they cannot take up tension when they are being pulled out. Screws, on the other hand, work very well in the latter type of tension (withdrawal). In general, a connection with nails performs better when the nails are smaller and more, than larger and few [40].

4.2.2 Prosthesis and interlocking

In case that any of the wooden elements that constitute to the connection is decayed or degraded, it is possible to cut off the deteriorated part and replace it with a new one. This new part, with the same material properties as the ones of the old element, is known as prosthesis [40]. It is of great importance, to ensure the continuity and right conjunction of the old and new part, which can be achieved with the use of specially designed glues, screws, steel or FRP rods, epoxy resins, etc.

Another matter that is holding a key role in case that a prothesis is used, is the good lateral “interlocking” between the wooden parts at the joint. The prothesis should be in good contact with the rest of the wooden elements at the joint and clearances should be minimized.

4.2.3 Bolts

In order to tighten and secure the connection from out-of-plane movements, it is possible to use bolts. They penetrate the entire section width and they are fixed on their ends with washers and nuts. The hole where the bolt will be put, has to be predrilled with a machine and its diameter should be the same or slightly smaller than that of the bolt to establish the friction between wood and bolt. The use of the right nut diameter is important because it ensures the fixing of the end and provides high strength in tension (Figure 4.1b) [21],[33],[40].

4.2.4 Steel plates

For a behavior closer to the one that is obtained by a monolithic connection, it is possible to use steel plates which are usually positioned and fixed upon the elements with nails or screws. Commercial steel plates with prefabricated hole patterns and variable thicknesses, facilitate the implementation of this strengthening technique which is usually applied when greater loads need to be carried by the structure [40]. As an alternative application technique, holes can be drilled through the entire width of the section and the steel plates that are positioned on each side can be bonded with bolts (Figure 4.1c) [41].

The number of nails and screws that will be used to position the steel plates, as well as the distances between them have to be predefined [20],[21],[33].

4.2.5 Steel flat bars or rods

It is possible to improve the flexural rigidity of a member or the overall rigidity of the connection with the use of embedded steel elements, like flat bars or rods, near the surface of the wood. The technique used is called near-surface mounting (NSM) and is quite common as a reinforcement method in concrete structures, but with the use of special glues, it can also be applied in timber structures. Special care should be taken, in order to secure the necessary anchorage length in any case (Figure 4.1d-e) [21],[40],[41].

4.2.6 Steel embedded connectors in specific connection locations

Another option, which is available on the market today, is a type of special steel embedded connectors that can be used in specific connection locations, as long as the anchorage length is provided within the accommodating area. This product is designed to join timber elements together and provides high tensile strength, while it replaces the mortise and tenon connections. It consists of a hollow steel connection tube with elongated slots where expanding cross pins are inserted to fix its ends. Its advantages are the simplicity of its installation, as well as the traditional appearance of the connection, which adds to its aesthetical point of view (Figure 4.1f) [42].

4.2.7 Use of innovative techniques - FRP materials (rods and sheets)

While timber and steel elements predominated in the traditional strengthening techniques for the connections of the timber-framed structures, an innovative material has started to gain ground in this area. The use of fiber reinforced polymers (FRP) is rising due to its simple and fast application, high strength and stiffness and mainly due to the very low weight that adds minimum loads to the structure [43].

Usually glass FRP sheets with their epoxy resins are used externally bonded over the connections. The glass fiber costs less while it has lower strength compared to carbon and aramid fibers, so it fits better for the strengthening of timber, which is not a material with high values of strength as concrete.

Nevertheless, it should be kept in mind that FRP's add stiffness but they reduce the overall ductility of the structure (Figure 4.1g) [28],[29],[44],[45].

Additionally, FRP rods or laminates can also be used with the NSM method (See 4.2.5) to improve the rigidity (Figure 4.1h) [39],[41].

Figure 4.1 - a) Nail and screws, b) Bolt, nut and washer, c) Types of steel plates, d) Steel flat bar, e) Steel rods, f) Steel embedded connectors, g) Types of FRP, h) Types of FRP rods [42],[43].

4.3 Description of the applied retrofitting techniques

After the tests of the unreinforced specimens were concluded, their final state was evaluated and several solutions were proposed in order to restore them. Most of the retrofitting techniques that were finally decided to be applied, were evaluated both under pull-out and in-plane cyclic tests. The response of the specimens under each type of test will be presented and discussed separately.

4.3.1 Specimens used for pull-out tests

As it was previously mentioned, all four specimens that had been used to perform the pull-out tests, had no significant damage apart from the bending of their nails into an "S" shape and a small vertical sliding crack parallel to the grain over and lower from the nail at the inner overlapping part of the post. The beams showed no signs of damage (See 3.5.4). Provided that, those specimens could be retrofitted without any further provision other than the simple removal of the nails.

4.3.1.1 Fixing point

Special attention was paid to the fact that the grip for the tests was ensured through 4 steel rods that passed through the holes of a steel U profile and they were fixed with nuts (See 3.5.1), as it was possible that failure could occur to that point instead of the connection under study.

In order to avoid this type of failure, it was decided to apply 2 uniaxial GFRP sheets with their fibers perpendicular to the timber grain, impregnated in epoxy resin for each side of the upper part of the post.

Shallow grooves of 2÷3mm were made to the front and posterior, upper parts of the post with a height equal to the one that is required from the steel profile (Figure 4.2a). After that, the area where the FRP would be applied was roughened with sandpaper and particles of wood along with dust were removed (Figure 4.2b).

The GFRP which was used is MapeWrap G UNI-AX and the epoxy resin was the MapeWrap 31, with medium viscosity (Figure 4.2c). The epoxy resin consists of two components which are mixed with a 4:1 ratio by weight. A precision electronic scale was used to ensure that the mixture preparation was right and subsequently it was stirred until it became homogeneous (Figure 4.2d).

With the use of a brush, the epoxy was applied on the surface of the timber (Figure 4.2f) and then a substantial amount of epoxy was used to impregnate the GFRP, which had been carefully cut in strips with the appropriate dimensions 8x24(cm) (Figure 4.2e). The direction of glue application has to remain parallel to the fibers to avoid their disorganization (Figure 4.2g). It is important to handle GFRP with protection for the hands as it can cause itching and irritation to the skin. The same applies for the epoxy resin.

After the impregnation, the GFRP sheet was positioned on the previously mentioned timber surface (Figure 4.2h) and with the use of a rolling paint brush, it was pressed against it to maximize the adherence of their surfaces. Another layer of epoxy was applied and then, the second GFRP sheet was positioned over the first one, following the same procedure. The same was done at the posterior side of the post.

After the placing of the GFRP sheets was completed for all 4 specimens, they were left for 7 days in order to obtain the maximum tensile strength of the epoxy resin (Figure 4.2i). Then, the holes for the positioning of the rods were drilled once more at their previous placing points.

Additionally, during the mounting of every pull-out test, after the rods were put in place, eight screws of ø8mm and 8cm length, were placed laterally, two above each rod with a distance of 6cm in between, as additional reinforcement to prevent bending of the rods (Figure 4.2j)[46].


a)


b)

c)

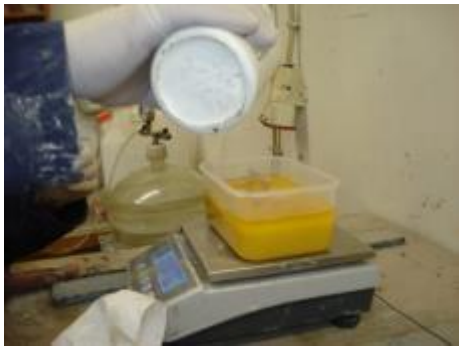
d)

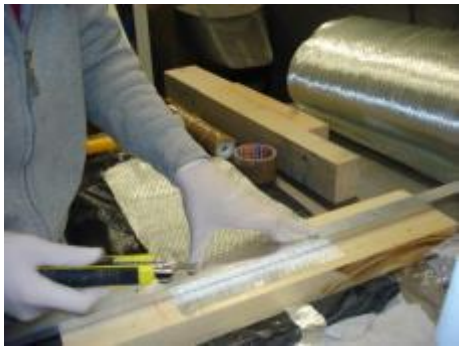
e)


f)


g)

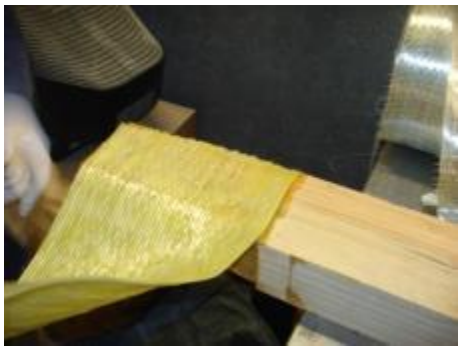
h)


i)

j)

Figure 4.2 - Photos a) - i) show the application procedure of the GFRP sheets on the fixing point of the posts and j) the laterally placed screws.

4.3.1.2 Screws

In this retrofitting case, four self-tapping screws with a length of 19cm and a diameter of 8mm (Figure 4.3a), were positioned laterally of the connection; two on each side under different angles. Two were positioned through the post sides while the other two through the beam sides. The ones that penetrated from the beam sides were placed under an angle of 45°, crossing one another forming an "X" and so did the ones that entered the connection from the post sides, but with an angle of 60°. The spacing between the screws and their distances from the end and edge recommended by the standards of Eurocode 5 could not be accommodated within the small width of the specimen, 12cm so they were appropriately modified to fit in the area (Figure 4.4). Small wooden wedges were created to ensure that the angles would be easily followed (Figure 4.3b).

It was necessary that the screws would be entering through the post sides from the back point of view, in order to obtain continuity between the post and the beam, which are interrupted on this side. It should be mentioned that it was very difficult to position these two screws. The capacity of the screwing machines that were used was not enough to place them until the end and about 2,5cm was left outside on both sides (Figure 4.3c).

All the screws were put into place by means of in plane positioning regarding the specimen and no other mechanical fasteners were used, e.g. nails or screws from the front side of the post.

This strengthening technique was easily implemented and its application on-site is facilitated by its lightness while it is also reversible.


a)


b)


c)

Figure 4.3 - a) Self-tapping screw, b) Wooden wedges were used to help follow the right angles, c) Difficulties were encountered when the screws were positioned through the posts.

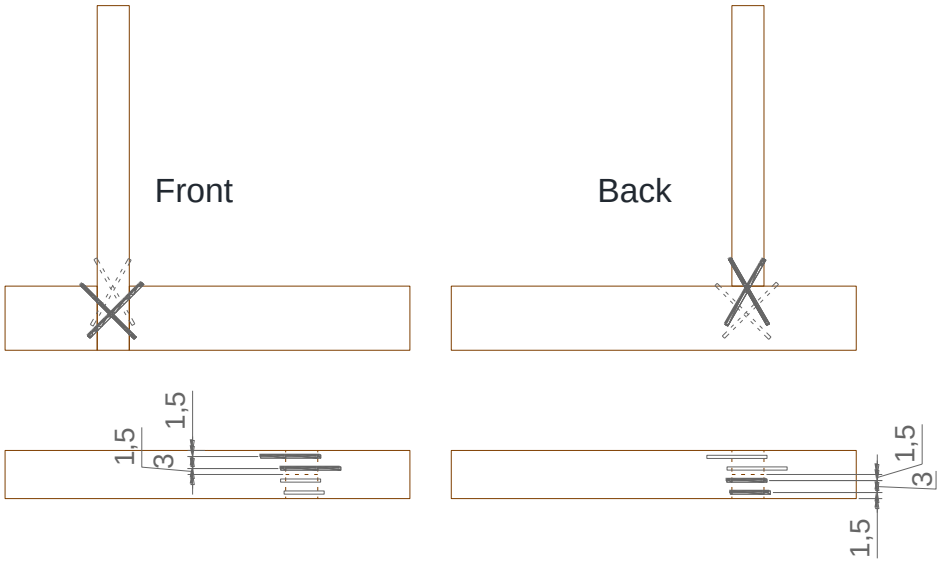

Figure 4.4 - Section configurations of the self-tapping screws positioning regarding front, back and upper point of view. (Dimensions in cm).

4.3.1.3 "T" GFRP

The same uniaxial GFRP sheet and epoxy resin that were used to strengthen the fixing point (See 4.3.1.1) were used to reinforce the connection under study.

One sheet placed vertically and another one placed horizontally, were used on each side forming an upside down "T". The width of the vertical sheet was equal to the post width, 8cm, while the sheet placed horizontally had a width of 14cm. In order to provide sufficient anchorage lengths for the FRP's, the sheets were positioned with an extension of 20cm to every side from the joint (left, right and above) [45]. The fibers were always parallel to the longer side of the sheets (Figure 4.5).

In the front side, where there is continuity of the post, the horizontal sheet was placed first (Figure 4.6a), to prevent out-of-plane displacements and to provide stiffness while, the vertical sheet was positioned on top of it (Figure 4.6b). On the other side, where there is no continuity between post and beam, the vertical sheet was applied first (Figure 4.6c) and the horizontal afterwards (Figure 4.6d).

The procedure which was followed for the preparation the resin mixture and the impregnation and application of the sheets, was similar to the one described earlier for the fixing point (See 4.3.1.1).

This technique is easy and fast to apply, although it requires special care in handling the materials. Additionally, it is light and it can be applied on site without rising any difficulties. However, it should be mentioned that while the final colour of the FRP's is yellow and it is not so much in contrast with the natural colour of the wood, it still fails to be regarded as a harmonious result. Nevertheless, this problem could be addressed through painting.

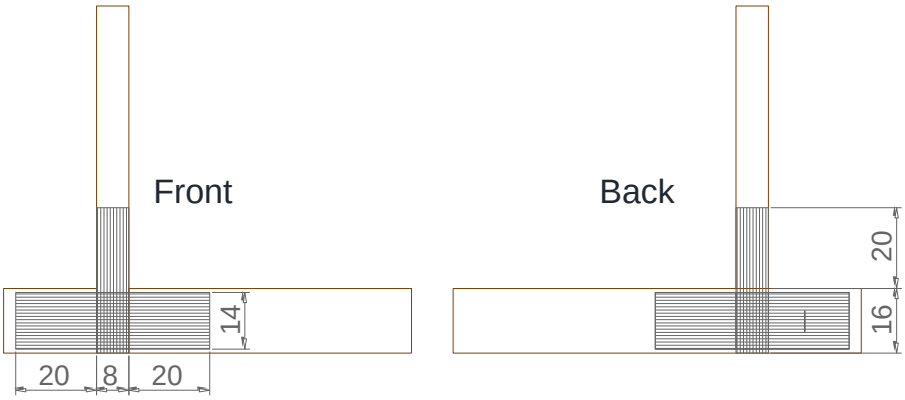

Figure 4.5 - Configurations of the positioning for the "T" GFRP and the steel plates regarding front and back. (Dimensions in cm).


a)

b)

c)

d)

Figure 4.6 - a) Horizontal GFRP sheet applied first at front, b) Vertical GFRP sheet placed on top of the horizontal forming an upside down “T”, c) Vertical GFRP sheet applied first at the back, d) Straightening of the horizontally placed GFRP sheet using a rolling paint brush.

4.3.1.4 Steel plates

Four steel plates with prefabricated hole patterns were used in this case. In each joint’s side two of them were placed, one horizontally and the other vertically (Figure 4.5). Four bolts of ø10mm were used to fix and confine the plates together, while another 18 screws of ø5mm and 5,5cm length were put on each side in order to induce better distributions of the stresses on the plates. The positioning locations of the screws were defined according to Eurocode 5 requirements.

Initially, the plates were drilled at the positions where the bolts would be put (Figure 4.7a) and then they were set above one another in the way that they would be placed and they were temporarily fixed (Figure 4.7b). Once more, the horizontal plate was positioned first in the front side and the vertical on top of it, while the opposite was done at the back to provide continuity between the connected members. The vertical plates were cut to fit the width of the post as they were larger (Figure 4.7c).

Afterwards, the holes for the bolts were drilled at the specimen and the bolts with their washers and nuts were placed and tightened. Subsequently, 18 screws were put on each side (Figure 4.7d).

This technique requires precision but, on the other hand, it is easy and fast to apply in on site conditions, while totally reversible, even though it adds extra weight to the structure.

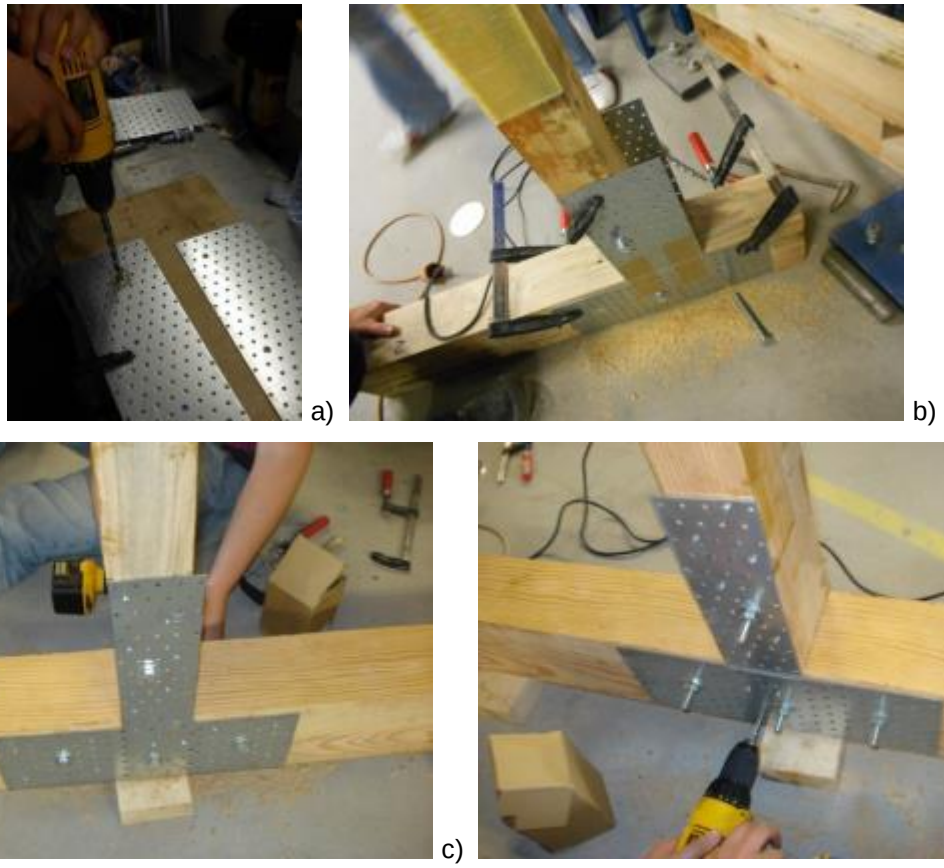

Figure 4.7 - a) Drilling of holes for the bolts, b) Temporarily fixed plates in order to drill the holes for the bolts. The vertical plates were cut. c) Front side – d) Back side and positioning of the screws.

4.3.1.5 NSM with steel rods

The technique of near-surface mounting was accomplished with the positioning of steel rods into shallow grooves which were previously created upon the surface of the connection and their filling with glue (Figure 4.8).

Initially, the specimen was positioned horizontally and it was temporarily fixed (Figure 4.9a). Then the grooves were created with a plunge router machine, with the alignment being ensured by using perfectly straight wooden elements (Figure 4.9b). It was important that the final depth of 15mm would be reached gradually, for the better operation of the machine (Figure 4.9c). A right machine head was used to achieve a width of 12mm. There was no need for depth differentiations as the rods had been welded together by the manufacturer. Two vertical grooves were made at the post part and the joint and one horizontal through the joint, at the beam. As they extended from the joint it was made sure that an anchorage length was provided (20cm) [45]. Once finished with the creating of the grooves in one side, the same procedure was followed for the opposite side.

Three steel rods of class 8.8 (minimum tensile strength 800MPa and minimum yield strength 640MPa) and ø10mm were welded together in an orthogonal configuration and positioned inside the grooves on each side to confirm that they could fit (Figure 4.8). Further depths of widths were implemented to the

grooves whenever needed in order to accommodate the welded steel rods. For this reason, it was essential that the welded rods would be perfectly straight. The grooves were then cleaned using a vacuum cleaner to remove any particles of sawdust (Figure 4.9d).

An epoxy gel glue, Mapewood Gel 120, was used to fill the void between the rods and the timber grooves, providing high adhesion. The glue consists of two parts which are mixed with a ratio of 4:1 (A:B) and it has to be stirred until homogeneity is achieved (Figure 4.9e). The mixture remains in a fluid form with medium viscosity until it dries. A precision electronic scale was used to ensure that the mixture preparation was correct.

Small pieces of wood were used as spacers to ensure that there would be glue underneath the rods and larger wood pieces were nailed at the edge of the post bottom to seal it temporarily and prevent the glue from running (Figure 4.9f).

A certain quantity of the glue was applied first to the grooves until the height of the spacers (Figure 4.9g). Next, the welded rods were positioned and then the grooves were filled until the surface (Figure 4.9h-j). The filling of the opposite side had to be done the next day, in order to allow the glue on one side to dry first. Finally, the complete hardening of the glue was reached after 7 days.

The application of this technique is time-consuming and invasive, while it cannot be done on site unless a glue with different consistency is used (paste glue). Other than that, if it is applied carefully it can have an aesthetically good final appearance, as its final color is brown. Additionally, wood peel can be placed on top of the groove leaving the surface looking almost intact. Also, it should be kept in mind that it adds extra self- weight to the structure.

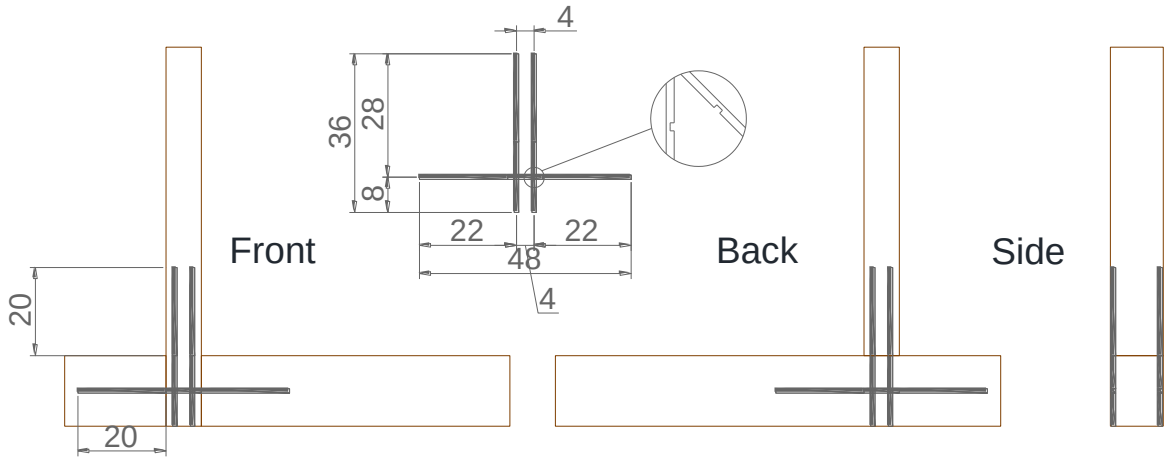

Figure 4.8 - Section configurations of the NSM of steel rods regarding front, back and side point of view and configuration of the welded rods. (Dimensions in cm).

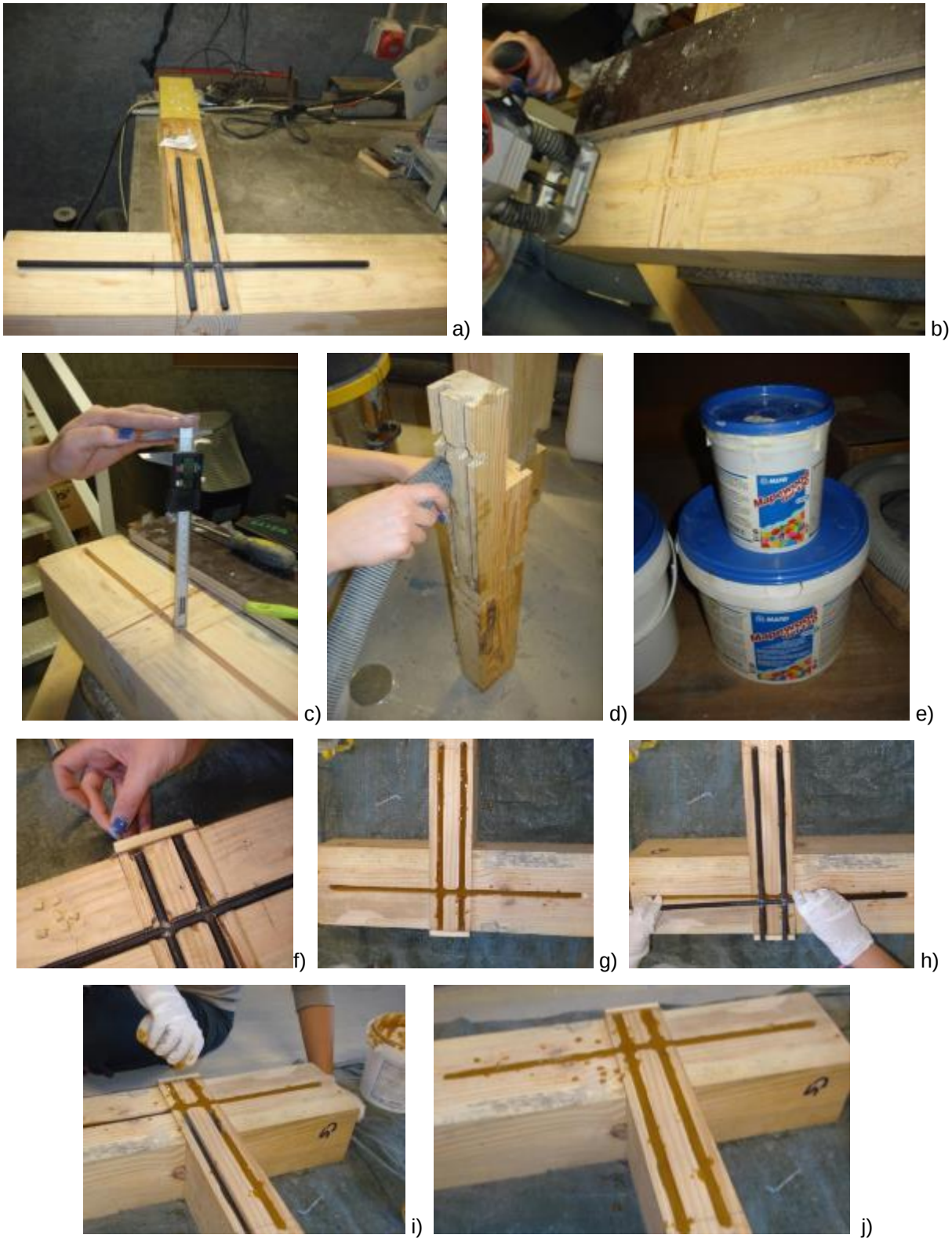

Figure 4.9 - Photos a) - j) show the application procedure of the NSM steel rods.

4.3.2 Specimens used for in-plane cyclic tests

Unlike the specimens that were previously used for the pull-out tests, the ones that were submitted to in-plane cyclic tests, suffered severe damages (See 3.6.4):

- Vertical, parallel to the grain (splitting-sliding) cracks underneath the nail position and around the “tenon” part of the post in the intersection with the beam;
- Horizontal, perpendicular to the grain (snapping) cracks on each side of the post at the points of intersection with the beam;
- Crashing cracks at the bottom of the tenon” part of the post (Figure 4.10a);
- In one case, post “tenon” was totally detached (C2_50);
- No significant damage was encountered at the beams.

Due to this, it was decided that all the posts of the ten specimens would be inspected and for the ones that had heavy damages, their “tenon” would be cut up to a point and a wooden prosthesis would be positioned in their place.

The posts were inspected separately, regarding to the vertical load that had been previously implemented on them during the tests (Figure 4.10b-g).

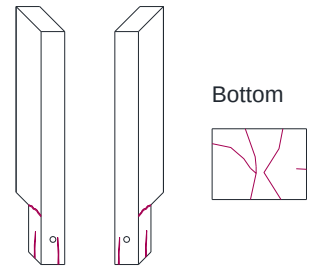

. a)

b)

c)

d)

e)


f)

g)

Figure 4.10 - Photos a) Crack patterns for in plane cyclic tests, b) - d) Front, back and side view of posts for the 25kN pre-compressive level, e) - g) Front, back and side view of posts for the 50kN pre-compressive level.

Out of all the specimens, only 3 were kept as they were to be used for further strengthening, because they had no permanent deformations concerning vertical alignment and their lateral snapping cracks had not propagated much, perpendicular to the grain. The list of all the inspected post specimens with their names regarding the unreinforced tests, along with the final decision about the prosthesis is given in Table 4.1.

Table 4.1 - List of the in-plane cyclic test specimens that will be retrofitted with a prosthesis

Ref.number	Type of test	Test name	Prosthesis
1	Cyclic	URT C1_25	✓
2	Cyclic	URT C2_50	✓
3	Monotonic	MONO25	✓
4	Monotonic	MONO50	✓
5	Cyclic	URT C3_25	✓
6	Cyclic	URT C4_25	Kept as is
7	Cyclic	URT C5_25	✓
8	Cyclic	URT C6_50	✓
9	Cyclic	URT C7_50	Kept as is
10	Cyclic	URT C8_50	Kept as is

4.3.2.1 Prosthesis

For the seven specimens that were decided to be retrofitted with prosthesis, three different solutions were proposed (Figure 4.11):

1. A wooden addition with an angle of 90° would be attached with gel glue to the preexisting post, which would be appropriately cut and prepared. This solution was not chosen due to the high uncertainty concerning its performance;
2. The second solution, involved the positioning of 2 steel rods within the section of the previously mentioned prosthesis and their anchorage within the preexisting post. This solution was also rejected as it limits the further retrofitting solutions that could be applied for the in plane cyclic tests;
3. Finally, a different solution was proposed and used. It required the cutting of a wooden prosthesis with 2 opposite orthogonal angles, in order to increase the contact surface of the

wooden elements and the glue. To secure the consolidation between the new and the older wooden member, 2 screws of ø6mm were positioned from the front at the mid-height of the prosthesis joint with a distance of 4cm between them. As their length surpassed that of the post width, their ends were cut.

The wood that was used by the carpenter to make the prosthesis members was of the same type of wood, which was used for the connection specimens. It be should mentioned here, that the geometry of the connections in some cases was rather bad as the members would not fit well together.

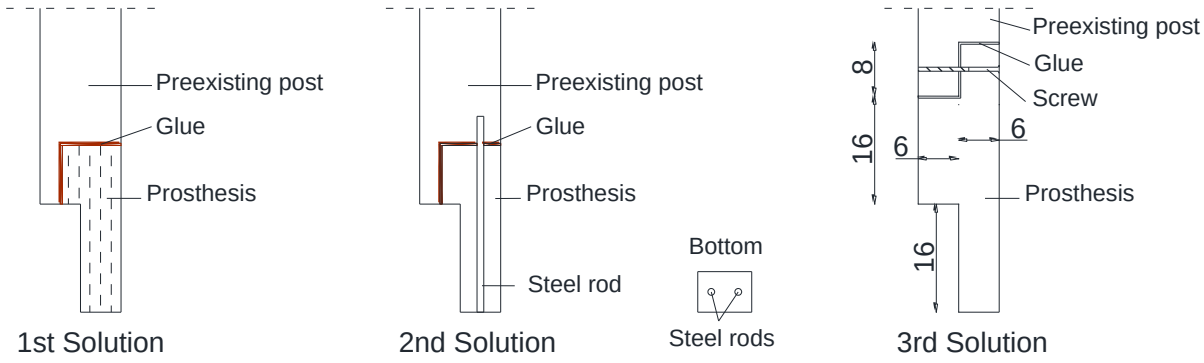

Figure 4.11 - Section configurations of the 3 solutions that were proposed for the prosthesis. On the right (3rd Solution) is the one that was finally applied. (Dimensions in cm).

Before the glue application, all the timber members were covered with paper tape at their edges to minimize the staining of their surfaces. For two of the specimens (MONO25, C5_50), instead of the epoxy gel glue, Mapewood Gel 120, another one with high viscosity was used (Mapewwod Paste 140). Mapewood Paste 140 is a thixotropic epoxy adhesive and it consists of two parts which are mixed with a ratio 2:1 (A:B). Its final color is very close to the natural beige color of wood. It was much more workable than the gel glue, while it was applied much faster and easier (Figure 4.12a-b). On the contrary, the implementation of gel was time consuming and it required further filling which was “injected” with a syringe (Figure 4.12c-d). Additionally the specimens had to be strapped around with paper tape, otherwise the members would detach.

The next day, two screws were placed at the prosthesis connection of each specimen as it was described earlier (Figure 4.12e-f) and then they were left for another 6 days until both glues reached complete hardening.

The performance of this retrofitting solution is time consuming and invasive, while it requires supporting to maintain the stability of the structure. Depending on the materials that will be used, the result can be good from the aesthetical point of view. Additionally, the originality of the initial state is reduced.

Figure 4.12 - a) - b) Application of paste glue for the prosthesis, c) Application of gel glue for the prosthesis, d) The gel was additionally filled with the help of a syringe, e) For the first two specimens on the left the prosthesis was placed with paste glue giving a better looking result, f) The positioning of the two screws at the prosthesis connection.

4.3.2.2 GFRP sheets and CFRP strips wrapped

After the evaluation of the damage patterns at the posts during the performance of the in-plane cyclic tests, an innovative solution was proposed and implemented. The proposed solution involves the simultaneous use of GFRP sheets and CFRP strips.

As far as it concerns the GFRP sheets they were placed laterally of the post up until the mid-width, so as to be applied on the side of the “tenon” from the bottom and exceed above the joint for 20cm as

anchorage length [45]. This was meant to delay the snapping perpendicular to the grain (Figure 4.13a).

Additionally, two CFRP strips with a width of 3cm each were wrapped; the first around the bottom of the “tenon” and the other around the post exactly above the intersection with the beam [41]. The latter intended the same as the GFRP while it also anchored it, while the one placed at the bottom would prevent the opening of the vertical sliding cracks.

For the application of the GFRP sheets the same procedure which was described earlier (See 4.3.1.1) was followed. A unidirectional CFRP was used, S&P C-Sheet 240 with a fiber weight of 200g/m^2 along with its resin epoxy, S&P Resin Epoxy 55/50, that consists of two components which were mixed in a ratio of 2:1 (resin: hardener) (Figure 4.13b) . It was important that the edges of the post would be rounded in order to wrap the CFRP strips, so this was done with a filer, only in the areas where the strips would be placed (Figure 4.13c). Other than that the procedure was the same as the one for the application of the GFRP’s except from the fact that the CFRP was protected with a transparent film that had to be replaced before its impregnation (Figure 4.13d-e).

This technique was applied to two specimens, one damaged and one that had been retrofitted with a prosthesis with paste glue. After seven days from the FRP’s implementation, the posts were positioned in the beams. For this reason the beams were laterally widened as the width of the posts was relatively bigger.

Finally, a hole was drilled at the specimen and a bolt of ø10mm with its washer and nut was placed at the position of the preexisting nail (Figure 4.13f).

While the positioning of a bolt is a reversible solution which could easily be implemented on site, the previously described solution could not be easily applied in this way, except if a retrofitting solution like the prosthesis would be done as well. Other than that the appearance is slightly poor, mainly due to the black color of the CFRP strips and another disadvantage is the fact that the dimensional changes which are caused to the wood, are not accommodated by the CFRP wrapping.

It was decided that these two specimens would be tested under the pull-out test procedure as well.


a)

b)


c)

d)

e)

f)

Figure 4.13 - Photos a) - f) show the application procedure of the GFRP sheets and CFRP strips and the bolt positioning at the specimen.

Apart from the last solution, which was applied on two of the 10 specimens that were used for the in-plane cyclic tests, another 4 were retrofitted with the previously mentioned “T” GFRP technique (See 4.3.1.3), 2 more with steel plates (See 4.3.1.4) and another 2 with NSM steel rods (See 4.3.1.5). The only differentiation was that the upper part of the rods had to be cut because their height was the same as the one of the positioning of the two screws for the prosthesis (Figure 4.14a-b).

Below, there is a table with all the specimens and the retrofitting solutions that were applied to them (Table 4.2).


a)

b)

Figure 4.14 - a) - b) The vertical rods were reaching up to the height of the screws so they were slightly cut.

Table 4.2 - List of all the specimens and the retrofitting solutions that were applied.

Ref.number	Type of test	Test name	Retrofitting soultions
1	Monotonic / Pull-out	URT PO1	"T" GFRP
2	Pull-out	URT PO2	Steel Plates
3	Pull-out	URT PO3	Auto-perforated screws
4	Pull-out	URT PO4	NSM Steel rods
5	Cyclic	URT C1_25	Prosthesis - NSM Steel rods (50KN)
6	Cyclic	URT C2_50	Prosthesis - "T" GFRP
7	Monotonic	MONO25	Prosthesis(paste) -GFRP sheet - CFRP strip wrap- bolt (50KN)
8	Monotonic	MONO50	Prosthesis - Steel Plates (50KN)
9	Cyclic	URT C3_25	Prosthesis - "T" GFRP
10	Cyclic	URT C4_25	"T" GFRP
11	Cyclic	URT C5_25	Prosthesis (paste)- NSM Steel rods (50KN)
12	Cyclic	URT C6_50	Prosthesis - Steel Plates (25KN)
13	Cyclic	URT C7_50	"T" GFRP
14	Cyclic	URT C8_50	GFRP sheet - CFRP strip wrap- bolt (50KN)

References

[13] Cardoso R., Lopes M., Bento R., Seismic evaluation of old masonry buildings. Part I: Method description and application to a case-study, Engineering Structures 27: (2005), 2024–2035

[20] Goncalves A.M., Ferreira J.G., Guerreiro L., Branco F., Seismic retrofitting of Pombalino “frontal” walls, World Conference of Earthquake Engineering, Lisbon 2012, Paper No. 5129

[21] Poletti E., Vasconcelos G., Seismic behaviour and retrofitting of timber frame walls. International conference on structural health assessment of timber structures (SHATIS’13) 4 - 6 September 2013, Trento, Italy (accepted).

[28] Cruz H., Moura J.P., Machado J.S., The use of FRP in the strengthening of timber-reinforced masonry load-bearing walls, Historical Constructions, Guimaraes, 2001, p.847-856

[29] Pilaon P., Experimental cyclic behavior of timber shear walls, SAHC Master Thesis, Civil Engineering Dept., University of Minho, Portugal 2010[33] European Committee for Standardization – European Standard EN 1995-1-1:2004, Eurocode 5: Design of timber structures - Part 1-1: General - Common rules and rules for buildings, Brussels, Belgium 2004

[38] Roca P., MSc SAHC Lecture, SA1.11 History of Conservation and Restoration Part 2/2, UNIPD, Padova, Italy, 2012-2013.

[39] Madhoushi M., Ansell M., Behaviour of timber connections using glued-in GFRP rods under fatigue loading. Part II: Moment-resisting connections, Composites Part B: Engineering Volume 39, Issue 2, March 2008, Pages 249–257

[40] Oikonomou N., Mpikas D., Avdelas A., Timber Structures – Notes for students (in Greek), Thessaloniki 2008-2009

[41] El-Hacha R., MSc SAHC Lecture, SA5 Repairing and Strengthening Techniques- Strengthening of Timber Structures, UNIPD, Padova, Italy, 2012-2013.

[42] Improving Timber Connections through Design, Ron Blank & Associates, 2009
Available at: http://www.ronblank.com/courses/tlx06a/tlx06a.pdf (8.7.2013)

[43] El-Hacha R., MSc SAHC Lecture, SA5 Repairing and Strengthening Techniques- Strengthening of Concrete Structures (II), UNIPD, Padova, Italy, 2012-2013.

[44] Vázquez E., MSc SAHC Lecture, SA6 Restoration and conservation of materials- Polymers and Composites 2012, UNIPD, Padova, Italy, 2012-2013.

[45] Jorge M.A.P., Experimental behavior of glulam-FRP systems, MSc Thesis, Department of Civil Engineering, University of Minho, Portugal 2010.

[46] Blass H.J., Bejtka I., Reinforcements perpendicular to the grain using self-tapping screws, Proceedings of the 8th World Conference on Timber Engineering, Volume I, Lahti, Finland, 2004

Chapter 5

Experimental results after retrofitting

5.1 Introduction

It is of great importance to understand and evaluate the mechanical behavior of each retrofitting solution in order to provide guidelines for future studies.

Since overlapping timber connections, which are typical for half-timbered walls have not been studied thoroughly and their strengthening is still at an experimental basis, it is necessary to obtain further knowledge towards their mechanical characterization through a series of tests, namely pull-out and in plane cyclic, following also the experimental approach defined in Chapter 3.

Through the observation of the performance that the overlapped connections will have during the tests, it is possible to review and adjust the retrofitting solutions, if they present any unwanted and unpredicted deformation or even failure patterns.

This chapter deals with the analysis of the cyclic performance of overlapped connections retrofitted with the various solutions that have been described in Chapter 4. The results for the strengthened connections are discussed for each distinct test configuration, namely for the pull-out and for the in plane cyclic test. Besides, the specimens are grouped according to the retrofitting technique selected. Additionally, regarding the specimens with the CFRP wrapped strips (See 4.3.2.2) that were subjected first to in-plane cyclic and then to pull-out tests, their pull-out performance will be reviewed at the end.

5.2 Pull-out tests

All 6 pull-out tests were performed cyclically. The test procedure was adjusted in order to impose very small displacements, as the stiffness of the specimens was expected to be higher after their strengthening (Table 5.1).

Table 5.1 – New procedure for the pull-out tests on the retrofitted specimens.

speed 1	0,01	mm/s					
speed 2	0,05	mm/s					
speed 3	0,15	mm/s					
speed 4	0,25	mm/s					
step	**nº of cycles**	**displacement**	total course per cycle	time per cycle	time per step		
		mm	[mm]	[s]	[s]	[min]	[h]
1	1	0,10	0,2	20	20,00	0,33	0,01
2	1	0,20	0,4	40	40,00	0,67	0,01
3	1	0,30	0,6	60	60,00	1,00	0,02
4	3	0,40	0,8	80	240,00	4,00	0,07
5	3	0,60	1,2	24	72,00	1,20	0,02
6	3	0,80	1,6	32	96,00	1,60	0,03
7	3	1,00	2	40	120,00	2,00	0,03
8	3	1,50	3	60	180,00	3,00	0,05
9	3	2,00	4	80	240,00	4,00	0,07
10	3	4,00	8	53,33	160,00	2,67	0,04
11	3	6,00	12	80	240,00	4,00	0,07
12	3	8,00	16	106,67	320,00	5,33	0,09
13	3	10,00	20	80	240,00	4,00	0,07
14	3	15,00	30	120	360,00	6,00	0,10
15	3	20,00	40	160	480,00	8,00	0,13
16	3	30,00	60	240	720,00	12,00	0,20
				tot	3588,0	59,8	1,0

The tests setup was the same as the one used in case of unreinforced specimens. However, in order to prevent the failure of the rods in the fixing U profile, screws were added laterally above them and two GFRP sheets were placed on each side on the top of the post, with their fibers perpendicular to the grain (See 4.3.1.1).

The monitoring instrumentation was similar to the one used in case of unreinforced specimens and consisted of the actuator, the computer and the LVDT's which measured the uplifting displacements of the post and the beam and whenever it was necessary the out-of-plane displacements.

5.2.1 "T" GFRP

As described in Chapter 4, a damaged specimen was strengthened with two uniaxial GFRP sheets on each side, one horizontal and other vertical (See 4.3.1.3). In this section the main results on damage patterns, force-displacement diagrams and performance indexes are provided and discussed.

Evaluation of the damage patterns

During the test, damages appeared in the following order (Figure 5.1):

- Initially, at the front, where there is post continuity, there was debonding of the horizontal GFRP sheet, which was applied on the beam, perpendicular at the 2 intersecting sides with the post (Figure 5.1a). Further outwards propagation of the debonding upon the beam happened gradually.
- During the 10th displacement step (4mm) the total and abrupt debonding of the vertical sheet from the post at the back side was observed. Additionally, snapping was present at the upper side of the beam laterally from the post. This was the first time that a beam suffered significant deformation during any test (Figure 5.1b).
- During the 14th step (15mm) there was disbandment and dispersion of the fibers that were previously debonding at the front part of the beam, which left the connection between post and beam free of fibers (Figure 5.1c). After that only friction was providing resistance to the induced displacements and there was a very small out-of-plane displacement (4mm).


a)


b)

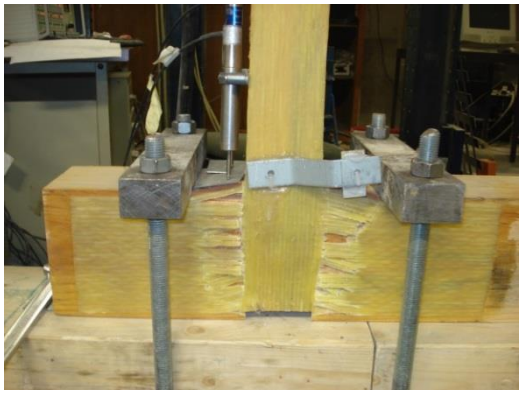

c)

Figure 5.1 – Details of the damage patterns that were observed during the pull-out test of the specimen with “T” GFRP strengthening a) - c).

Analysis of the Force – Displacement diagram

Comparing the envelop curves of the unreinforced and retrofitted specimen (Figure 5.2), it is evident that after the retrofitting, the stiffness and the maximum force were extremely high, being the maximum force 16 times bigger than the maximum load in the unreinforced specimen. The debonding of the GFRP at the back of the specimen resulted in an abrupt and remarkable loss of resistance which was then partially recovered. This recovering is attributed to the still effective horizontal sheet at the front of the connection, even though further losses appeared due to disbandment of its fibers. After that, the specimen works as if it was unreinforced.

Additionally, the dissipated energy at the first hysteresis loops was not significantly large, as the displacement steps were very small, while pinching is present after the debonding of the vertical sheet at the back. Once the specimen was free of any reinforcement there was uplift for the rest of the displacement steps, while the achieved force values were lower than those of the unreinforced specimen.

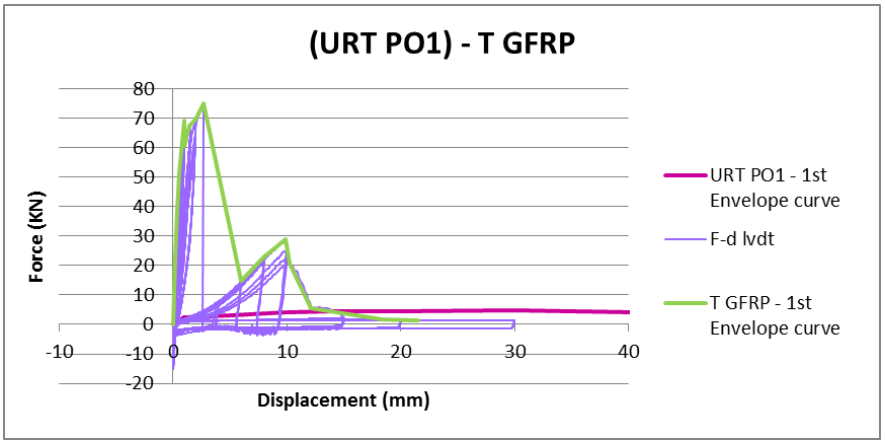

Figure 5.2 – Pull-out force-displacement diagram of the specimen with “T” GFRP strengthening.

5.2.2 Steel Plates

As described in Chapter 4, when steel plates were adopted, the specimen was retrofitted with 4 steel plates: two on each side positioned vertically and horizontally connected to the wood elements through 4 bolts penetrating the specimen. Additionally, 18 screws were placed on each side through the holes of the plates (See 4.3.1.4).

Evaluation of the damage patterns

It is important to mention that during the pull-out test, work both the bolt at the overlapping connection and the vertical plate at the back of the specimen which provides continuity between the beam and post members, while it prevents the uplifting. The rest of the strengthening is meant for better distribution of the stresses and anchorage.

This test was not performed completely, as the actuator which was used has a load capacity of 150kN in compression while its capacity in tension is much lower, reaching 80kN. Once the maximum force was ranged, it was not possible to proceed with the rest of the test.

This force was achieved at the 9th step (2mm) and until then there was no visible damage at the strengthened specimen (Figure 5.3a). Also, some uplifting of the beam was registered due to the stiffness of the joint which performed close to monolithically (Figure 5.3b).

a)

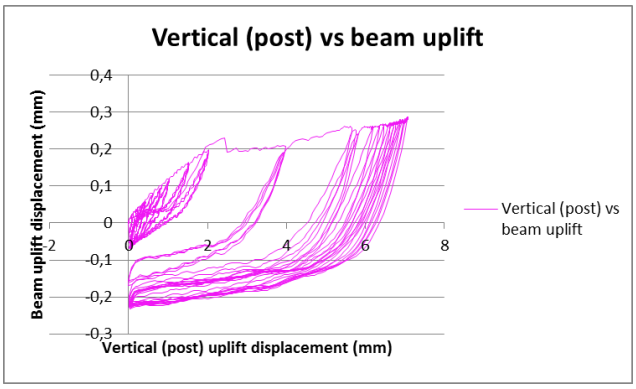

b)

Figure 5.3 - a) The specimen had no deformations, b) Graph showing the presence of beam uplift.

Analysis of the Force – Displacement diagram

The specimen exhibits a large stiffness and maximum force increase compared to the unreinforced specimen and the hysteresis loops where gradually increasing as expected, although it is not possible to perceive its post-peak behavior without having a diagram with softening (Figure 5.4). Note that its maximum force was up to 28 times higher at this point, although this actuator could not reach higher forces.

It is also evident that pinching behavior is increasing as the displacement increases, which should be associated to the local deformation developed around the main bolt as it was submitted to direct shear.

This specimen was kept at the laboratory of the University of Minho and it will be tested in the future to obtain further information about its global performance, including the post-peak behavior.

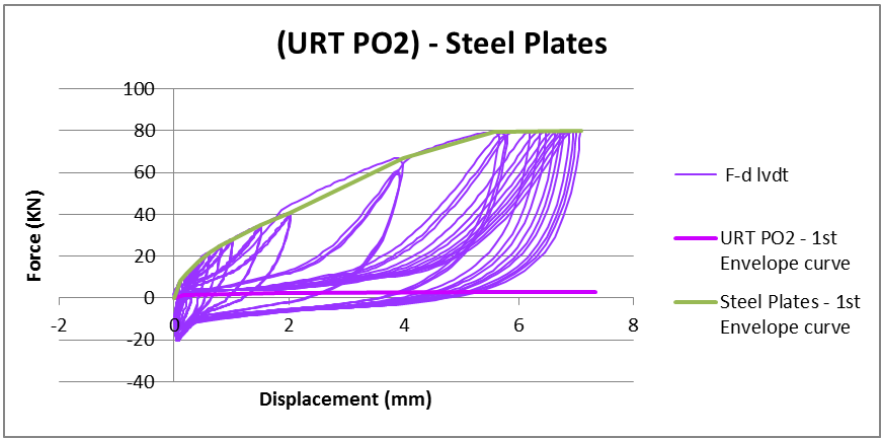

Figure 5.4 - Pull-out force-displacement diagram of the specimen with steel plates strengthening.

5.2.3 Screws

Four screws were placed under different angles laterally of the specimen: two through the post forming an “X” and another two through the beam forming one more “X” (See 4.3.1.2).

Evaluation of the damage patterns

The main damage patterns observed during the tests are summarized as follows:

- In the adjacent top surface of the beam to the post “tenon”, at the continuous part of the connection two cracks developed in the direction parallel to the grain: one above and one at the front, forming corners which were gradually detaching and uplifting along with the post. The same happened to the left side of the beam, at the discontinuous part of the connection a little after the one on the right appeared (Figure 5.5a).
- Regarding the screws that were inserted through the post at the “back”, as they were moving upwards and downwards they induced grain disorganization, which eventually turned into wood dust (Figure 5.5b).
- Since the uplifting of the post was prevented, especially at the beginning of the test, there was some beam uplifting which rapidly decreased as the stiffness of the connection decreases, being almost zero for high uplift displacements (Figure 5.5c).
- After the dismantling of the connection it was found that the screws had been deformed, although not significantly (Figure 5.5d).

a)

b)

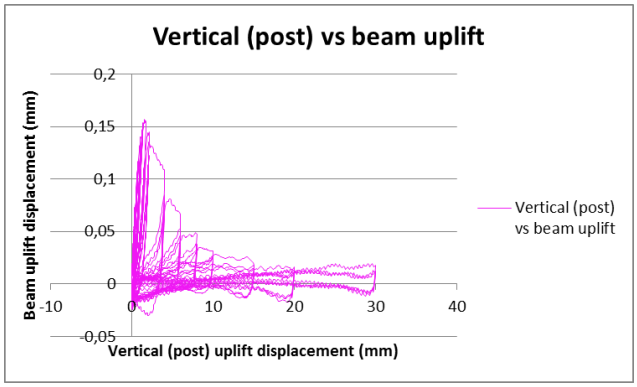

c)

d)

Figure 5.5 – a) Front side of the specimen showing the deformations of the beam, b) Back side of the specimen and the effect of the uplifted screws, c) Graph showing the presence of beam uplift, d) The screws suffered permanent deformations.

Analysis of the Force – Displacement diagram

This strengthening technique provided high stiffness and a maximum force that increased 7 times compared to the one of the unreinforced state (Figure 5.6a).

Beyond the maximum force, softening happened gradually and not abruptly as in the case of the specimen with “T” GFRP. This resulted to a gradual degradation of the stiffness, while the dissipated energy was relatively high, even though there was pinching, due to the remaining deformations of the timber elements at each step. The connection is able to work for high displacements imposed, even though there is resistance and stiffness degradation.

It should be noticed that the cyclic behavior is considerably close to the unreinforced specimen regarding the shape of the hysteresis loops (Figure 5.6b). In both cases: (1) the unloading stiffness is significantly high, being almost vertical; (2) the recovery of the displacement is accompanied by the development of compressive forces at the connections, which is particularly important in case of the retrofitted specimen; (3) the pinching behavior in the re-loading branch.

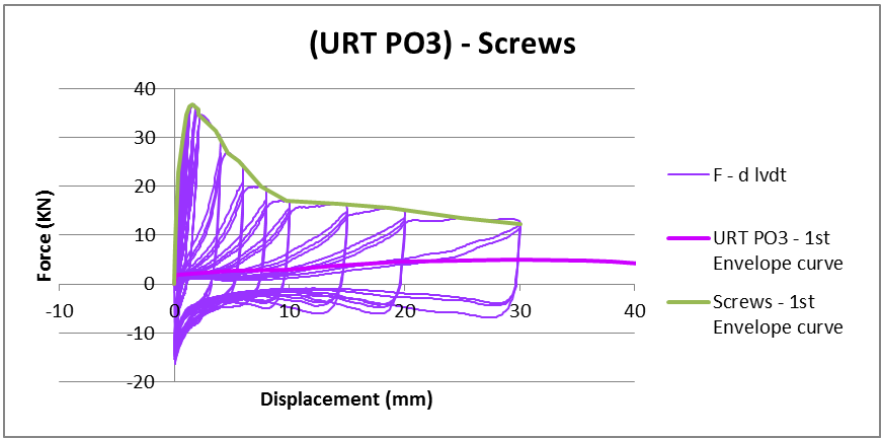

a)

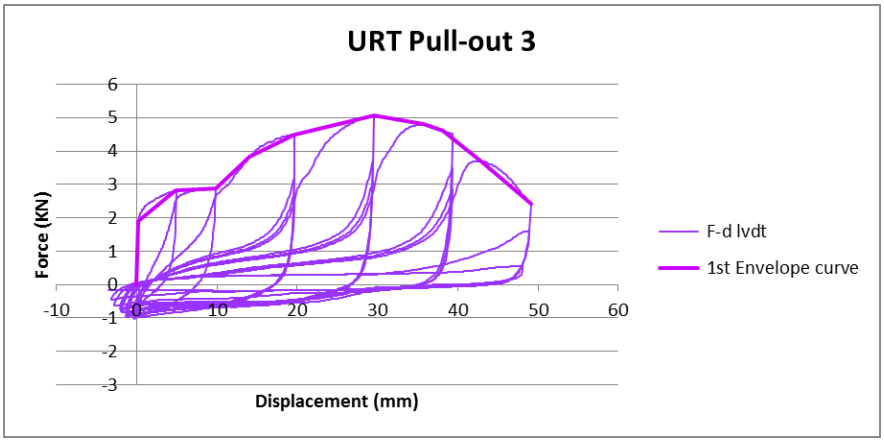

b)

Figure 5.6 - Pull-out force-displacement diagram: a) retrofitted specimen with screws; b) corresponding unreinforced specimen.

5.2.4 NSM with steel rods

Three steel rods were welded, with one of them being horizontal, and positioned into shallow grooves within each surface of the specimen. The void of the grooves was filled with gel glue (See 4.3.1.5).

Evaluation of the damage patterns

This test was not performed until the end of the procedure because the ultimate capacity of the actuator in tension was reached at 80kN (See 5.2.3).

Nevertheless, some damage occurred as in the following order:

- Splitting cracks parallel to the grain appeared above and beneath the horizontal rod in the front side of the beam (Figure 5.7a).
- Splitting cracks parallel to the grain above the beam laterally of the post and uplifting of the beam (Figure 5.7b). Due to this uplifting, the imprints of the lateral fixing plates were left upon the upper surface of the beam (Figure 5.7c-d). The uplift of the beam is the result of the huge increase on the connection stiffness. If fact, given the great stiffness of the connection, the bottom beam is submitted to bending. In this case the uplift is still increasing, even though in a

nonlinear trend, until the maximum load is reached. This should be attributed to the low level of the developed damage.


a)

b)

c)
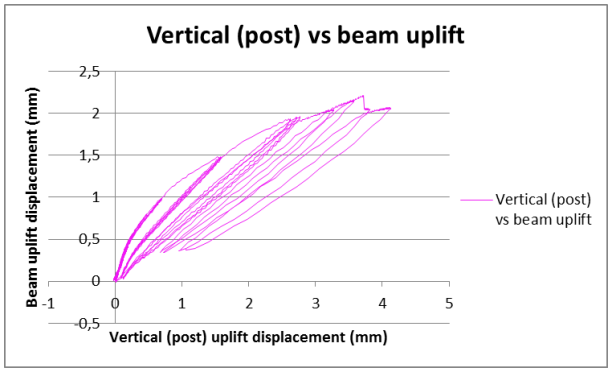

d)

Figure 5.7 – Photos a) – b) show the progressive damages of the NSM strengthened specimen during the pull-out test, d) Graph showing the presence of beam uplift.

Analysis of the Force – Displacement diagram

In this case the maximum force was acquired much earlier that the one with the steel plates, which is an indication of higher stiffness.

Regarding the maximum force of the unreinforced state, it is at least 25 times higher than the resistance of the unreinforced specimen. This value should be higher, taking into account the behavior of the connection, until the maximum force of the actuator in tension was acquired (80kN).

It is necessary to obtain a behavior with softening in order to evaluate the hysteresis loops which were still increasing until that point without any pinching effect, despite the apparent degradation of the stiffness.

An interesting feature of the cyclic force-displacement diagram of this retrofitting technique is associated to the unloading branch. The stiffness of the unloading is much lower, indicating a great level of recoverable deformation, without inducing significant compressive stresses. Exception should be made for almost zero values of the displacement.

This specimen was kept at the laboratory of the University of Minho and it will be tested in the future to obtain further information about its performance.

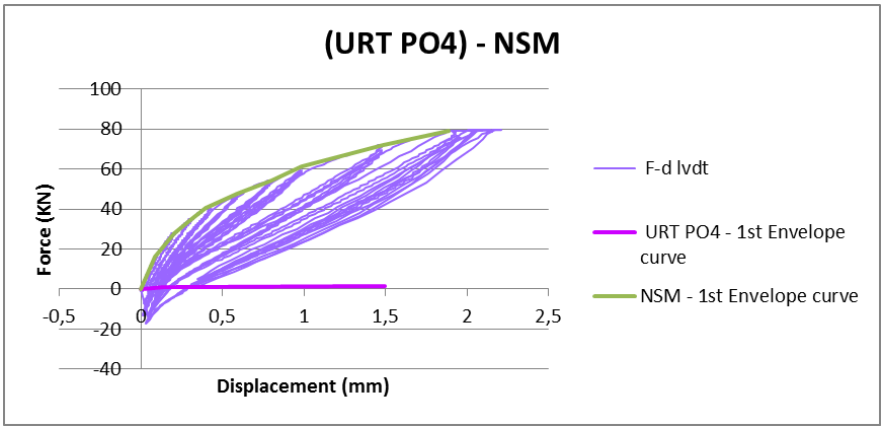

Figure 5.8 - Pull-out force-displacement diagram of the specimen with NSM strengthening.

5.2.5 Comparison of all retrofitting techniques

The first envelope curves of all the retrofitting techniques were gathered in one diagram to facilitate their comparison (Figure 5.9).

In terms of strength, an initial observation is that the techniques of NSM and steel plates surpass the other two retrofitting techniques, although their further performance is essential in order to be able to correlate them with one another and with the rest of the specimens.

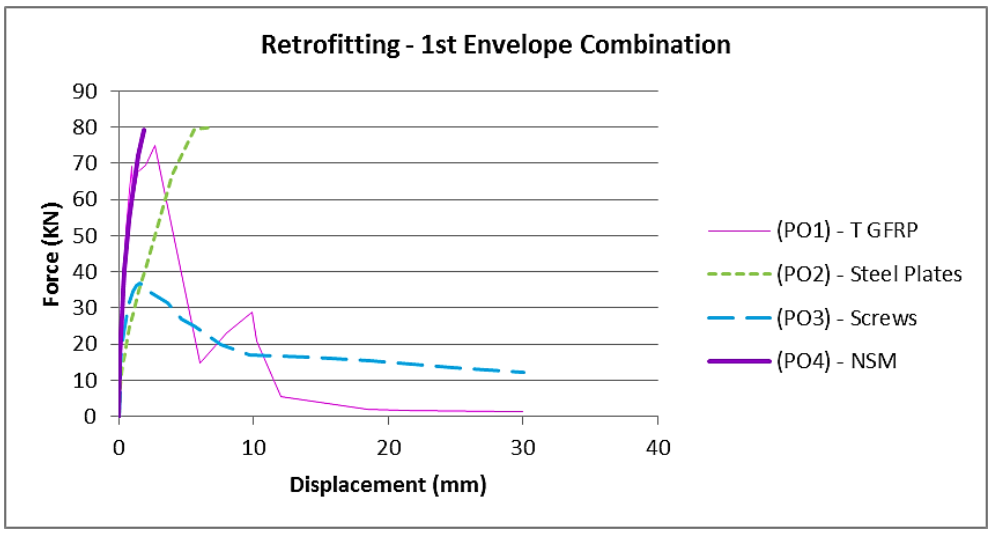

Figure 5.9 – Comparative diagram of the F-d envelope curves for all the retrofitted specimens, obtained from the pull-out tests.

The “T”GFRP solution shows abrupt force differentiations, which is associated to premature failure of the GFRP sheets. On the other hand, the solution with the screws appears to maintain a certain load capacity with small and gradual force losses. In spite of the higher resistance, the retrofitting with screws appears to be much more efficient that the GFRP sheets, at least with the configuration adopted in this work.

It is interesting to notice that until the rupture of the GFRP sheets, the monotonic envelops is practically superimposed with the envelop corresponding to the retrofitting with NSM technique.

Analysis of the Dissipated energy and stiffness

The dissipated energy for the first cycles of every step was calculated and in Figure 5.10, the accumulative dissipated energy is presented as a function of the vertical uplift. It is observed that energy dissipation increases in all cases as the vertical displacement increases.

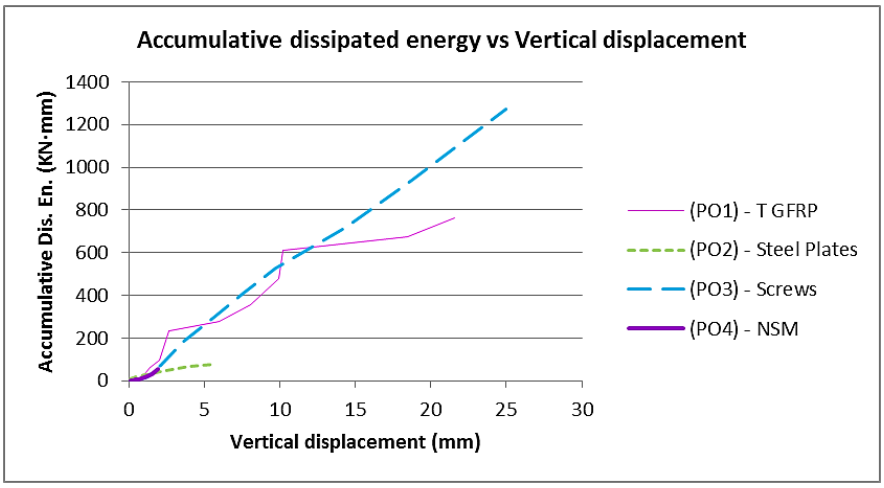

Figure 5.10 - Accumulative dissipated energy for the increasing vertical displacements of all the retrofitted specimens, obtained from the pull-out tests.

For the steel plates and the NSM solutions there is a clear trend of increasing but it is not possible to derive any conclusions from those results given the low levels of vertical displacements that were possible to be imposed.

A stable increase of the accumulative dissipated energy of the screws retrofitting technique is shown, which verifies the earlier observations, while differentiations are apparent in the case of “T” GFRP due to the abrupt changes of the force values. A clear reduction at the final displacement steps is also obvious for this case, where there was pinching with very low force values, as it was previously discussed.

The results of all the specimens were also evaluated in terms of the equivalent viscous damping ξ_{eq}, and they are presented in Figure 5.11, where it is shown that there is a clear trend for reduction of the damping after the maximum load capacity is reached. This result is related to the cases of “T” GFRP and screws, as the test was still in early stages for the other two cases.

The increasing branch at the final vertical displacement step for the case of screws is due to the increasing of the unloading forces, as there were remaining deformations. The maximum equivalent viscous damping increases in case of the retrofitting with screws, when compared to the unreinforced specimen. In case of retrofitting with GFRP sheets, there are no considerable advantages in terms of

equivalent viscous damping, particularly for high deformations. In any case, once again, it is seen that the retrofitting with screws is more favorable when compared to the retrofitting with GFRP sheets.

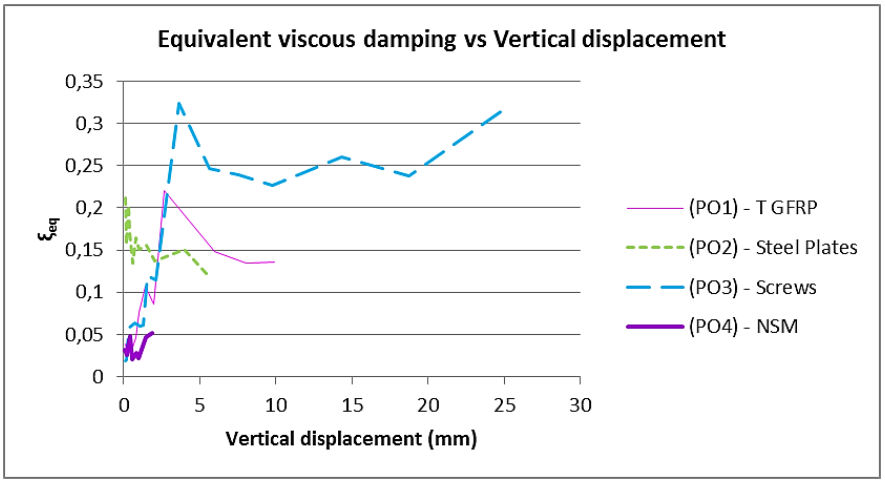

Figure 5.11 - Combination of the equivalent viscous damping graphs for all the retrofitted specimens, obtained from the pull-out tests.

The values of the initial stiffness for each strengthening case are presented in Table 5.2. It is possible to verify them through the correlation with the comparative diagram of the F-d envelope curves for all the retrofitted specimens, in Figure 5.9.

Regarding the cyclic stiffness, as expected there is a degradation which is obvious for all the strengthening cases, even for the tests that were not concluded (Figure 5.12). Gradual degradation (exponential) happens to the case of screws, while in the case of "T" GFRP this degradation does not happen in a continuous way which is verified by all the previous observations. It should be noticed that the degradation of stiffness is very similar in the cases of NSM and GFRP retrofitting techniques, at least for low levels of displacements.

Table 5.2 - Calculated initial stiffness for the first envelope curve of all the retrofitted specimens, obtained from the pull-out tests.

	Fmax	v40%Fmax	v10%Fmax	K
(PO1) - T GFRP	74,89	0,285	0,06	99,853
(PO2) - Steel Plates	79,94	1,285	0,11	20,410
(PO3) - Screws	36,72	0,168	0,018	73,440
(PO4) - NSM	79,21	0,255	0,044	112,621

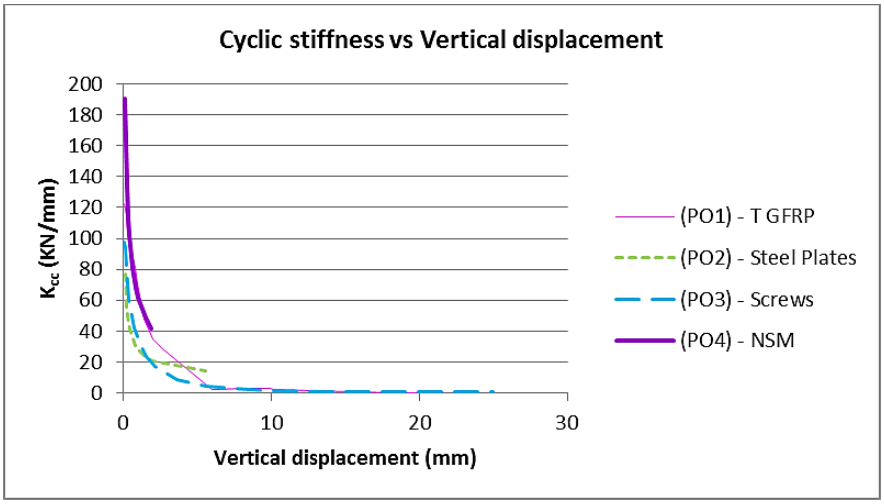

Figure 5.12 - Combination of the cyclic stiffness graphs for all the retrofitted specimens, obtained from the pull-out tests.

The difference between the values shown in Table 5.2 and the graphs in Figure 5.12 exist because the cyclic stiffness is calculated for every cycle, while initial stiffness takes into consideration the maximum force obtained from the whole test, which leads to not directly comparable results (See equations 3.6 and 3.7 in 3.6.4).

5.3 In-plane cyclic tests

The remaining 10 in-plane cyclic tests were performed cyclically and their procedure was the one that derived from the yield value of the monotonic tests, which were performed using two unreinforced specimens, one for each vertical load case (See Table 3.6).

The monitoring instrumentation consisted once more of the actuator, the computer and the LVDT's which measured the horizontal displacements and the uplifting of the post, the out-of-plane displacement and, whenever it was necessary, the uplifting at the prosthesis connection.

The tests will be discussed in groups according to the retrofitting solutions that were applied.

5.3.1 "T" GFRP

This technique was applied to four specimens: two damaged and two which were further strengthened with a wooden prosthesis that had been glued to the preexisting part of the post, while two screws were also positioned at the front side of their connected parts (See 4.3.2.1).

5.3.1.1 Damaged specimens

Evaluation of the damage patterns

During both tests, for a lower and a higher vertical load on the previously damaged unreinforced specimens, rupture of the vertical GFRP sheets occurred laterally of the intersecting points with the beam. The rupture was perpendicular to the uniaxial fibers and it happened in both the front and back

sides. As the horizontal displacements at the top of the post increased, initially, it was witnessed in one side laterally, but once the displacement changed direction, rupture appeared at the other lateral side too (Figure 5.13a-b). Eventually, it propagated towards the center until the entire width of the sheet was ruptured (Figure 5.13c). After this, the damaged timber section continued deteriorating although it was not clearly visible due to the existence of the GFRP sheets (Figure 5.13d).

It is important to comprehend that during the in-plane cyclic test, the horizontal sheet at the front side, prevents the out-of-plane displacements and the uplifting of the post, while the vertical sheets at both front and back sides are meant to also withhold the uplifting of the post. The horizontal sheet at the back of the specimen is placed in order to provide anchorage to the vertical one (Figure 5.13a-b).

The uplifting at the lower part of the post did not present any significant differentiations for the two applied vertical loads. Additionally, no considerable out-of-plane displacements were registered.

a)


b)

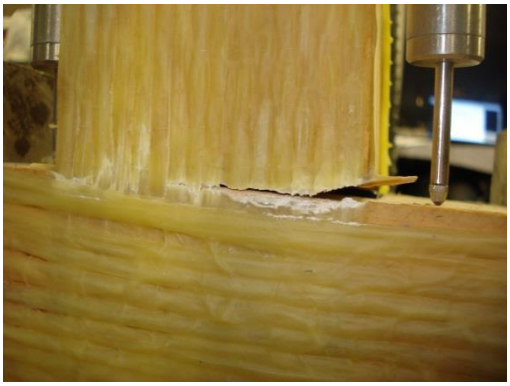
c)

d)

Figure 5.13 – Photos a) – d) show the progressive damage patterns that appeared during the in-plane cyclic tests of the damaged and strengthened with “T” GFRP specimens.

Analysis of the Force – Displacement diagrams

The two experimental force – displacement diagrams of the two specimens that were tested for different pre-compression loads are presented in Figure 5.14 (a-b). The first envelope curves of the unreinforced specimens are also shown in the graphs.

As it would be expected, a higher stiffness is visible in the case of the vertical load of 50kN due to the higher pre-compression. Both cases failed to surpass the anterior behavior of the unreinforced specimens which indicates that this strengthening technique is not adequate for the retrofitting of cases where damages are present.

Nevertheless, it is observed that for the lower vertical load, although the initial load capacity was not achieved, it was still able to maintain most of its strength and present a gradual softening, even though there was significant pinching.

On the other hand, the pinching was less due to the high pre-compressive load for the other case, but it showed a significant deterioration compared to its original strength, while rocking is evident on both sides after the displacement of 20mm was surpassed.

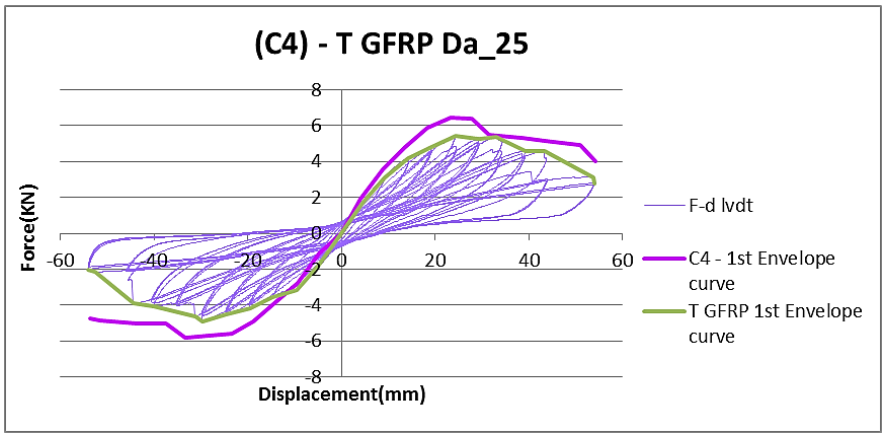

a)

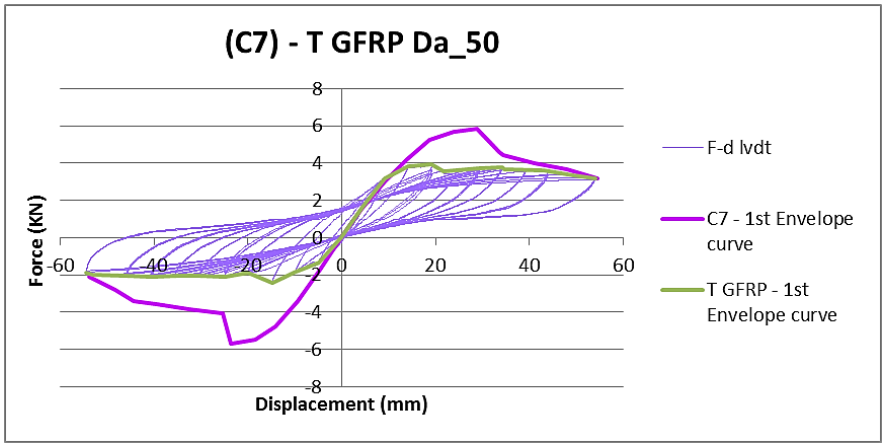

b)

Figure 5.14 – F-d graph for the strengthened with “T” GFRP specimens, which were subjected to in-plane cyclic tests and had: a) a vertical load of 25kN and b) a vertical load of 50kN.

5.3.1.2 Specimens with prosthesis

Evaluation of the damage patterns

Since there were differences at the damage patterns between the two applied vertical loads, they will be discussed separately.

Vertical load of 25kN

There was rupture of the vertical GFRP sheet perpendicular to the uniaxial fibers on the back side at the intersecting point between post and beam, which propagated through the width of the sheet (Figure 5.15a). In the front side, rupture of the horizontal GFRP sheet appeared perpendicular to the uniaxial fibers due to some initial out-of-plane clearances (Figure 5.15b).

Additionally on the 6th step (29,85mm), there was a separation between the prosthesis part and the older part of the post on both lateral sides (Figure 5.15c). After this point, fundamentally the connection between the post and the prosthesis part was being tested, instead of the actual connection between the post and beam parts (Figure 5.15d).

a)

b)

c)

d)

Figure 5.15 - Photos a) – d) show the progressive damage patterns that appeared during the in-plane cyclic tests of the strengthened with prosthesis and “T” GFRP specimens for a vertical load of 25kN.

Vertical load of 50kN

Some of the damages that were previously mentioned for the lower vertical load case, appeared here as well (Figure 5.15a-b). Furthermore, there were two vertical sliding cracks parallel to the vertical GFRP sheet fibers one at the front and one at the back side of the post between the screws that connect the preexisting post part to the prosthesis, which progressed (Figure 5.16a).

The glue between the post and the prosthesis failed laterally of the post on both sides and there was debonding of the vertical GFRP sheet at the back side of the post (Figure 5.16b).

A snapping crack perpendicular to the grain of the wood appeared laterally of the post at the intersection between post and beam (Figure 5.16c).

Finally, a big triangular like part of the prosthesis failed with two vertical, sliding cracks; one at the front and one at the right side. The previously mentioned part was still attached to the preexisting post. After this point the part that failed was only rocking, while the remaining prosthesis member was not working anymore (Figure 5.16d-f).

Figure 5.16 - Photos a) – e) show the progressive damage patterns that appeared during the in-plane cyclic tests of the strengthened with prosthesis and “T” GFRP specimens for a vertical load of 50kN.

Analysis of the Force – Displacement diagrams

It is possible to compare the two force – displacement graphs of the two specimens that were tested for different pre-compression loads in Figure 5.17 (a-b). The first envelope curves of the unreinforced specimens are also shown in the graphs.

A first observation is that the overall capacity was raised for both specimens in terms of strength and maximum load, which was almost 1,7 times higher for both cases, as well as in terms of stiffness.

After the failure of the prosthesis connection, the force is diminished in both cases, but for the higher pre-compressive load the strength still remains higher than that of the unreinforced case and with less pinching in the hysteresis loops.

For the lower vertical load, it is not realistic to derive conclusions from the results that correspond to the displacement steps beyond the failure of the prosthesis connection, since after that, the actual connection between the post and beam parts was no longer being tested (Figure 5.15d).

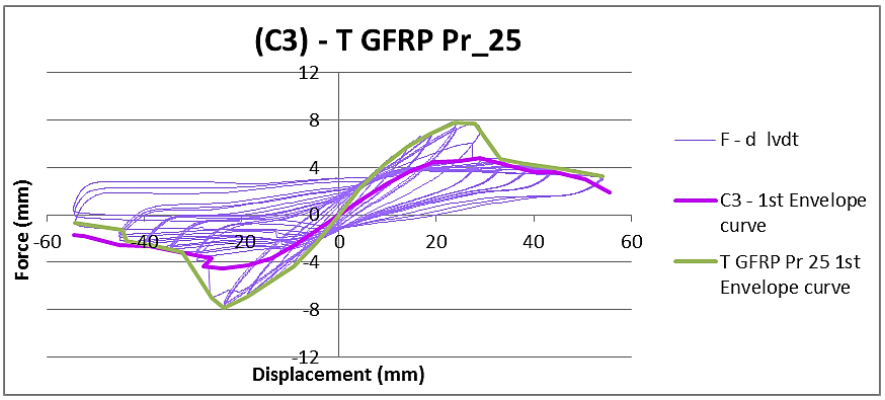

a)

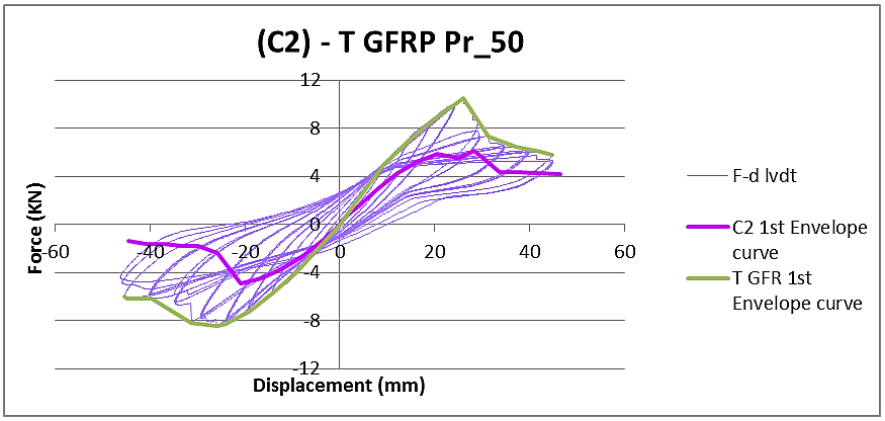

b)

Figure 5.17 - F-d graph for the strengthened with prosthesis and “T” GFRP specimens, which were subjected to in-plane cyclic tests and had: a) a vertical load of 25kN and b) a vertical load of 50kN.

Comparison of the Force – Displacement diagrams for all the specimens with "T" GFRP strengthening

A comparison among the first envelope curves of all the specimens that were retrofitted with the "T" GFRP solution (Figure 5.18) could lead to the conclusions that uniaxial GFRP sheets cannot reinforce members which are meant to undergo flexure. In the case of prosthesis it was not the "T" GFRP that worked as the vertical sheets ruptured, while the prosthesis solution appeared to perform well only in the case of higher pre-compression load. Nevertheless, the solution of prosthesis seems to not present a good mechanical behavior for displacements further than 25±5mm.

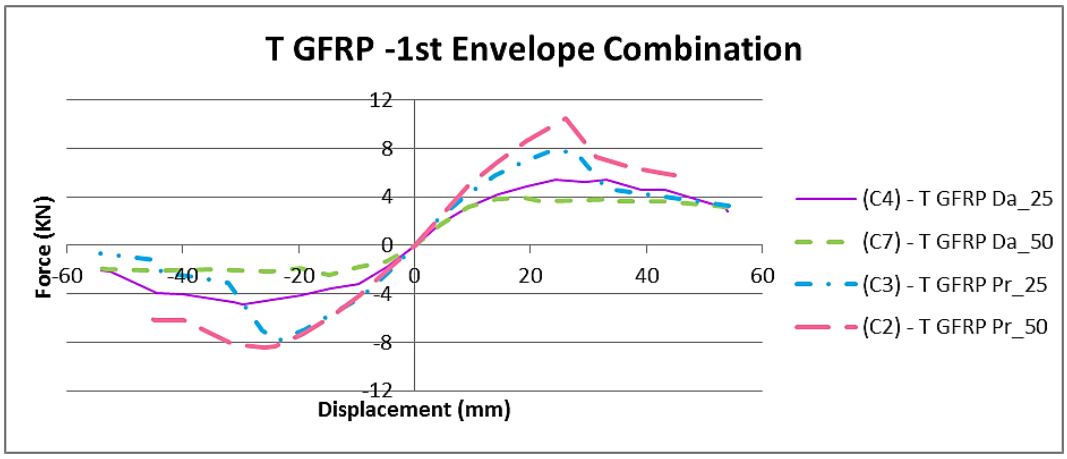

Figure 5.18 - Comparative diagram of the F-d envelope curves for all the retrofitted with "T" GFRP specimens, which were subjected to in-plane cyclic tests.

Analysis of the Dissipated energy and stiffness

In terms of accumulative dissipated energy correlated to the drift percentage (Figure 5.19), as expected, it is higher for the specimens with prosthesis.

A large part of the branch concerning the prosthesis reinforced specimen with lower vertical load cannot be taken into consideration, as the studied connection between post and beam had stopped working.

Among the two damaged and retrofitted with "T" GFRP sheets specimens, the one with higher vertical load appears to have high accumulative dissipated energy, which is due to the decreased pinching that it had, compared to the one with a vertical load of 25kN. Nevertheless, the latter had an overall better performance in terms of strength, as it was previously discussed.

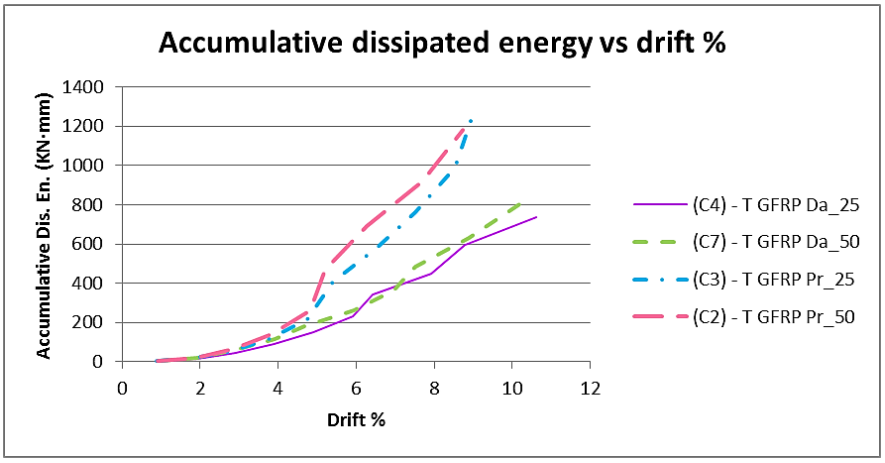

Figure 5.19 - Comparative diagram of the accumulative dissipated energy – drift % for all the retrofitted with "T" GFRP specimens, which were subjected to in-plane cyclic tests.

The results of all the specimens were also evaluated in terms of the equivalent viscous damping ξ_{eq} (Figure 5.20).

An increase is apparent for all the strengthened specimens. Among the damaged retrofitted specimens, the higher values of the equivalent viscous damping correspond to the one with the higher pre-compression load and thus, less pinching. A clear decreasing trend is evident once the maximum capacity is surpassed and rocking was present.

In a similar manner, both cases that were tested with a lower vertical load presented pinching so the corresponding equivalent viscous damping for them is inferior.

A part of the branch related to the specimen with the prosthesis and lower vertical load, is not realistic, as the studied connection between post and beam had stopped working.

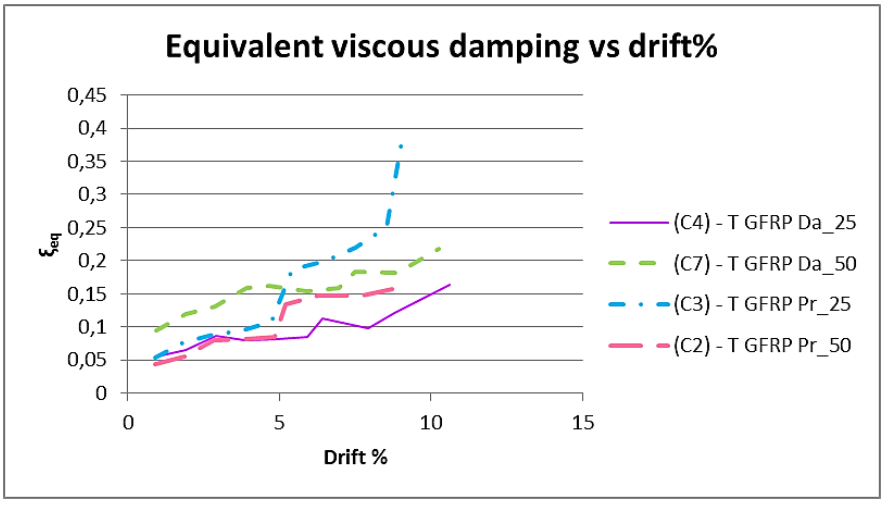

Figure 5.20 - Comparative diagram of the equivalent viscous damping – drift % for all the retrofitted with "T" GFRP specimens, which were subjected to in-plane cyclic tests.

Additionally, the degradation of the cyclic stiffness is clearly shown in Figure 5.21. As expected, higher degradation happened to the damaged specimens that had the lower initial cyclic stiffness values.

One more observation is that the initial cyclic stiffness of the retrofitted with prosthesis and “T” GFRP specimen, which was tested for the higher vertical load value, is the highest as it could have been foreseen.

There is a distinctive correlation between this diagram and the one in Figure 5.18. Furthermore, the calculated values of the initial stiffness for all the retrofitted with “T” GFRP specimens, which are presented in Table 5.3 are also verified through this comparison.

Once more a part of the branch related to the specimen with the prosthesis and the lower vertical load should not be taken into consideration.

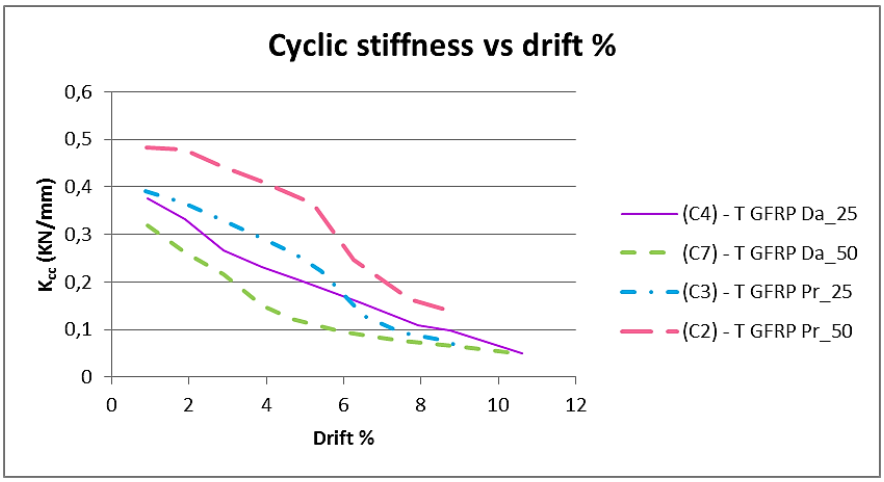

Figure 5.21 - Comparative diagram of the cyclic stiffness – drift % for all the retrofitted with “T” GFRP specimens, which were subjected to in-plane cyclic tests.

Table 5.3 - Calculated initial stiffness for the first envelope curve of all the retrofitted with “T” GFRP specimens, which were subjected to in-plane cyclic tests.

Specimen		Fmax	v40%Fmax	v10%Fmax	K (kN/mm)	mean K (KN/mm)
(C4) - T GFRP Da_25	(+)	5,43	5,75	1,01	0,344	0,346
	(-)	4,89	5,13	0,93	0,349	
(C7)- T GFRP Da_50	(+)	3,96	4,185	0,745	0,345	0,313
	(-)	2,12	2,27	0,01	0,281	
(C3) - T GFRP Pr_ 25	(+)	7,82	6,13	1,23	0,479	0,479
	(-)	7,88	6,275	1,34	0,479	
(C2) - T GFRP Pr_50	(+)	10,46	7,6	1,885	0,549	0,491
	(-)	8,47	7,695	1,815	0,432	

5.3.2 Steel Plates

This strengthening technique was applied on two specimens that had already been retrofitted with a prosthesis. One of them was tested with an applied vertical load of 25kN and the other with 50kN.

Evaluation of the damage patterns

As different damage patterns were observed the tests will be discussed separately in terms of vertical load values.

Vertical load of 25kN

During the 4th displacement step (19.90mm) the preexisting post was detached from the glued prosthesis member laterally on both sides (Figure 5.22a-b). After that, only the connection between the preexisting post part and the prosthesis was tested, while the remaining part of the prosthesis and its connection to the beam remained undeformed until the test was completed (Figure 5.22c,f).

The only damages that were observed at the prosthesis member after it was dismantled, were some vertical sliding cracks at the positions of the screws at the front of the post and a detached part which had remained glued at the connection with the preexisting post (Figure 5.22d).

An important finding was the significant lack of gel glue at the inner part of the connection between the prosthesis and the preexisting post (Figure 5.22e).

a)

b)

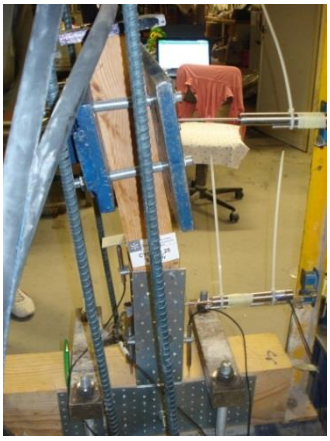
c)


d)

e)

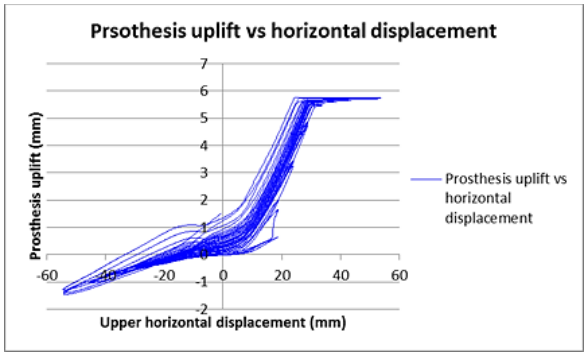

f)

Figure 5.22 - Photos a) – e) show the progressive damage patterns that appeared during the in-plane cyclic tests of the strengthened with prosthesis and steel plates specimens for a vertical load of 25kN, f) Graph showing the lateral uplift of the prosthesis.

Vertical load of 50kN

In this case, while the test was in progress, vertical sliding cracks parallel to the grain were observed at the lateral sides of the prosthesis. Additionally, the vertical steel plates were bending in and out-of-plane and a snapping crack occurred laterally of the prosthesis at the left side of the intersection with the beam (Figure 5.23a).

After the completion of the test, the plates were removed and the connection was dismantled. Permanent deformations were witnessed at the vertical plates (Figure 5.23b), while no apparent deformation existed on the horizontally positioned plates.

It should be noted that during the in-plane cyclic test, the horizontal steel plate at the front side, prevents the out-of-plane displacements and the uplifting of the post, while the vertical steel plates at both front and back sides are meant to also withhold the uplifting of the post. The horizontally positioned steel plate at the back of the specimen is helping towards better distribution of the stresses and anchorage.

Other than that, there were damages on the “tenon” part of the prosthesis that resembled the damage patterns of the unreinforced specimens that were subjected to in-plane cyclic tests, although the degree of permanent deformations was smaller (See 3.7.4) (Figure 5.23c).


a)

b)


c)

Figure 5.23 - Photos a) – c) show the progressive damage patterns that appeared during the in-plane cyclic tests of the strengthened with prosthesis and steel plates specimens for a vertical load of 50kN.

Analysis of the Force – Displacement diagrams

Concerning the diagram of the specimen which was tested for a lower vertical load value (Figure 5.24a), it is realistic to consider only the first 4 displacement steps as the connection stopped working beyond that point, which is the point corresponding to the maximum force value. Nevertheless, until the failure of the prosthesis connection, the strengthening presented a considerably better behavior than the unreinforced specimen in terms of maximum load capacity and stiffness, especially for the displacements towards the left direction, which exceeded its previous corresponding load value by 1,7 times.

The stiffness provided by the steel plates strengthening contributed to the increased stiffness and the absence of pinching effect.

For the case with the higher vertical load, a behavior with softening was achieved (Figure 5.24b), as the prosthesis member did not fail. The previous monotonic load capacity was surpassed by 0,80kN but once the 7th step (34.83mm) was reached, there was a constant load decrease in consequence of the plastic deformation of the steel plates.

Additionally, it could be mentioned that the hysteresis loops were wide without pinching until the completion of the test due to the high pre-compression level.

A comparison between the two specimens, until the point where the prosthesis connection failed, indicates the same stiffness at the first cycle, which was provided by the steel plates.

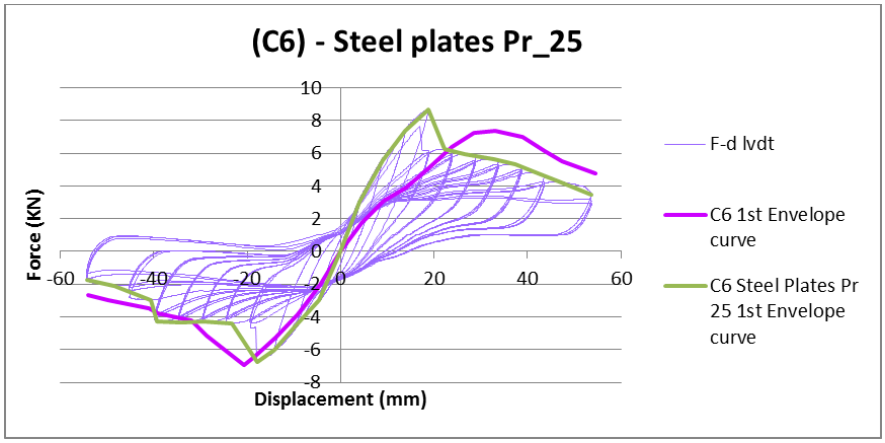

a)

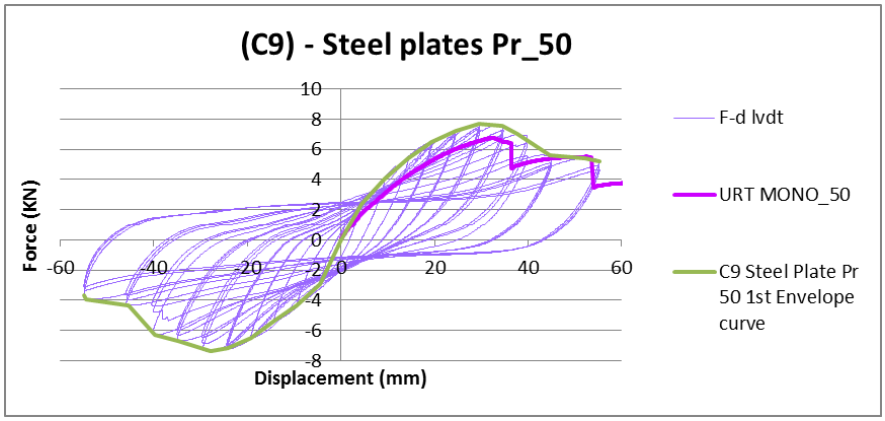

b)

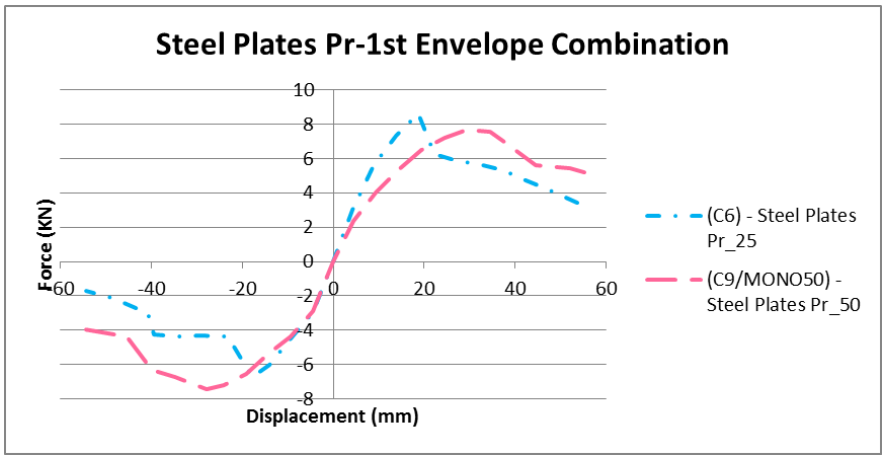

c)

Figure 5.24 - F-d graph for the strengthened with prosthesis and steel plates specimens, which were subjected to in-plane cyclic tests and had: a) a vertical load of 25kN and b) a vertical load of 50kN, c) Comparative diagram of their F-d envelope curves.

Analysis of the Dissipated energy and stiffness

A clear comparison among the two specimens is not realistic as the prosthesis connection failed during the 4th step of the test with the lower vertical load.

However, the comparative graphs for the accumulative dissipated energy, equivalent viscous damping and cyclic stiffness correlated to the lateral drift percentage, are given in Figure 5.25a-c. The failure of the prosthesis connection occurred at a drift of 4%.

Respectively, a gradual increase of the accumulative dissipated energy is observed, while there is a trend for increase of the equivalent viscous damping as well, which would be expected after the evaluation of the results in the previous cases, unreinforced and retrofitted that were tested in a similar way.

The gradual degradation of the cyclic stiffness is evident, while the higher cyclic stiffness concerning the first four steps, of the specimen with the lower vertical value is verified by the comparison with the graph in Figure 5.24c. The calculated values of the initial stiffness for all the retrofitted with steel plates specimens, which are presented in Table 5.3 are also verified through this comparison.

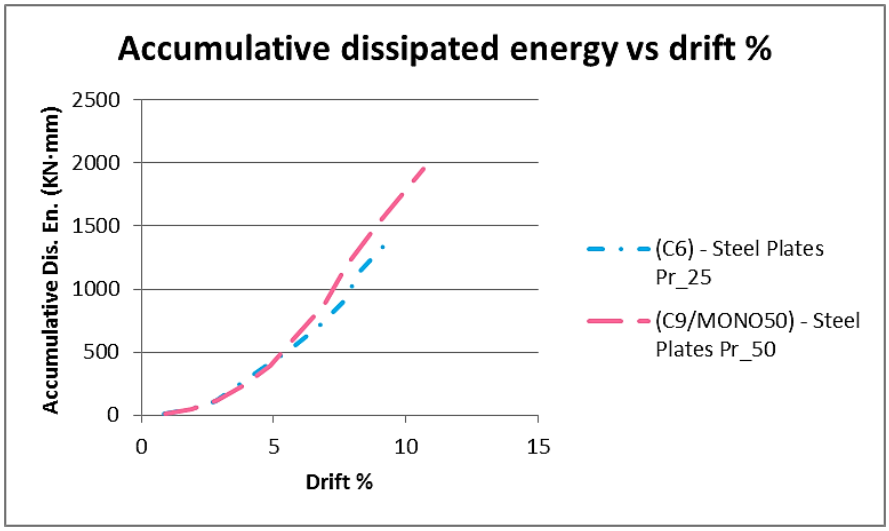

a)

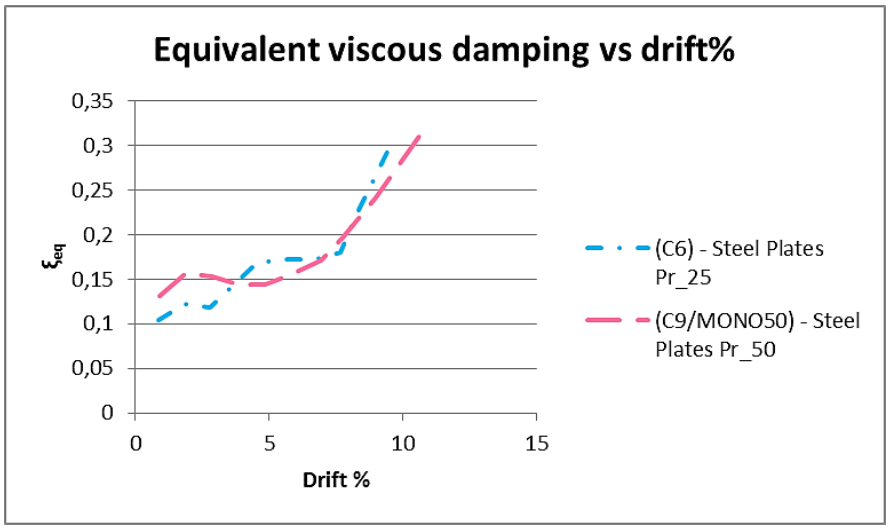

b)

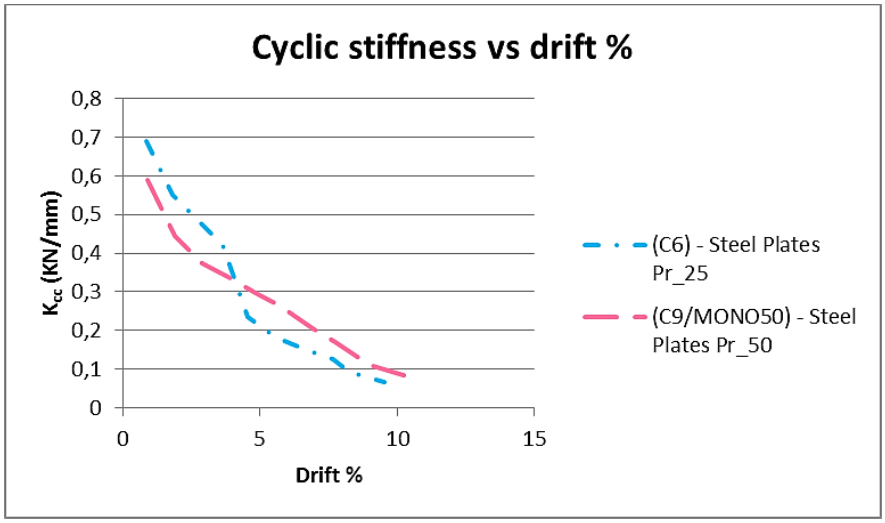

c)

Figure 5.25 - Comparative diagram of: a) the accumulative dissipated energy – drift%, b) the equivalent viscous damping – drift%, c) the cyclic stiffness – drift % for all the retrofitted with prosthesis and steel plates specimens, which were subjected to in-plane cyclic tests.

Table 5.4 - Calculated initial stiffness for the first envelope curve of the retrofitted with prosthesis and steel plates specimens, which were subjected to in-plane cyclic tests.

Specimen		Fmax	$v_{40\%Fmax}$	$v_{10\%Fmax}$	K (kN/mm)	mean K
(C6) - Steel Plates Pr_25	(+)	8,64	4,525	0,775	0,691	0,616
	(-)	6,73	3,68	-0,05	0,541	
(C9/MONO50) - Steel Plates Pr_50	(+)	7,67	5,9	0,65	0,438	0,486
	(-)	7,4	3,513	-0,645	0,534	

5.3.3 NSM with steel rods

This strengthening technique was applied on two specimens that had already been retrofitted with a prosthesis. Both of the specimens were tested with an applied vertical load of 50kN in order to avoid the previously observed failure of the prosthesis connection.

Evaluation of the damage patterns

During the test, cracks were observed on the surface of the NSM filling glue (Figure 5.26a).

Even though a higher vertical load was applied, the failure at the prosthesis connection was not prevented. During the displacement of the 4th step (19.90mm) the glued preexisting post, detached laterally from the prosthesis on both sides. Note that in this case the paste glue type was used (Figure 5.26b). After that, only the connection between the preexisting post part and the prosthesis was tested.

At the top of the prosthesis member at the front cracks parallel to the grain appeared, between the screws and eventually there was crashing at that part (Figure 5.26c).


a)


b)

c)

Figure 5.26 - Photos a) – c) show the progressive damage patterns that appeared during the first in-plane cyclic test of the strengthened with prosthesis and NSM steel rods specimens for a vertical load of 50kN.

Since it was noticed that the application of a higher vertical load does not ascertain preventing the prosthesis connection failure, it was decided to place two steel plates with prefabricated hole patterns laterally of the post and fix them with screws above and underneath the connection.

However, the prosthesis connection failed and after that, the plates prevented further opening of the connection and deterioration. The NSM continued working only towards the right side of the cycle since the glue had not failed completely on that side (Figure 5.27a-b).

For higher displacement steps, the NSM worked again for a while and snapping cracks occurred laterally of the post at the intersection with the beam (Figure 5.27c).

Permanent deformations were also evident at the steel plates after the test completion.


a)

b)

c)

Figure 5.27 - Photos a) – c) show the progressive damage patterns that appeared during the second in-plane cyclic test of the strengthened with prosthesis and NSM steel rods specimens for a vertical load of 50kN.

Analysis of the Force – Displacement diagrams

It is more realistic to discuss the behavior of the strengthening until the 4th step, because this is when the prosthesis failed in both cases (Figure 5.28a-b), although in the second specimen it is obvious that the strengthening continued working for displacements towards the right direction (3rd quadrant – negative values) (Figure 5.28b).

In both cases the overall behavior was better in terms of strength and stiffness, while the maximum load for the final displacement value of the 4th step was higher by 1,8 and 1,9 times, respectively. It could also be mentioned that no pinching was observed.

A comparison among the first envelope curves of the two retrofitted cases (Figure 5.28c), indicates a higher maximum load capacity for the second specimen which could be attributed to the positioning of the steel plates laterally of the post.

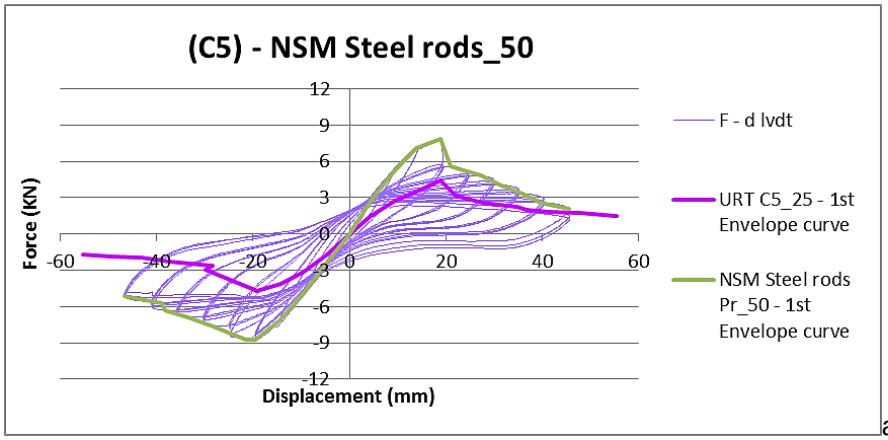

a)

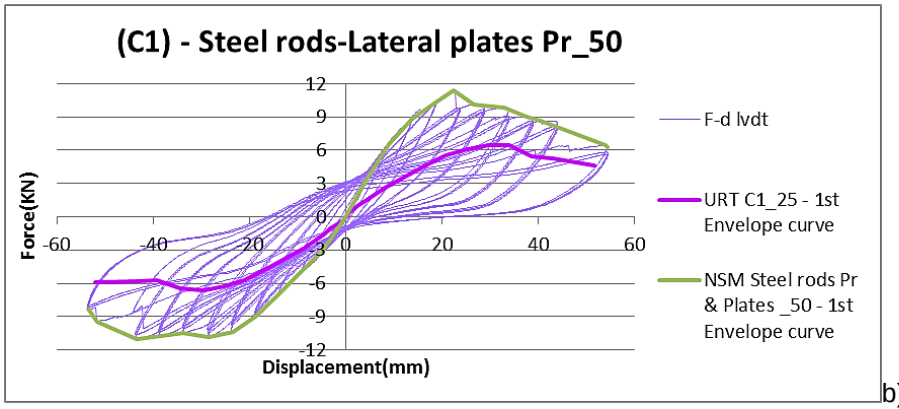

b)

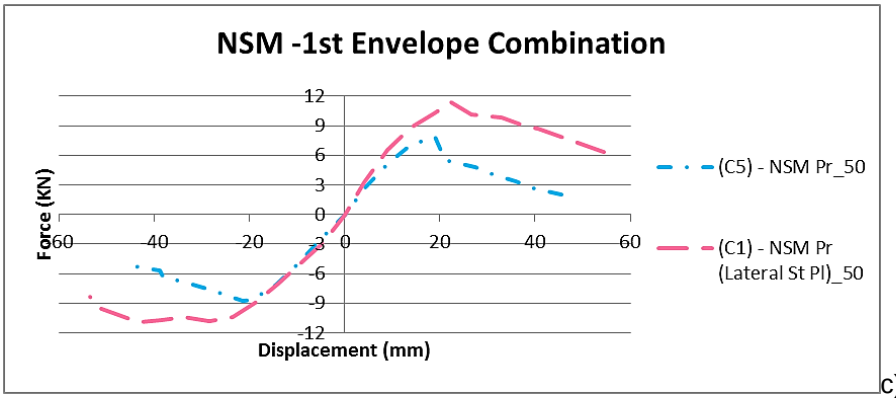

c)

Figure 5.28 – a)-b) F-d graphs for the strengthened with prosthesis and NSM steel rods specimens, which were subjected to in-plane cyclic tests with a vertical load of 50kN.(Case b) with lateral steel plates, c) Comparative diagram of their F-d envelope curves.

Analysis of the Dissipated energy and stiffness

A clear comparison among the two specimens is not realistic as the prosthesis connection failed during the 4th displacement step for both tests.

However the comparative graphs for the accumulative dissipated energy, equivalent viscous damping and cyclic stiffness correlated to the lateral drift percentage, are given in Figure 5.29a-c. The failure of the prosthesis connection occurred at a drift of 4%. The latter can explain the differences that are apparent in the graphs b) and c) of Figure 5.29 after that point.

Once more, there is an increase for the accumulative dissipated energy, as well as the equivalent viscous damping and progressive degradation of the cyclic stiffness. The higher cyclic stiffness of the specimen with the laterally placed steel plates is verified by the comparison with the graph in Figure 5.28c. The calculated values of the initial stiffness for all the retrofitted with NSM steel rods specimens, which are presented in Table 5.5 are also verified through this comparison.

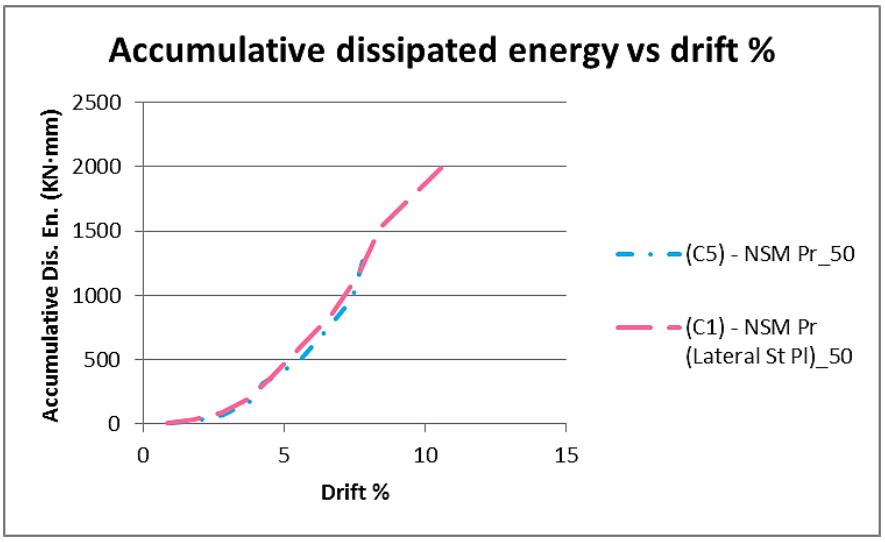

a)

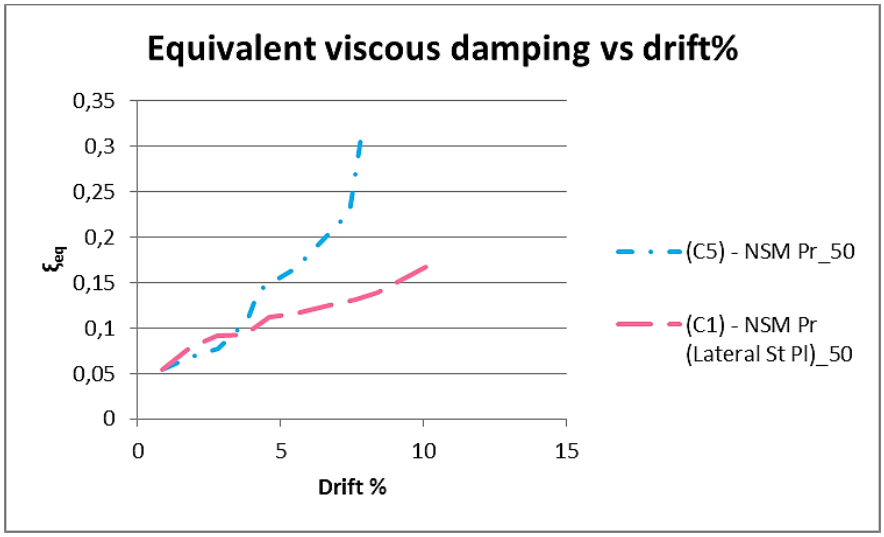

b)

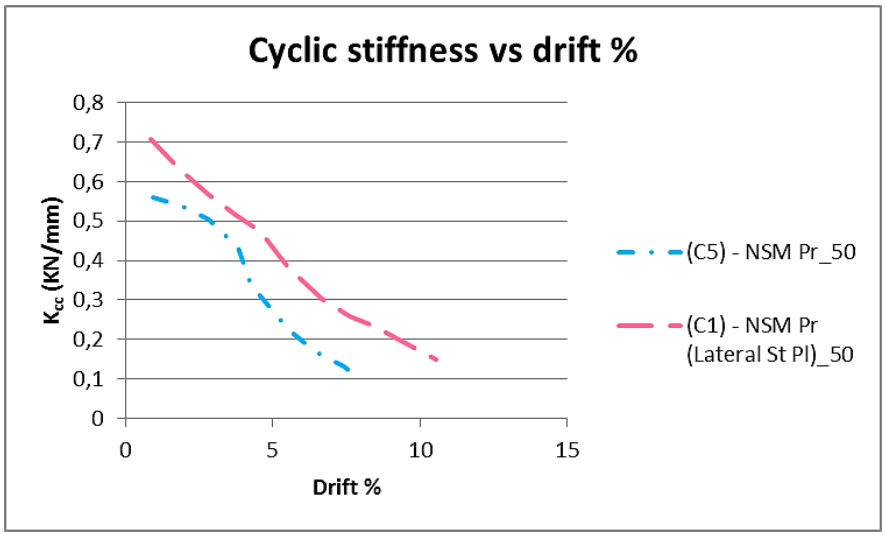

c)

Figure 5.29 - Comparative diagram of: a) the accumulative dissipated energy – drift%, b) the equivalent viscous damping – drift%, c) the cyclic stiffness – drift % for all the retrofitted with prosthesis and NSM steel rods specimens, which were subjected to in-plane cyclic tests.

Table 5.5 - Calculated initial stiffness for the first envelope curve of the retrofitted with prosthesis and NSM steel rods specimens, which were subjected to in-plane cyclic tests.

Specimen		Fmax	v40%Fmax	v10%Fmax	K (kN/mm)	mean K (KN/mm)
(C5) - NSM Pr_50	(+)	7,85	4,71	0,933	0,624	0,590
	(-)	8,77	6,35	1,63	0,557	
(C1) - NSM Pr (Lateral St Pl)_50	(+)	11,4	5,43	0,385	0,678	0,599
	(-)	10,86	7,355	1,095	0,520	

5.3.4 GFRP sheets and CFRP strips wrapped

Finally, this strengthening technique was applied on two specimens; one damaged and one that had already been retrofitted with a prosthesis. Each specimen was reinforced laterally with GFRP sheets and its section was wrapped in two positions with CFRP strips. Additionally, a single bolt fixes the overlapped connection (See 4.3.2.2).

Both of the specimens were tested with an applied vertical load of 50kN in an attempt to avoid the previously observed failure of the prosthesis connection.

After the completion of the in-plane cyclic tests, these specimens were meant to be tested further with the pull-out procedure.

Evaluation of the damage patterns

The same patterns were manifested during the tests for both specimens.

Specifically, there was rupture of the GFRP sheets, perpendicular to their fibers, at the intersecting points between the post and beam (Figure 5.30a). This occurred earlier for the case of the damaged specimen (4^{th} step – 19.90mm), which could lead to the assumption that the existence of prosthesis contributed to the withstanding of bigger displacements.

Subsequently, snapping cracks were observed laterally of the post at the intersecting points with the beam on both sides, which propagated perpendicular to grain (Figure 5.30b). For the case of the damaged specimen, those cracks already existed to a certain extension, but there was further propagation (Figure 5.30c).

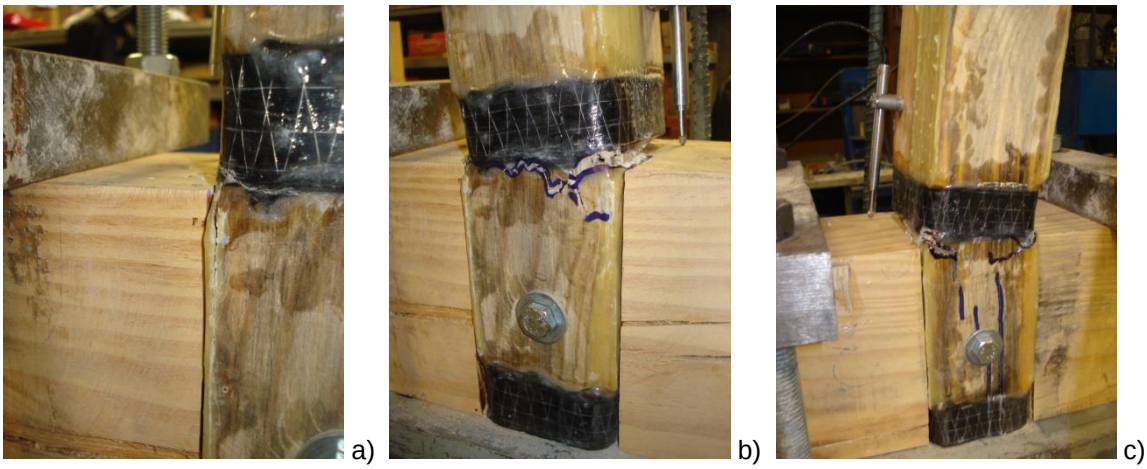
a) b) c)

Figure 5.30 - Photos a) – c) show the progressive damage patterns that appeared during the in-plane cyclic test, for a vertical load of 50kN, of the strengthened with GFRP sheets and CFRP strips wrapped specimens: a), b) with a prosthesis, c) damaged.

Analysis of the Force – Displacement diagrams

Regarding the overall behavior of the previously damaged, retrofitted specimen , no remarkable improvement is observed, apart from the stiffness, provided by the strengthening at the first cycle (Figure 5.31a). Other than that, there was mainly rocking after the GFRP rupture.

Better results were given, for the case of prosthesis, which contributed in order to withstand bigger displacements, without concurrent loss of load capacity (Figure 5.31b), while there was a surpassing in terms of stiffness and maximum load than the previously performed monotonic test (for a vertical load of 25kN). The latter was exceeded by 1,2 times. The effect of rocking and pinching is obvious during the propagation of the snapping cracks, perpendicular to the grain.

A comparison among them (Figure 5.31c) shows higher stiffness, as well as maximum load capacity for the case with the prosthesis. Additionally, larger hysteresis loops are observed as they would be expected for the case of prosthesis.

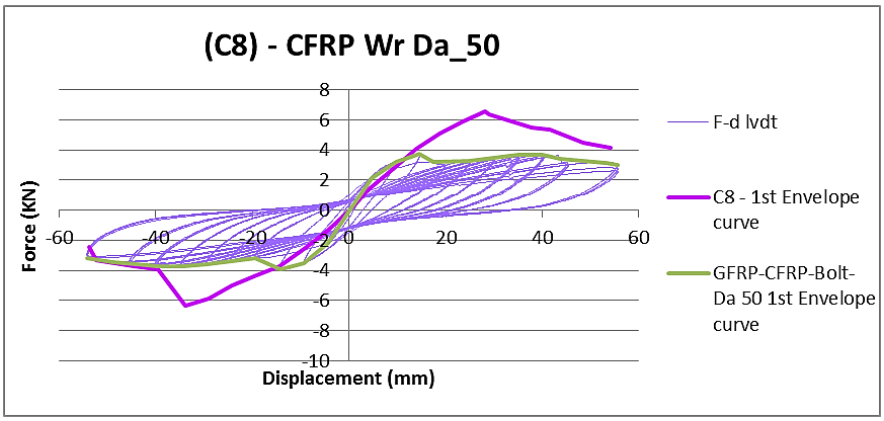

a)

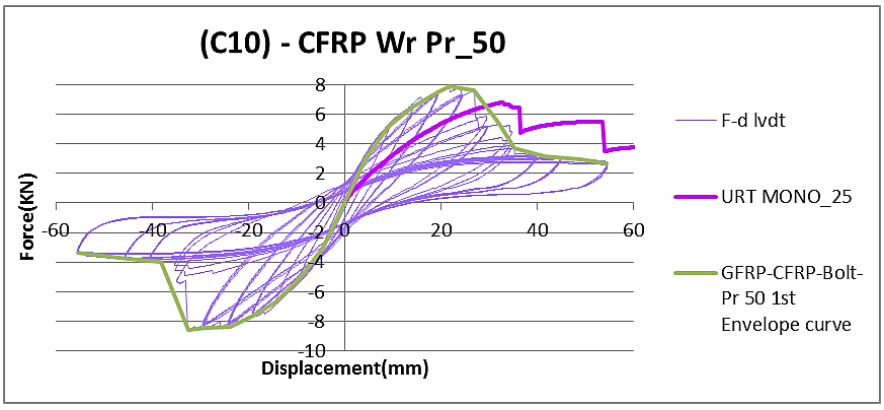

b)

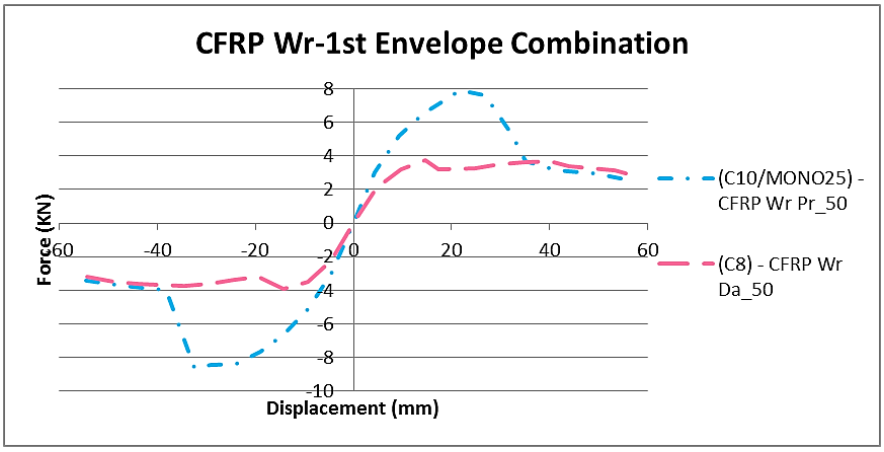

c)

Figure 5.31 – a)-b) F-d graphs for the strengthened with GFRP sheets and CFRP strips wrapped specimens, which were subjected to in-plane cyclic tests with a vertical load of 50kN.(Case b) with a prosthesis, c) Comparative diagram of their F-d envelope curves.

Analysis of the Dissipated energy and stiffness

It is more realistic to take into consideration the results of the damaged specimen until the 4th displacement step (19.90mm) because the retrofitting technique stopped being effective after that point.

The comparative graphs for the accumulative dissipated energy, equivalent viscous damping and cyclic stiffness correlated to the lateral drift percentage, are given in Figure 5.32a-c. The failure of the strengthening technique for the damaged specimen occurred at a drift of 4%. The latter can explain the differences that are apparent in all the graphs after that point.

As expected after the analysis of all the previous retrofitted and unreinforced cases for the in-plane cyclic tests, there is an increase for the accumulative dissipated energy, as well as the equivalent viscous damping and progressive degradation of the cyclic stiffness.

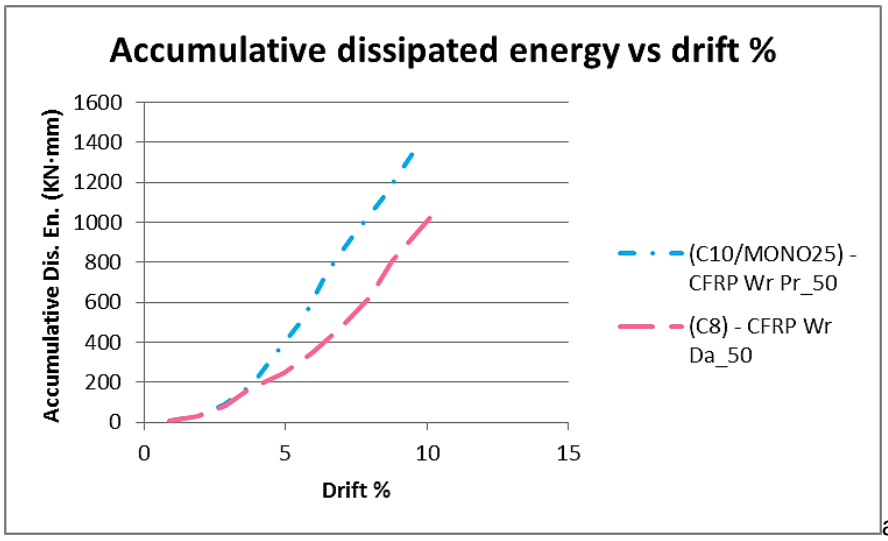

a)

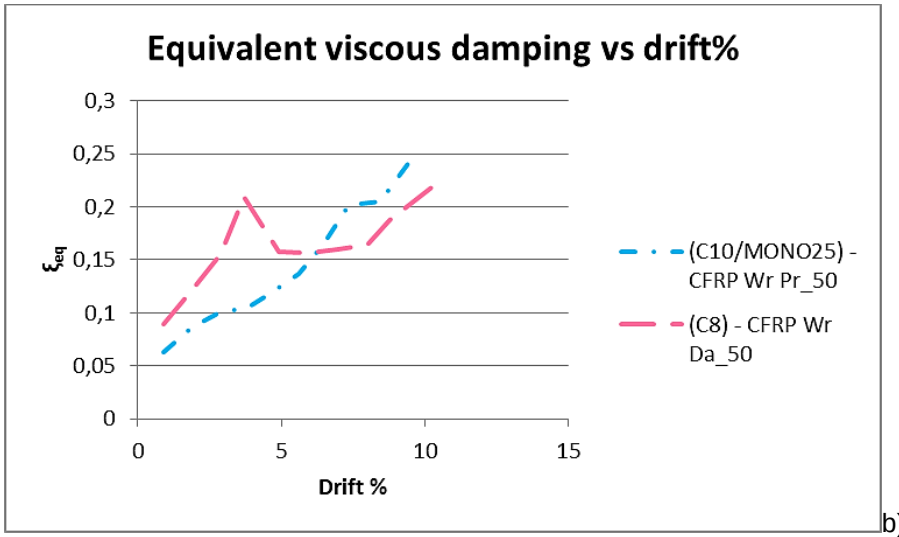

b)

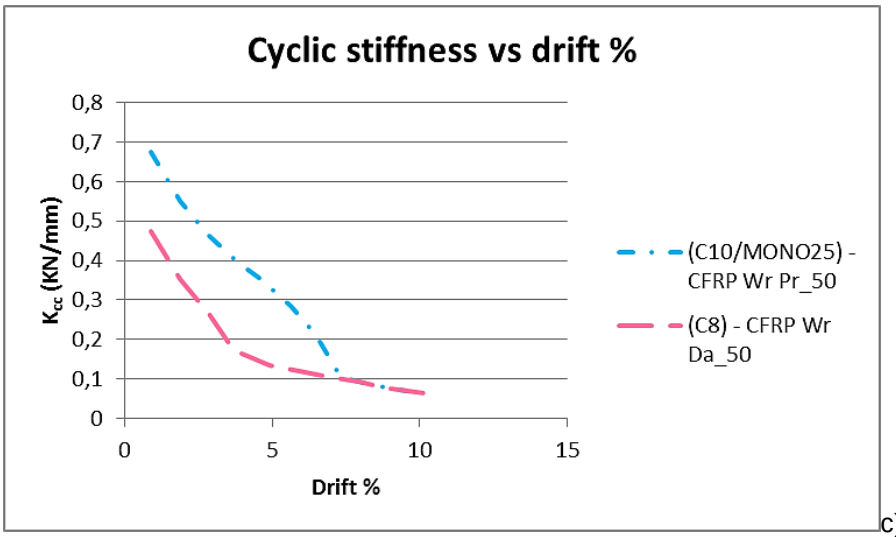

c)

Figure 5.32 - Comparative diagram of: a) the accumulative dissipated energy – drift%, b) the equivalent viscous damping – drift%, c) the cyclic stiffness – drift % for all the retrofitted with GFRP sheets and CFRP strips wrapped specimens, which were subjected to in-plane cyclic tests.

The higher accumulative dissipated energy, as well as cyclic stiffness of the specimen with the prosthesis member is verified by the comparison with the graph in Figure 5.28c. The calculated values of the initial stiffness for all the retrofitted with GFRP sheets and CFRP strips wrapped specimens, which are presented in Table 5.6 are also verified through this comparison.

Table 5.6 – Calculated initial stiffness for the first envelope curve of all the retrofitted with GFRP sheets and CFRP strips wrapped specimens, which were subjected to in-plane cyclic tests.

Specimen		Fmax	v40%Fmax	v10%Fmax	K (kN/mm)	mean K (KN/mm)
(C10/MONO25) - CFRP Wr Pr_50	(+)	7,91	4,1	0,705	0,699	0,686
	(-)	8,6	4,555	0,726	0,674	
(C8) - CFRP Wr Da_50	(+)	3,72	2,62	0,25	0,471	0,451
	(-)	3,9	2,44	-0,271	0,432	

5.4 Pull-out tests of GFRP sheets and CFRP strips wrapped

The pull-out tests for these specimens were initially decided in order to evaluate the contribution of the fixing bolt at the overlapped connection, in the uplifting of the post.

However, after the cyclic tests and the failure of the retrofitting solution, the bolt was no longer expected to provide significant resistance, concidering the fact that the perpendicular snapping cracks had propagated through almost the entire width of the section in both cases and the bolt was fixed underneath that level. Nevertheless, the pull-out tests were performed so that the remaining load capacity of the specimens could be evaluated.

Before the tests, the fixing points of the specimens at the top of the posts were strengthened as it has previously been mentioned with GFRP sheets and laterally placed screws above the fixing rods of the steel U profile (See 4.3.1.1). The tests were performed with the same procedure as the rest of the retrofitted specimens that were subjected to pull-out tests (See Table 5.1).

An extra LVDT was positioned at the bottom of the post to register the uplifting at that point and compare it with the uplifting of the post at the top. Through the evaluation of these results it is possible to realize the resistance of the bolt to the uplifting displacements of the post.

Evaluation of the damage patterns

The failure of the specimens occurs thorugh the tensile cracking parallel to the grain of the wood section of the post at the level of the top surface of the beam (Figure 5.33a-b). The bolt worked mainly for the case of the damaged specimen, where the snapping of the grain occurred for larger induced uplifting displacements (Figure 5.34a-b).

Although it was expected that after the unmounting of the specimens with the completion of the tests, the posts would be unstable they were found to be stable. In fact, the task of detaching the post from its bottom part, took effort in the case with the prosthesis member, and a hammer was needed (Figure 5.33c). The latter happened because a part of the grain had detached in a form which provided good interlocking (Figure 5.33d).


a)

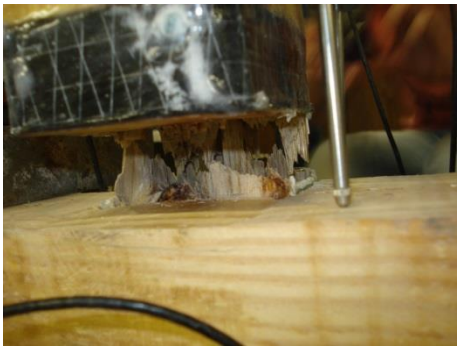
b)


c)

d)

Figure 5.33 - Photos a) – d) show the progressive damage patterns that appeared during the pull-out tests of the strengthened with GFRP sheets and CFRP strips wrapped specimens: a) with a prosthesis, b)-d) damaged.

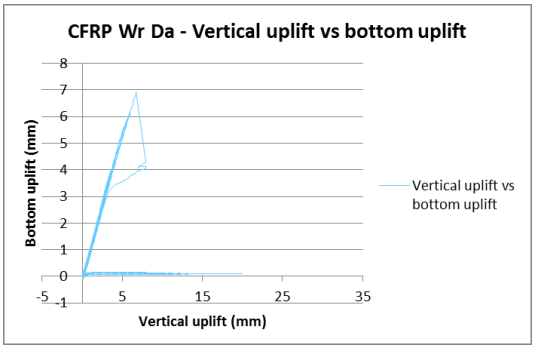

a)
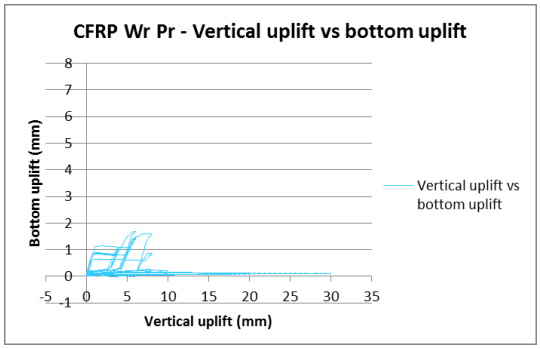

b)

Figure 5.34 – Graphs showing the uplifting at the bottom of the post for the induced uplifting displacements at the top od the post during the pull-out tests of the strengthened with GFRP sheets and CFRP strips wrapped specimens: a) damaged, b) with a prosthesis.

Analysis of the Force – Displacement diagrams

The additional resistance of the bolt to the uplifting displacements of the post, until total development of smeared tensile cracking and detachment-snapping of the grain occurred, is evident once the graphs in Figure 5.35 and Figure 5.34 are compared. In the case of the damaged specimen (Figure 5.35a), there was more resistance which leaded to a considerably higher maximum load, of about 3,4 times (Figure 5.35c). It should be noticed that in spite of the damage imposed during the lateral cyclic test, the retrofitted specimen is able to exhibit more than the double of the maximum resistance found in the unreinforced specimens presented in Chapter 3, which was of 5kN.

In the case of the specimen with the prosthesis, during the reset to the initial position there was resistance due to the difficulty imposed by the grain rearrangement (Figure 5.35b).

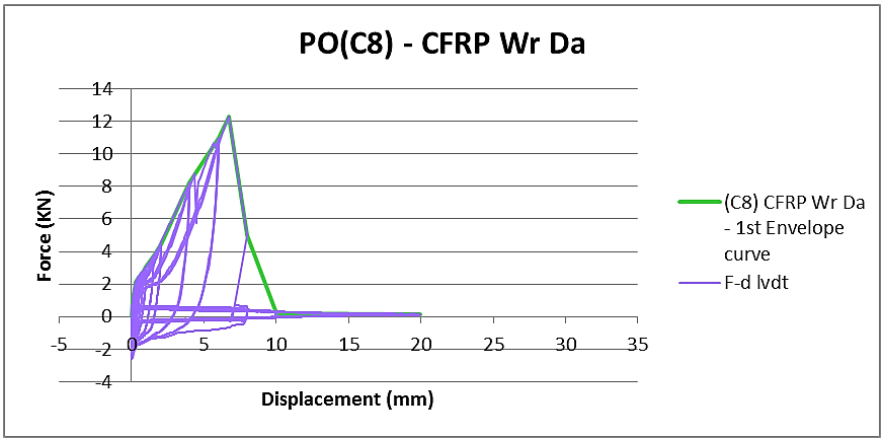

a)

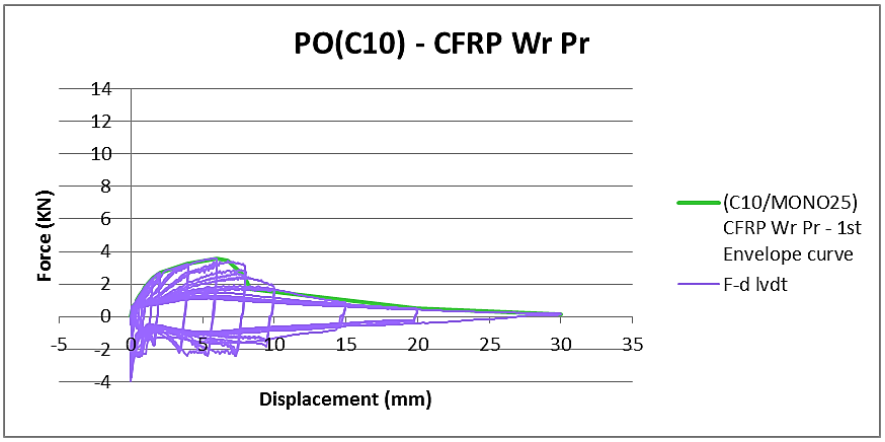

b)

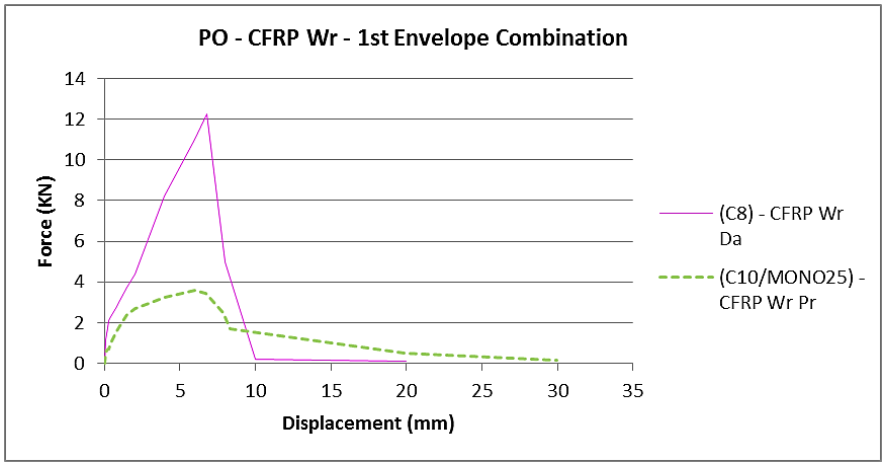

c)

Figure 5.35 - a)-b) F-d graphs for the strengthened with GFRP sheets and CFRP strips wrapped specimens, which were subjected to pull-out tests.(Case b) with a prosthesis, c) Comparative diagram of their F-d envelope curves.

Analysis of the Dissipated energy and stiffness

It is more realistic to take into consideration the results until the 12th displacement step (8mm) because the retrofitting technique stopped being effective after that point.

The comparative graphs for the accumulative dissipated energy, equivalent viscous damping and cyclic stiffness correlated to the lateral drift percentage, are given in Figure 5.36a-c.

As it was previously mentioned, in the case with the prosthesis, during the reset to the initial position there was resistance due to the difficulty imposed by the grain rearrangement. The latter can explain the increasing part of the equivalent viscous damping in Figure 5.36b, which should be decreasing once the maximum load is surpassed, in the case of pull-out tests as it was previously encountered (See 5.2.2), as well as the one regarding the accumulative dissipated energy in Figure 5.36a.

A gradual increasing of the accumulative dissipated energy in the case of the damaged specimen is also observed, as it was expected (Figure 5.36a). The higher accumulative dissipated energy, as well as cyclic stiffness of the damaged specimen is verified by the comparison with the graph in Figure 5.35c. Once again, the gradual degradation of the cyclic stiffness is evident in Figure 5.36c.

The values of the initial stiffness were also calculated and they are presented in Table 5.7. The difference between those values and ones in the graphs in Figure 5.36c exist because the cyclic stiffness is calculated for every cycle, while initial stiffness takes into consideration the maximum force obtained from the whole test, which leads to not directly comparable results (See equations 3.6 and 3.7 in 3.6.4).

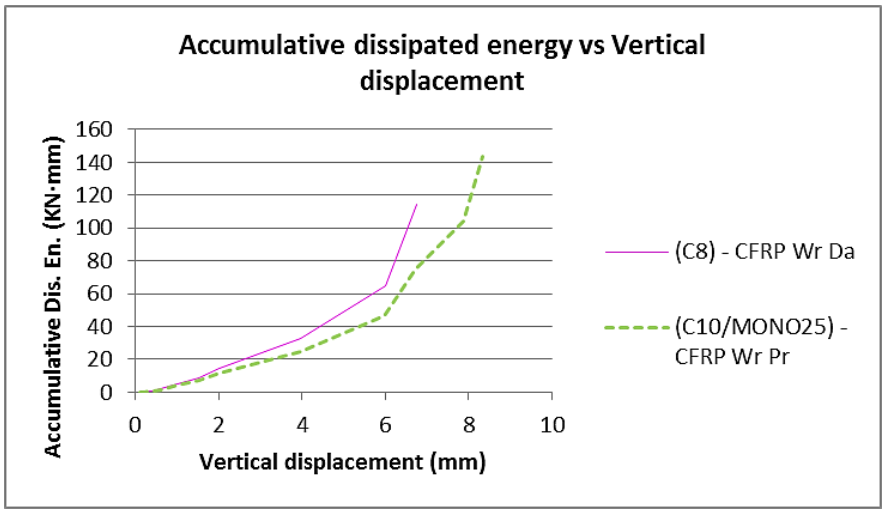

a)

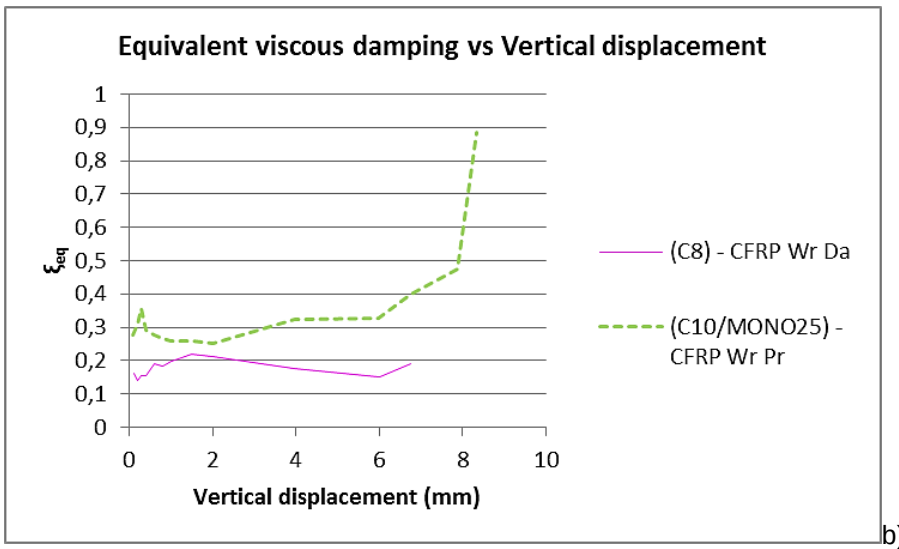

b)

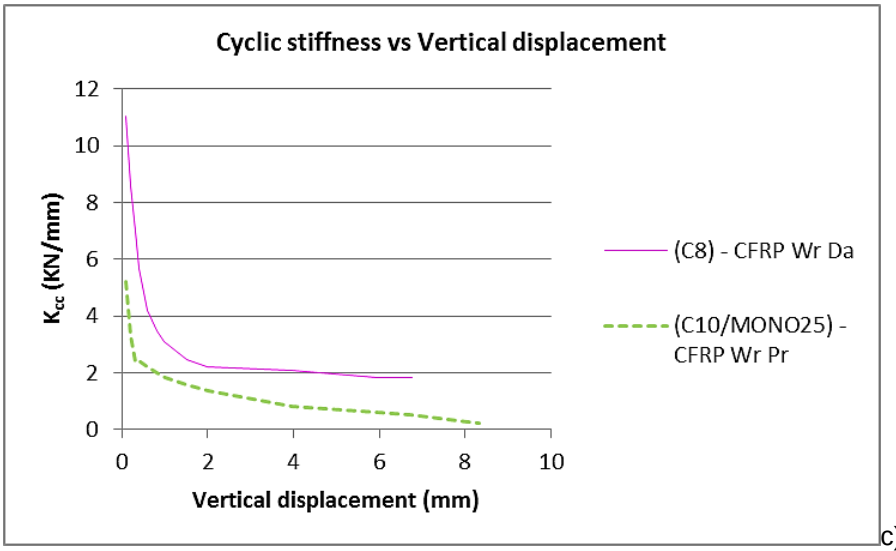

c)

Figure 5.36 - Comparative diagram of: a) the accumulative dissipated energy – drift%, b) the equivalent viscous damping – drift%, c) the cyclic stiffness – drift % for all the retrofitted with GFRP sheets and CFRP strips wrapped specimens, which were subjected to pull-out tests.

Table 5.7 – Calculated initial stiffness for the first envelope curve of all the retrofitted with GFRP sheets and CFRP strips wrapped specimens, obtained from the pull-out tests

	Fmax	v40%Fmax	v10%Fmax	K
(C8) - CFRP Wr Da	3,59	0,685	0,03	1,644
(C10/MONO25) - CFRP Wr Pr	12,26	2,188	0,1	1,761

Chapter 6

Conclusions

The purpose of this dissertation was to identify the mechanical behavior of a traditional overlapped connection, which is encountered in a half-timbered wall, regarding seismic loads,

During previous experimental campaigns on real size half-timbered walls, it was observed that their overall behavior was governed by their connections [4]. In general, the important uplift of the posts was recorded at the lower side of the walls, when they were submitted to shear and flexure associated to the lateral cyclic loads that were imposed at the top of the walls.

Therefore, it was decided to inspect the behavior of a single overlapped connection which is considered to be representative of a connection at the base of the walls, under cyclic pull-out and in-plane lateral loading. Note that a simplification was adopted, which consists of the non-consideration of the diagonal element converging to the overlapped connection. The lateral in-plane cyclic tests were performed for two different pre-compression vertical loads, namely 25kN and 50kN, as it was the case for the walls. In total, 14 specimens were tested, being 4 of them subjected to pull-out cyclic loading and the remaining 10 connections submitted to in-plane cyclic tests, 5 for each vertical load case.

From the results obtained in the experimental campaign the following conclusions can be provided:

- Regarding the pull-out tests, the mechanical behavior of the connection was mainly influenced by the shear resistance-load carrying capacity of the nail, while further strength was obtained whenever friction was present due to the good geometry of the specimen, which minimized the lateral clearances between the beam and the post “tenon”. Apart from the permanent deformation of the nail, that bended into an “S” shape no significant visible damages were present after the completion of the tests. It is important to mention the noticeable out-of-plane displacement that occurred during the performance of these tests, which is similar to what happens in the timber frame walls as well. This out-of-plane displacement is associated to a great extent, to the geometry of the connections, which can be considered asymmetric in the thickness of the wall.
- As far as it concerns the in-plane cyclic tests, it was noticed that preexisting natural defects of the timber post, as well as its physical properties in general, hold a key role to its mechanical behavior. All the damage patterns were localized mainly to the lower part of the post, close to its intersection with the beam, where it was affected by flexural and shear forces at the same time. Damages appeared sooner when the applied vertical load was higher, which indicates that the applied vertical load has an important role as well, on the damage patterns and the resistance of the connections.

After the evaluation and analysis of the results that derived from the previous tests, the specimens were retrofitted with different techniques and in some cases with a combination of retrofitting solutions. Specifically the following retrofitting solutions were applied:

- Positioning of screws to specimens that would be subjected to pull-out tests.

- Application of uniaxial GFRP sheets to a specimen that would be subjected to a pull-out test and to others that would be subjected to in-plane cyclic tests, which were damaged or further strengthened with a glued wooden prosthesis.
- Retrofitting with steel plates and bolts to a specimen that would be subjected to a pull-out test and to others that would be subjected to in-plane cyclic tests, which were further strengthened with a glued wooden prosthesis.
- Near-surface mounting of steel rods to a specimen that would be subjected to a pull-out test and to others that would be subjected to in-plane cyclic tests, which were further strengthened with a glued wooden prosthesis.
- Use of an innovative way which combines GFRP sheets and CFRP strips to specimens that would initially be subjected to in-plane cyclic tests and then to pull-out tests, which were damaged or further strengthened with a glued wooden prosthesis.

A new experimental campaign was carried out on the retrofitted specimens. Once it was completed the results were analyzed and along with the previously observed performance of each case during the tests, the following conclusions were drawn concerning the:

Pull-out tests

- The higher level of stiffness, which was provided to the connections through the retrofitting, leaded to a behavior which was closer to monolithic. Moreover, this leaded to the development of permanent deformations to the beam, which had not been witnessed during the tests that were performed on the unreinforced specimens. Additionally, uplifting displacements of the beam are attributed to the same reason.
- The GFRP solution was effective, providing remarkably high values in terms of stiffness and maximum load capacity. However its close-to-brittle failure should be taken into consideration, as after the failure of the sheets, the specimen behaves as if it was unreinforced.
- The solution with the addition of screws, provided an altogether good behavior in terms of strength, stiffness and dissipated energy for the pull-out test, but a complimentary retrofitting solution would be advised in order for it, to bear flexural and shear forces regarding in-plane cyclic tests.
- In a similar way, if the solution with the GFRP sheets and CFRP strips was subjected to a pull-out test before the in-plane cyclic, it would have performed in a significantly better manner. However, it was seen that the damaged specimen presented double of the resistance, when compared to the maximum pull-out resistance recorded in unreinforced specimens, which was due to the existence of the bolt.
- The tests conducted upon the specimens with the NSM and the steel plates retrofitting solutions were inconclusive, since they were not completed, as the load capacity of the actuator was not sufficient. However, it should be pointed out that a considerable increase

regarding stiffness and resistance was observed. The major issues related to the incomplete tests were the maximum force and the post-peak behavior.

In-plane cyclic tests:

- It was concluded that uniaxial GFRP sheets cannot reinforce members which are meant to undergo flexure, due to their early rupture and in some cases debonding. This was noticed without exception in all the cases, where GFRP sheets had been used.
- The prosthesis solution failed to perform as a unified element with the preexisting part of the post and in 5 out of the 7 specimens where it was applied, a plastic hinge was developed in their connection, once the 4^{th} displacement step (19,90mm) was reached. Furthermore, the gel glue, which was used to join the two members, appeared to create problems due to its consistency, as it was found that there was not a sufficient quantity of glue between the connected parts in a few cases. Nevertheless, even when paste glue was used, a plastic hinge developed.
- A preliminary assumption could be that the solutions with steel plates and NSM steel rods performed closer to the anticipated way and provided good results in terms of load capacity and stiffness, although for the case of NSM, the plastic hinge at the prosthesis connection occurred before the overlapped connection started to work effectively. Considering that the NSM solution is invasive and time consuming, the retrofitting solution with the steel plates might be preferable.

After the enumeration of all the conclusions that derived during the development of the dissertation, it is possible to provide recommendations for further study:

- Although the prosthesis solution appeared to not work during this study, a different prosthesis solution and its performance could be investigated, with or without further retrofitting.
- Retrofitting with multi-directional glass or carbon FRP, should present a better behavior regarding flexural and shear forces that are anticipated during in-plane cyclic tests. This means that certain strengthening techniques that were applied and did not work for this study do not have to be completely abandoned. After all, experimental campaigns are meant to function through the process of “trial and error”.
- An experimental campaign should be carried out on new specimens that will be retrofitted again, without having been subjected to previous tests, in order to reach safe conclusions regarding the most appropriate retrofitting solution. The retrofitting should be made after taking into consideration the previous recommendations.

References

[4] Poletti E,, Vasconcelos G,, Oliveira D.V., Influence of infill on the cyclic behaviour of traditional half-timbered walls. In: Proceedings of International Conference on Rehabilitation and Restoration of Structures, Chennai, India, 2013.

References

[1] Penelis G.G., Kappos A.I., Earthquake resistant constructions from concrete (in Greek), ZITIS Publising, Thessaloniki 1999

[2] Kappos A.I., Kouris L.A., Modelling of Traditional Timber-Framed Masonry Structures (in Greek), 3rd National Conference on Earthquake Engineering and Engineering Seismology, 5-6 of November 2008, Paper No. 2013

[3] Paula R., Coias V., Rehabilitation of Lisbon's old seismic resistant timber framed buildings using innovative techniques, International Workshop on "Earthquake Engineering on Timber Structures", Coimbra, Portugal, November, 2006

[4] Poletti E,, Vasconcelos G,, Oliveira D.V., Influence of infill on the cyclic behaviour of traditional half-timbered walls. In: Proceedings of International Conference on Rehabilitation and Restoration of Structures, Chennai, India, 2013.

[5] Stilianidis K., Ignatakis C., Masonry Structures (according to Eurocodes 6 and 8) (in Greek), Thessaloniki 2010

[6] Morphology - Rhythmology, Theory of Architectural Forms & Rhythms, Traditional Architecture (in Greek), Student Notes from Democritus University of Thrace, Ksanthi
Available at: http://morfologia.arch.duth.gr/3o_etos/3o_exam_VI/paradosiaka.pdf (7.7.2013)

[7] Langenbach R., From "Opus Craticium" to the "Chicago Frame": Earthquake-Resistant Traditional Construction, International Journal of Architectural Heritage (2007),1:1, 29 — 59

[8] Copani P., Timber-Frame Buildings in Scandinavia: High Deformation Prevent the System from Collapse, ICOMOS IWC - XVI International Symposium: From Material to Structure - Mechanical Behaviour and Failures of the Timber Structures, Florence, Venice and Vicenza, 11th -16th November 2007

[9] Gülkan P., Langenbach R., The earthquake resistance of traditional timber and masonry dwellings in turkey, 13th World Conference on Earthquake Engineering, Vancouver, B.C., Canada, August 1-6, 2004, Paper No. 2297

[10] Tsakanika-Theohari E., Mouzakis H., A post-byzantine mansion in Athens. The restoration project of the timber structural elements, World Conference on Timber Engineering 2010

[11] Anastasiadis C., Papadopoulos D., Restoration and energy efficiency of a historical building in Ano Poli, Master Thesis, Civil Engineering Dept., Aristotle University of Thessaloniki, 2010

[12] Koukouviki A.M., Inspection of insulation efficiency of a rural area residence in Megalo Seirini, Grevena, Greece, according to the Regulation of Energy Performance of Buildings and

suggestions on its improvement (in Greek), Master Thesis, Civil Engineering Dept., Aristotle University of Thessaloniki, 2011

[13] Cardoso R., Lopes M., Bento R., Seismic evaluation of old masonry buildings. Part I: Method description and application to a case-study, Engineering Structures 27: (2005), 2024–2035

[14] The Hobbit House Illustrated Glossary of Woodworking terms - Joinery terms: http://www.hobbithouseinc.com/personal/woodpics/_joineryterms.htm (7.7.2013)

[15] Meireles H.A., Seismic vulnerability of Pombalino buildings. PhD Thesis. UTL, Instituto Superior Tecnico, Lisbon 2012

[16] Mascarenhas J., Construction systems – V (in Portuguese). Livros Horizonte, Lisbon 2004

[17] Ignatakis C., Eftichidis S., Investigation of masonry infilled timber structures-Modelling proposal and analysis procedure (in Greek), 3rd National Conference on Earthquake Engineering and Engineering Seismology, 5-6 of November 2008, Paper No. 2072

[18] Roca P., Kabele P., Lourenco P., MSc SAHC Lecture, SA2.1 Purpose and Possibilities of Structural Analysis, UNIPD, Padova, Italy, 2012-2013.

[19] Gülhan D., Güney I.O., The behaviour of traditional building systems against earthquake and its comparision to reinforced concrete frame systems; experiences of Marmara earthquake damage assesment studies in Kocaeli and Sakarya.
Available at ICOMOS International Wood Committee :
http://www.icomos.org/iiwc/seismic/Gulhan.pdf (7.7.2013)

[20] Goncalves A.M., Ferreira J.G., Guerreiro L., Branco F., Seismic retrofitting of Pombalino “frontal” walls, World Conference of Earthquake Engineering, Lisbon 2012, Paper No. 5129

[21] Poletti E., Vasconcelos G., Seismic behaviour and retrofitting of timber frame walls. International conference on structural health assessment of timber structures (SHATIS’13) 4 - 6 September 2013, Trento, Italy (accepted).

[22] Branco J., Influence of the joints stiffness in the monotonic and cyclic behavior of traditional timber trusses. Assessment of the efficacy of different strengthening techniques, Ph.D. Thesis, Civil Engineering Dept., University of Minho, Portugal 2008

[23] Palma P., Garcia H., Ferreira J., Appleton J., Cruz H., Behaviour and repair of carpentry connections – Rotational behaviour of the rafter and tie beam connection in timber roof structures, Journal of Cultural Heritage 13S (2012) S64–S73

[24] Parisi M.A., Cordie C., Mechanical behavior of double-step timber joints, Construction and Building Materials: Volume 24, Issue 8, August 2010, Pages 1364–1371

[25] Koch H., Eisenhut L., Seim W., Multi-mode failure of form-fitting timber connections - Experimental and numerical studies on the tapered tenon joint, Engineering Structures 48 (2013) 727–738

[26] Feio A., Lourenco P., Machado J., Testing and modeling of a traditional timber mortise and tenon joint, Materials and Structures: DOI 10.1617/s11527-013-0056-y, 2013

[27] Shanks J.D., Walker P., Experimental performance of mortise and tenon connections in green oak, The Structural Engineer – 6 September 2005, p.40-45

[28] Cruz H., Moura J.P., Machado J.S., The use of FRP in the strengthening of timber-reinforced masonry load-bearing walls, Historical Constructions, Guimaraes, 2001, p.847-856

[29] Pilaon P., Experimental cyclic behavior of timber shear walls, SAHC Master Thesis, Civil Engineering Dept., University of Minho, Portugal 2010

[30] International Organization for Standardization – International Standard ISO 3131: Wood - Determination of density for physical and mechanical tests, Switzerland 1975

[31] International Organization for Standardization – International Standard ISO 3130: Wood - Determination of moisture content for physical and mechanical tests, Switzerland 1975

[32] Brites R., MSc SAHC Lecture, SA4 Inspection and Diagnosis: Non-destructive evaluation of timber structures, UNIPD, Padova, Italy, 2012-2013.

[33] European Committee for Standardization – European Standard EN 1995-1-1:2004, Eurocode 5: Design of timber structures - Part 1-1: General - Common rules and rules for buildings, Brussels, Belgium 2004

[34] Drdácký M., Panizza M., MSc SAHC Lecture, SA4 Inspection and Diagnosis: Laboratory and in situ testing, UNIPD, Padova, Italy, 2012-2013.

[35] International Organization for Standardization – International Standard ISO/DIS 21581: Timber structures — Static and cyclic lateral load test method for shear walls, Switzerland 2008

[36] Magenes G., Calvi M., In-plane seismic response of brick masonry walls, Earthquake Engineering and Structural Dynamics, VOL. 26, 1091-1112 (1997)

[37] European Committee for Standardization – European Standard EN 12512: Timber structures - Test methods - Cyclic testing of joints made with mechanical fasteners Brussels, Belgium 2001

[38] Roca P., MSc SAHC Lecture, SA1.11 History of Conservation and Restoration Part 2/2, UNIPD, Padova, Italy, 2012-2013.

[39] Madhoushi M., Ansell M., Behaviour of timber connections using glued-in GFRP rods under fatigue loading. Part II: Moment-resisting connections, Composites Part B: Engineering Volume 39, Issue 2, March 2008, Pages 249–257

[40] Oikonomou N., Mpikas D., Avdelas A., Timber Structures – Notes for students (in Greek), Thessaloniki 2008-2009

[41] El-Hacha R., MSc SAHC Lecture, SA5 Repairing and Strengthening Techniques- Strengthening of Timber Structures, UNIPD, Padova, Italy, 2012-2013.

[42] Improving Timber Connections through Design, Ron Blank & Associates, 2009
Available at: http://www.ronblank.com/courses/tlx06a/tlx06a.pdf (8.7.2013)

[43] El-Hacha R., MSc SAHC Lecture, SA5 Repairing and Strengthening Techniques- Strengthening of Concrete Structures (II), UNIPD, Padova, Italy, 2012-2013.

[44] Vázquez E., MSc SAHC Lecture, SA6 Restoration and conservation of materials- Polymers and Composites 2012, UNIPD, Padova, Italy, 2012-2013.

[45] Jorge M.A.P., Experimental behavior of glulam-FRP systems, MSc Thesis, Department of Civil Engineering, University of Minho, Portugal 2010.

[46] Blass H.J., Bejtka I., Reinforcements perpendicular to the grain using self-tapping screws, Proceedings of the 8th World Conference on Timber Engineering, Volume I, Lahti, Finland, 2004

Appendix A: F - d graphs of the tests on unreinforced timber connections

URT Pull-out tests:

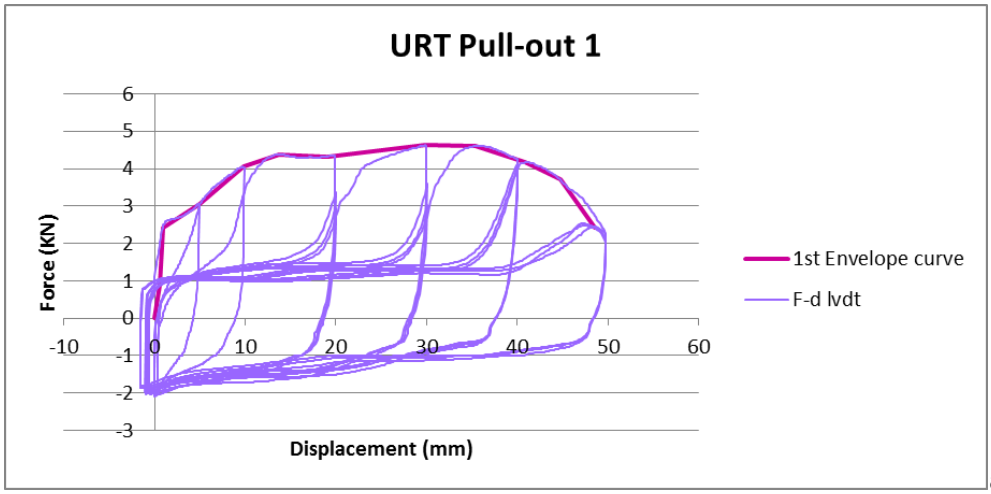

a)

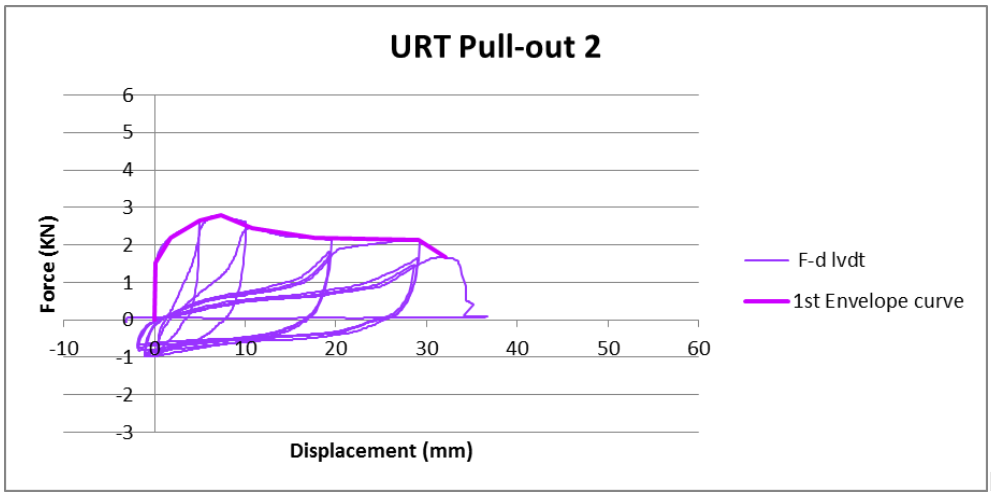

b)

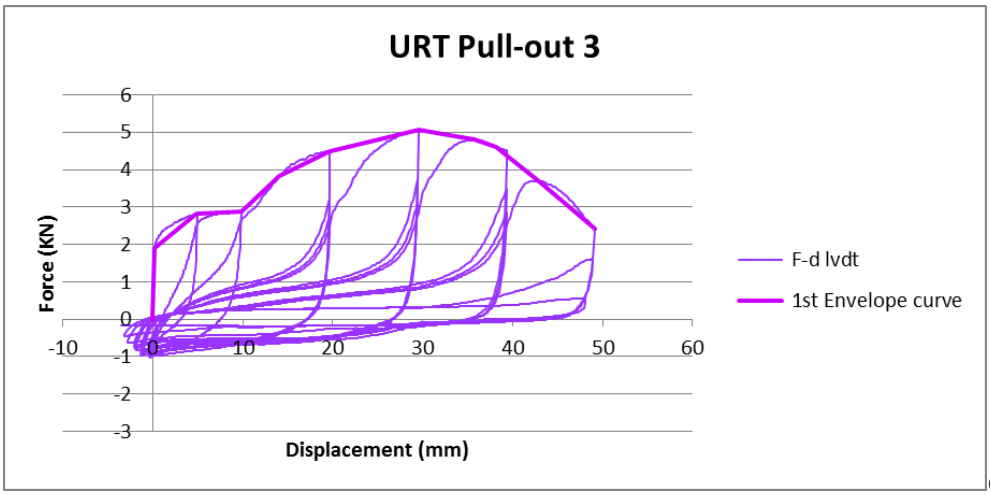

c)

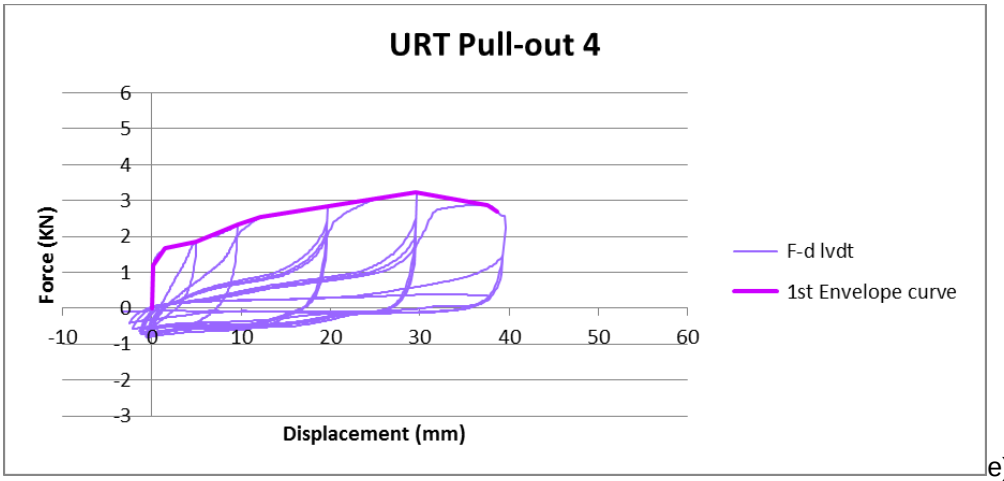

e)

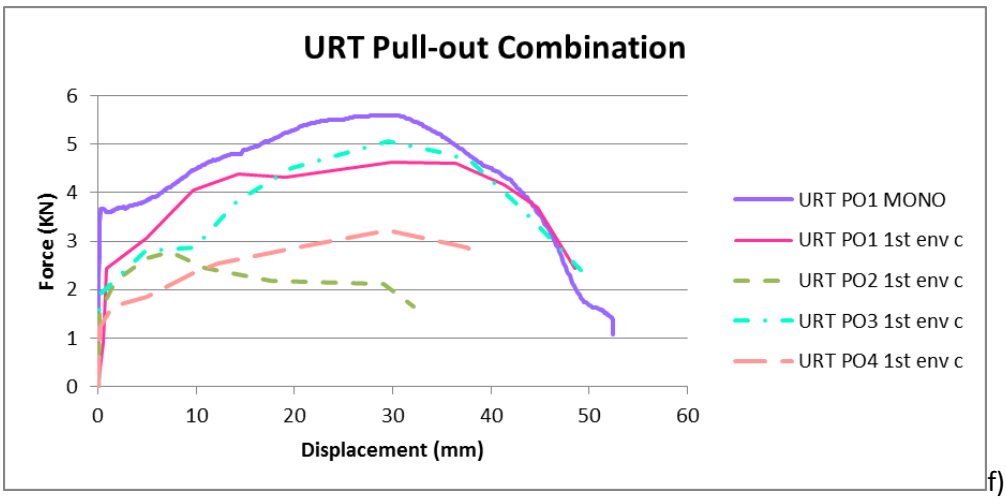

f)

Figure A.1 – a) F-d graph of PO1, b) F-d graph of PO2, c) F-d graph of PO3, d) F-d graph of PO4, e) Combination of F-d envelope curve graphs for all the pull-out tests. (URT: Unreinforced timber, PO: Pull-out test).

URT in-plane cyclic tests:

Vertical load 25KN:

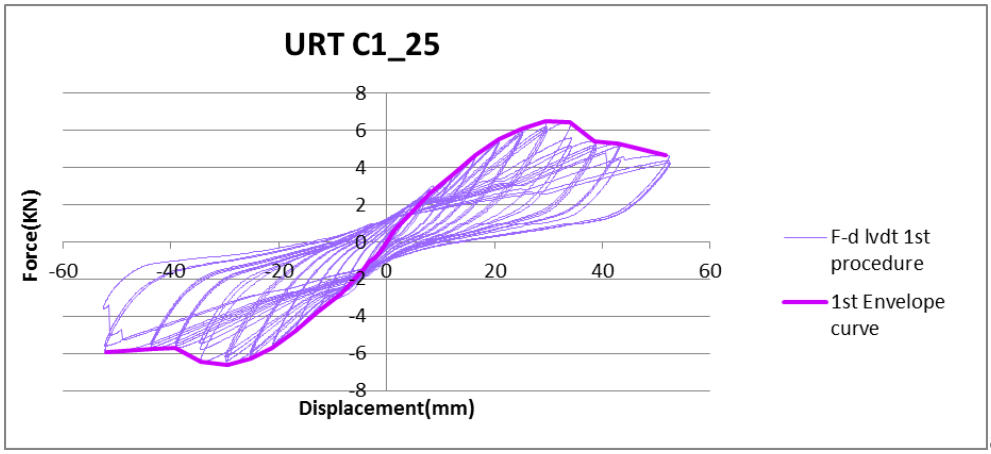

a)

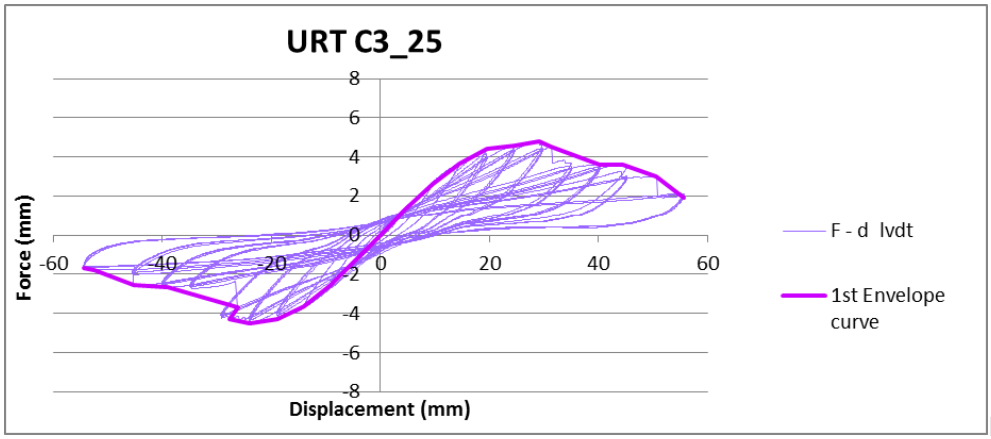

b)

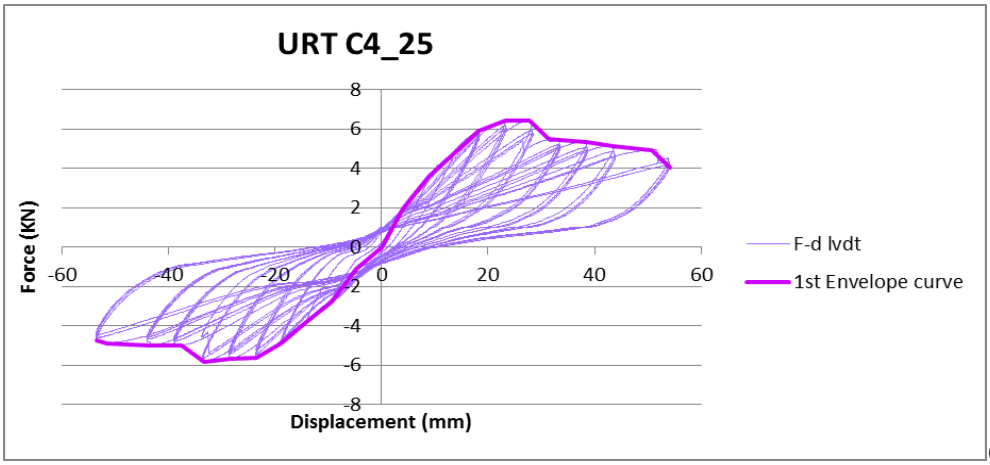

c)

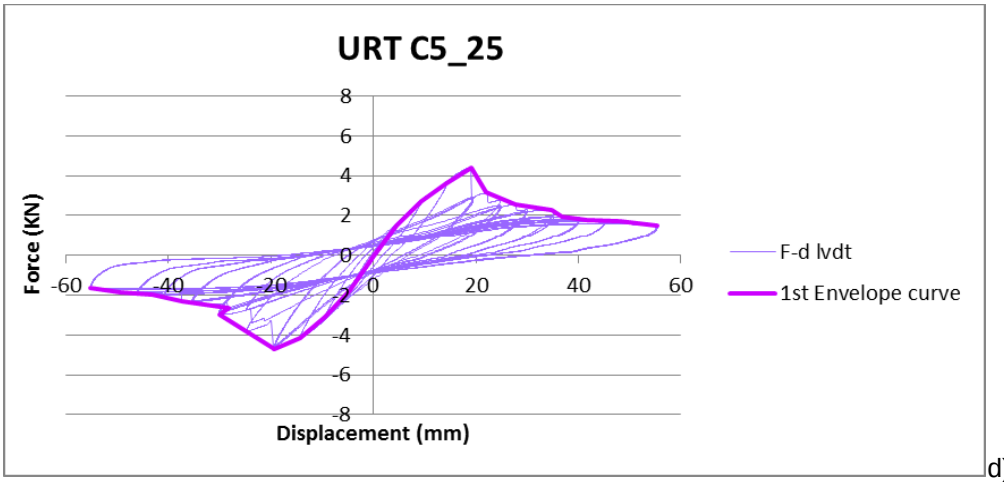

d)

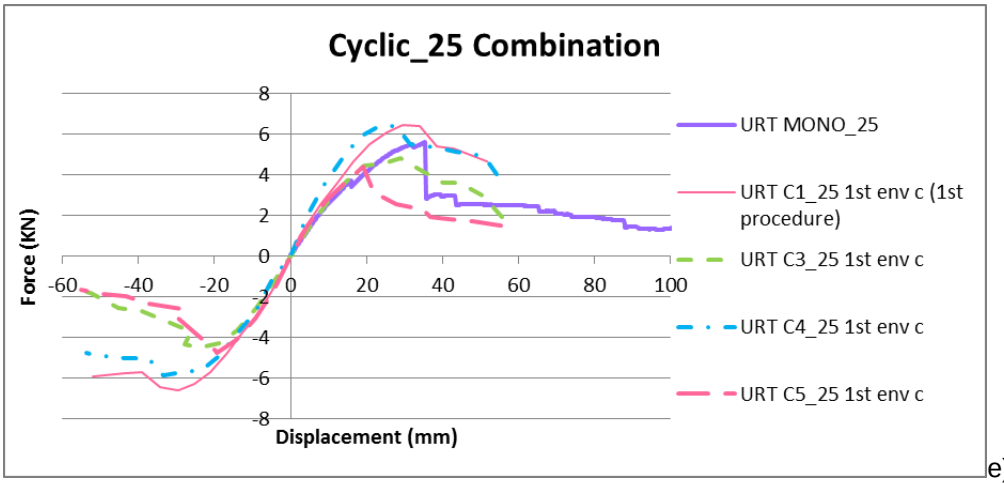

e)

Figure A.2 – F-d graph and 1st envelope curve of: a) C1, b) C3, c) C4, d) C5 and e) Combination of F-d monotonic and envelope curve graphs for all the cyclic tests with a vertical load of 25KN. (C: Cyclic test).

Vertical load 50KN:

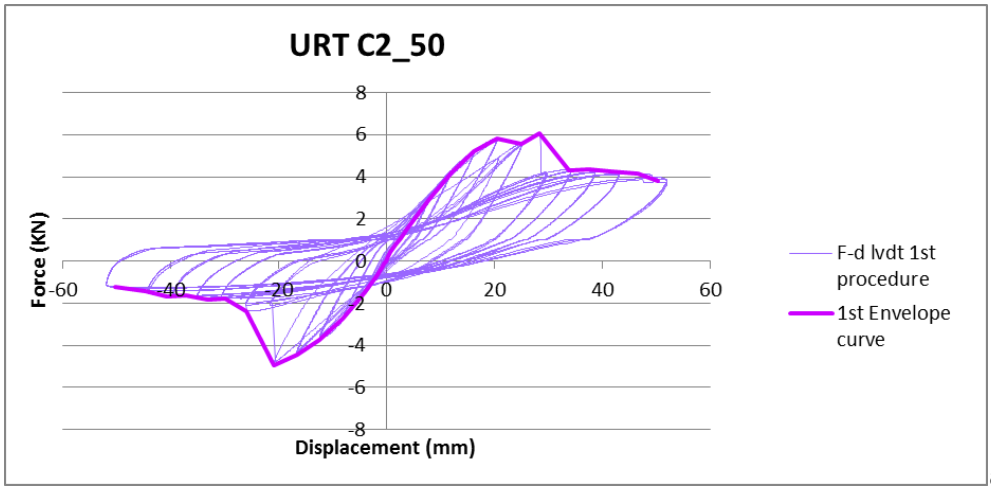

a)

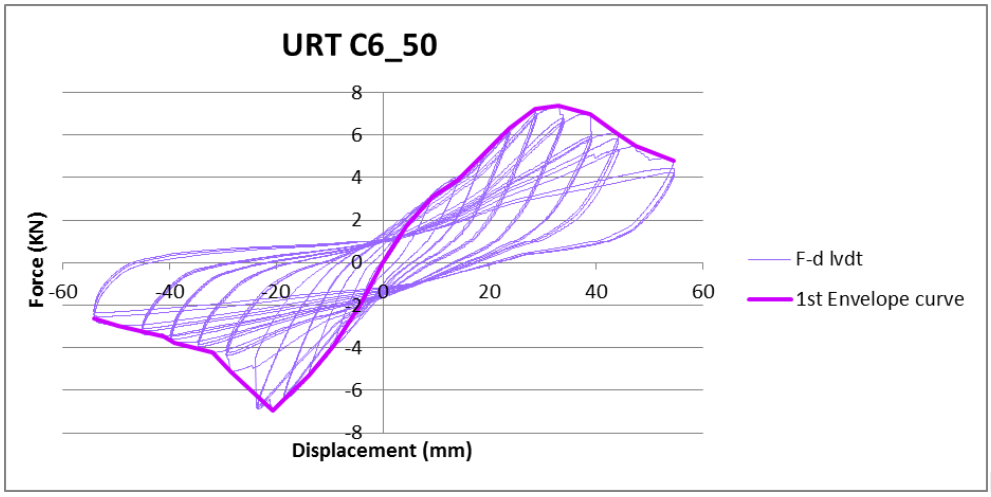

b)

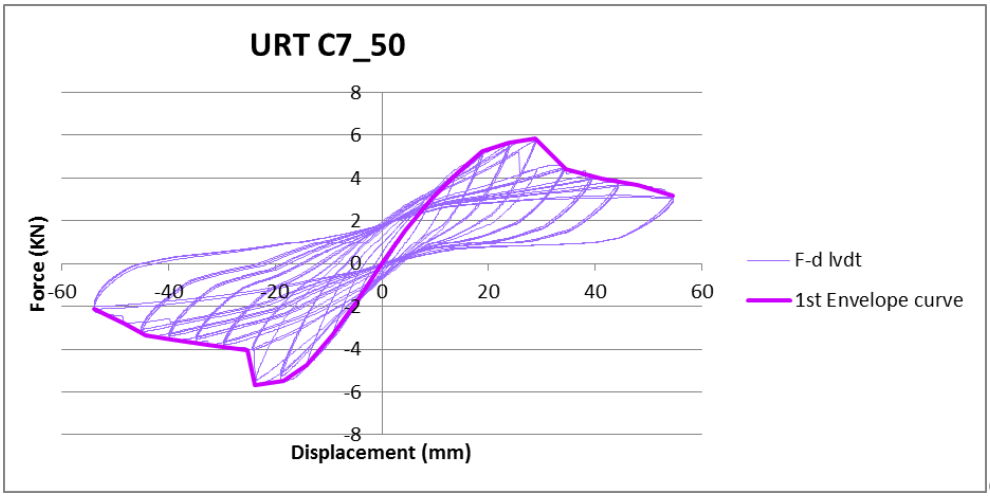

c)

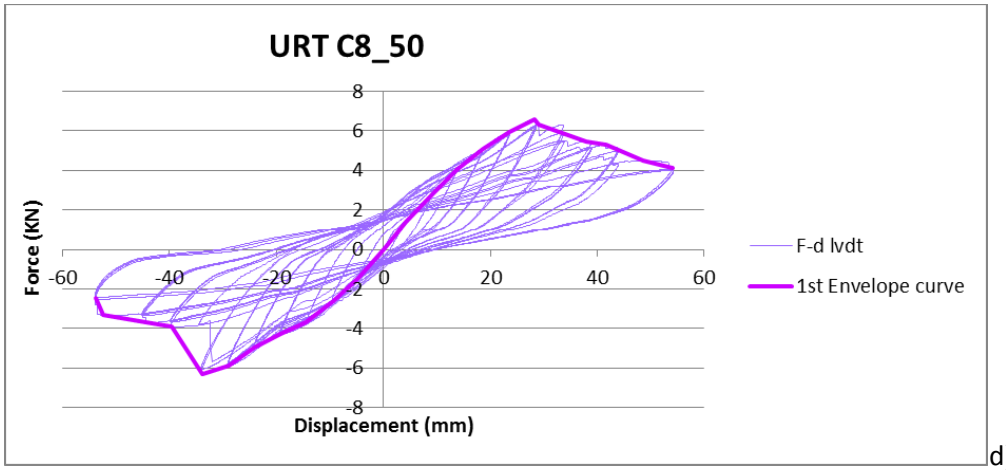

d)

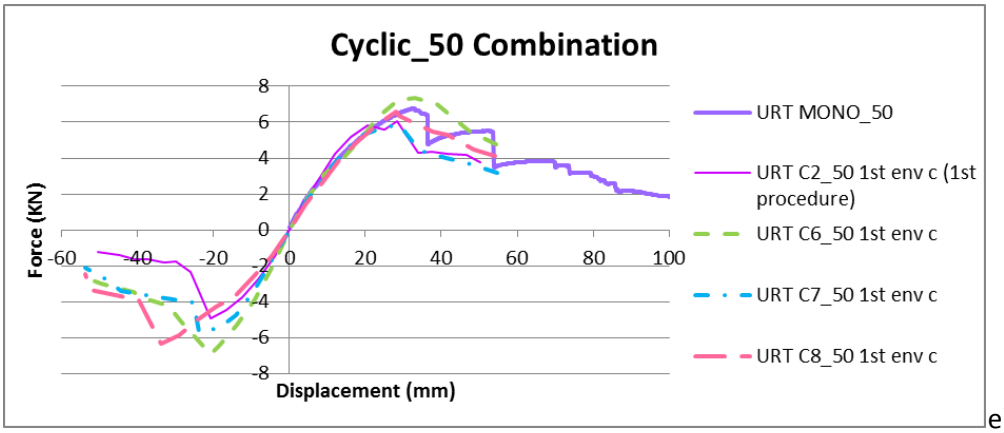

e)

Figure A.3 – F-d graph and 1st envelope curve of: a) C2, b) C6, c) C7, d) C8 and e) Combination of F-d monotonic and envelope curve graphs for all the cyclic tests with a vertical load of 50KN. (C: Cyclic test).

Appendix B: Vertical versus out-of-plane displacement graphs of the pull-out tests on unreinforced timber connections

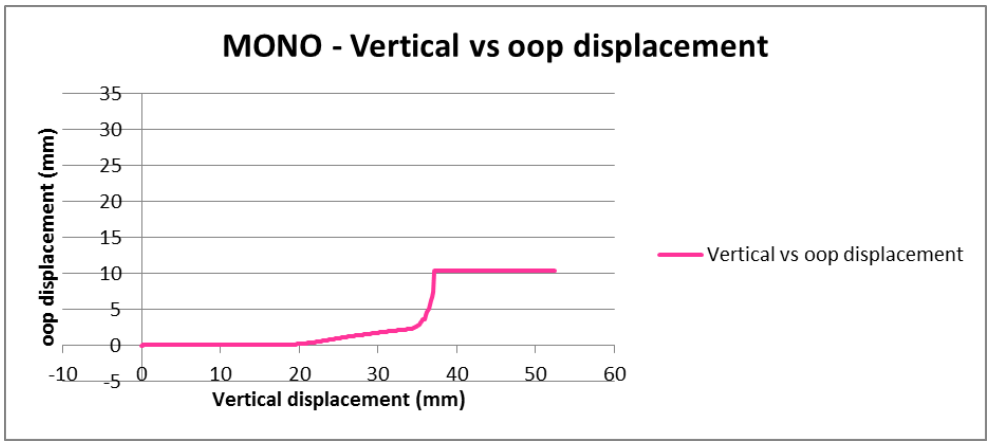

a)

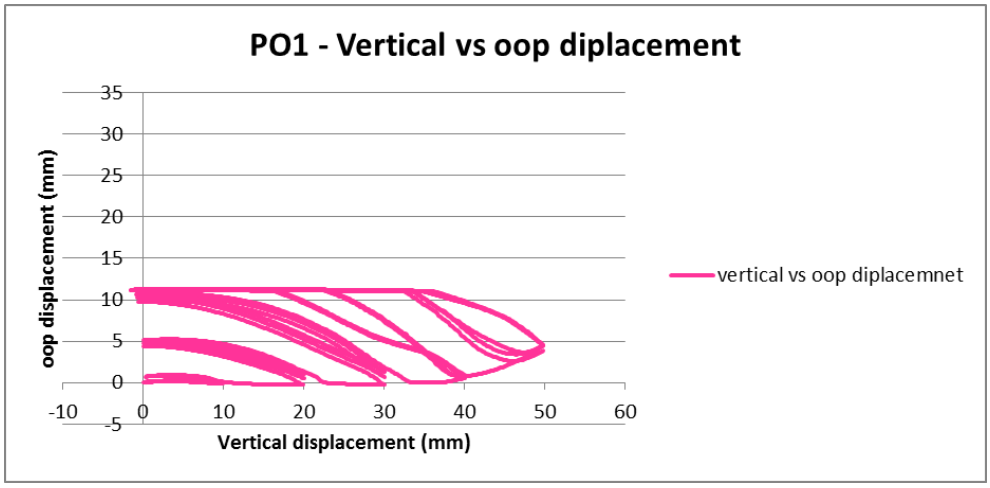

b)

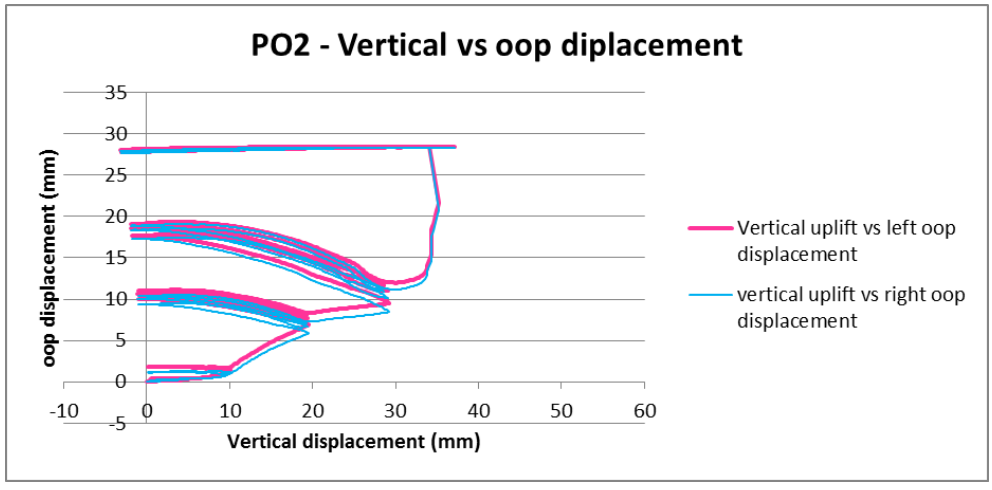

c)

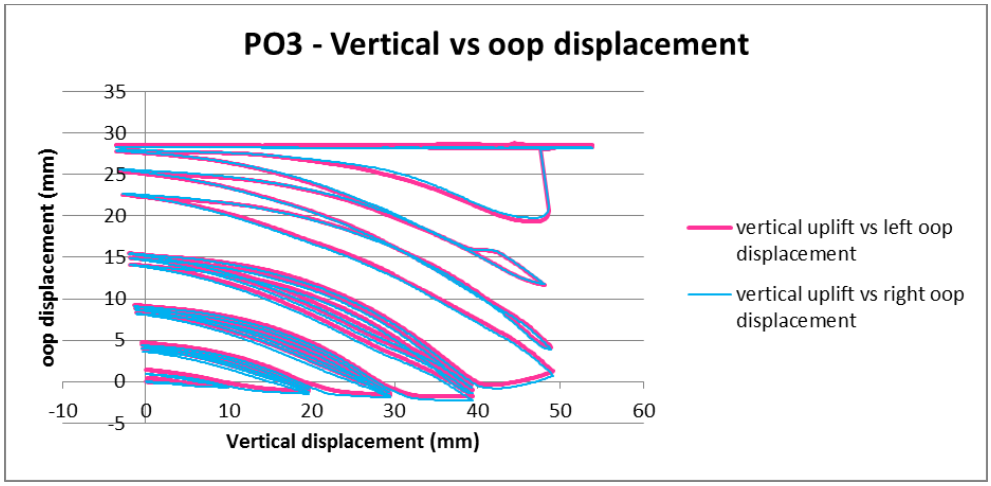

d)

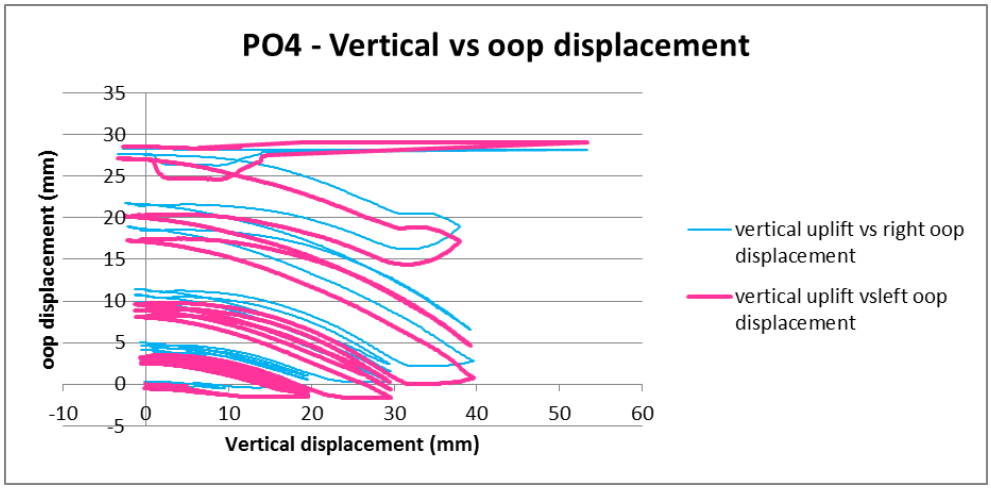

e)

Figure B.1 – Vertical versus oop displacement: a) monotonic pull-out test, b) PO1, c) PO2, d) PO3, e) PO4. (PO: Pull-out test).